Joint Synchronization and Channel Estimation for Burst Mode OFDM

Martino Freda

Department of Electrical & Computer Engineering
McGill University
Montreal, Canada

October 2004

A thesis submitted to McGill University in partial fulfilment of the requirements of the degree of Master of Engineering.

Your file Votre référence
ISBN: 0-494-06552-4
Our file Notre référence
ISBN: 0-494-06552-4

Abstract

The performance of orthogonal frequency division multiplexing (OFDM) is known to be highly sensitive to synchronization errors at the receiver. Inaccurate synchronization can increase channel estimation errors which further degrade OFDM performance. While effective independent synchronization techniques exist, performance gains can be expected by jointly estimating all synchronization errors and channel parameters.

The research presented in this thesis aims to improve the performance of synchronization and channel estimation in burst mode OFDM systems by employing the non-linear recursive least squares algorithm (NL-RLS) to perform joint synchronization and channel estimation. This thesis presents two joint synchronization and channel estimation algorithms. The joint carrier-frequency-offset and channel estimation and compensation algorithm (CFOCE-C) is first presented and possible applications are discussed. The Cramer Rao Lower Bound (CRLB) is derived to evaluate the efficiency of the estimator by measurement of its variance. Simulation is used to evaluate the advantage of the time domain approach used by the CFOCE-C in a typical burst mode system and a 2 dB gain in system performance is observed over an alternative joint frequency domain approach. The sensitivity of the CFOCE-C algorithm to sampling frequency offset (SFO) motivates the development of a second technique: the joint carrier-frequency-offset, sampling-frequency-offset, and channel estimation and compensation algorithm (CFOSFOCE-C). The variance of this estimator is also compared to the CRLB. A gain of 1.5 dB is observed in comparison to a joint estimation algorithm that uses a frequency domain approach.

Sommaire

La qualité de transmission du multiplexage par répartition orthogonale de la fréquence (OFDM) est sensible aux erreurs de synchronisation au récepteur. De plus, une synchronisation imprécise peut avoir comme conséquence un accroissement d'erreur dans l'estimation du canal. La synchronisation indépendante est souvent utilisée. Cependant, la synchronisation et l'estimation du canal de façon commune pourraient améliorer la qualité de transmission.

La recherche présentée dans ce mémoire de maîtrise a pour but l'utilisation de la version non linéaire de l'algorithme récursif des moindres carrés (NL-RLS) pour effectuer la synchronisation et l'estimation du canal afin d'améliorer la performance de transmission d'un system OFDM en fonctionnement en rafale. Deux algorithmes sont présentés dans ce mémoire. En premier lieu, l'algorithme d'estimation et de compensation commune du décalage de fréquence des porteuses et du canal (CFOCE-C) est présenté. La borne inférieure Cramer Rao (CRLB) est dérivée pour évaluer l'éfficacité de l'estimation en mesurant sa variance. L'avantage de l'approche en domaine temporel qui est employé par l'algorithme CFOCE-C est mesuré par simulation. L'algorithme CFOCE-C donne un gain de 2 dB comparé à une approche en domaine fréquentiel. Ensuite, un deuxième algorithme: l'algorithme d'estimation et de compensation commune du décalage de fréquence des porteuses, du décalage de la fréquence d'échantillonnage, et du canal (CFOSFOCE-C) est présenté pour remédier à la sensibilité de l'algorithme CFOCE-C au décalage de la fréquence d'échantillonnage (SFO). La variance de l'estimation de l'algorithme CFOSFOCE-C est comparée à la CRLB. Un gain de 1.5 dB est obtenu par l'utilisation de l'algorithme CFOSFOCE-C comparé à une approche en domaine fréquentiel.

Acknowledgments

I would first like to thank my supervisor, Prof. Tho Le-Ngoc for his advise and support throughout my graduate studies at McGill University. I learned a great deal from his experience, hard work, and extent of knowledge that will serve me well in my professional career. I would like to acknowledge NSERC for the financial support they provided through their postgraduate scholarship and other grants.

I am greatly indebted to Dr. Jianfeng Weng, whose encouragement and expertise in the area of my research proved to be invaluable in completion of my thesis. I would also like to thank all my fellow researchers and graduate students from McGill's Broadband Communications Lab for providing interesting and stimulating discussions that have taught me a great deal. A special thanks to Ying Lin Xu for proofreading this thesis and to Frederic Monfet for reviewing the French abstract.

I would like to thank my close friends Karol, Mike, and Sam who have given me much advice over the last two years which has made my graduate studies more fruitful. I wish to give my deepest gratitude to my family for their unending support through this and all other challenges in my life. Finally, I would like to thank my girlfriend Elena for her encouragement and understanding throughout my graduate studies.

Contents

List of Figures

List of Tables

List of Symbols

A	Magnitude of the decision error on a subcarrier
B_c	Channel coherance bandwidth
B_d	Channel Doppler spread
$C_{\mathcal{M}}$	Cost function after $\mathcal{M}$ iterations
$\boldsymbol{D}$	Deterministic frequency domain noise vector from decision feedback
$\mathcal{D}_i$	Mean square deviation of the coefficient vector at iteration i
E_s	OFDM symbol energy
F	Number of paths in Multipath channel
H_k	Channel frequency response at subcarrier index k
$\bar{H}_k$	Effective channel frequency response when the effect of SFO is considered
$\widehat{H}_k$	Estimate of the channel frequency response at subcarrier index k
$\boldsymbol{I}$	Identity matrix
$I_{k,l}$	Frequency domain ICI suffered by subcarrier k of symbol l
$\boldsymbol{K}$	Weight error vector correlation matrix
L_1	Number of long training symbol samples using the approximate gradient
L_2	Number of long training symbol samples using the exact gradient
M	QAM constellation size
$\mathcal{M}$	Size of input vector or size of a collection of samples
N	FFT/IFFT size
N_g	Length of the cyclic prefix
N_s	Number of samples in the OFDM symbol including cyclic prefix
P	Long training sequence cyclic prefix
$\boldsymbol{P}$	NL-RLS inverse correlation matrix
$\mathcal{P}_{ex}(i)$	The excess MSE at iteration i
$\mathcal{P}_0$	The optimum MSE for the estimation
R	Number of realizations used in obtaining estimate of statistical quantities
$\boldsymbol{R}$	Input vector correlation matrix

S	Number of training symbols for channel estimation
$\mathcal{S}$	Channel scattering function
T	Transmitter sampling period
T'	Receiver sampling period
T_i	ith long training symbol
$X_{k,l}$	Transmitted sample at subcarrier index k of OFDM symbol l
$\bar{X}_{k,l}$	Training sample at subcarrier index k of OFDM training symbol l
$Y_{k,l}$	Received sample at subcarrier index k of OFDM symbol l
$W_{k,l}$	AWGN noise sample added to subcarrier index k of symbol l
$\boldsymbol{c}$	Weight vector for the linear problem
$\widehat{\boldsymbol{c}}_m$	Estimate of $\boldsymbol{c}$ at time instant m
$\boldsymbol{d}$	Deterministic time domain noise vector from decision feedback
$\boldsymbol{e}_i$	Weight error vector at iteration i
e_m	Non-linear estimation error at time instant m
$\widetilde{e}_m$	Linear estimation error at time instant m
f	Passband carrier frequency
$f()$	Non-linear function for a system's received samples
$g()$	Adaptive algorithm weight update function
$\boldsymbol{g}$	NL-RLS adaptation gain vector
$\bar{\boldsymbol{g}}$	NL-RLS alternative adaptation gain vector
$\boldsymbol{h}$	CIR vector
h_r	rth element of the CIR vector
$\bar{\boldsymbol{h}}$	Effective CIR vector considering SFO effects
$\widehat{\boldsymbol{h}}_{(m)}$	Estimate of the CIR vector at time instant m
$\widehat{\boldsymbol{h}}^i_{(m)}$	Estimate of the CIR vector at time instant m for the ith realization
$\widehat{h}_{r_{(m)}}$	Estimate of the rth element of the CIR vector at time instant m
$\widehat{h}_{r_{(n,l)}}$	Estimate of h_r at time when receiver processes sample n of symbol l
$\boldsymbol{h}_{(i),eff}$	Effective CIR vector after i iterations in the long training symbols
$h(t;\tau)$	Time-varying CIR
i	Iteration index
k	Subcarrier index
l	OFDM symbol number
m	Absolute time index based on number of transmitted samples x_m
m^i	Absolute time index corresponding to NL-RLS iteration i
n	OFDM sample index $(0, 1, ..., N-1)$
t_i	ith short training symbol

$t_{n,l}$	Absolute sampling time associated with sample n of OFDM symbol l
v	Length of the CIR
w_m	Time domain AWGN noise sample at time instant m
$w_{n,l}$	Time domain AWGN noise sample added to sample n of symbol l
$\boldsymbol{w}$	Weight vector for the non-linear problem
$\dot{\boldsymbol{w}}$	Weight vector excluding the parameter θ
$\widehat{\boldsymbol{w}}_{(m)}$	Estimate of $\boldsymbol{w}$ at time instant m
$\widehat{\boldsymbol{w}}_{(n,l)}$	Estimate of $\boldsymbol{w}$ at time when the receiver processes sample n of symbol l
$\widehat{\dot{\boldsymbol{w}}}$	Estimate of $\dot{\boldsymbol{w}}$
x_m	Transmitted sample at time instant m
$x_{n,l}$	Transmitted sample n of symbol l
$\boldsymbol{x}_m$	Transmitted vector of samples at time instant m in non-linear estimation
$\widetilde{\boldsymbol{x}}_m$	Transmitted vector of samples at time instant m in linear estimation
$\dot{\boldsymbol{x}}$	Transmitted data samples (no CP) accounting for the effect of SFO
$\dot{\boldsymbol{x}}_{m_{n,l}}$	Estimate of $\dot{\boldsymbol{x}}$ at iteration for sample n of symbol l
$\dot{x}^q_{m_{n,l}}$	qth element of $\dot{\boldsymbol{x}}_{m_{n,l}}$
y_m	Received sample at time instant m in non-linear estimation
$y_{n,l}$	Received sample at sample n of symbol l
$\widehat{y}_m$	Estimate of the received sample at time instant m
$\widetilde{y}_m$	Received sample at time instant m in linear estimation
$y_{n,l}$	nth sample of the lth received OFDM symbol
Γ	SFO parameter multiplying factor
Ω	NL-RLS SFO step-size reduction factor
α	Complex channel path attenuation
$\widetilde{\alpha}$	Modified complex channel path attenuation
ϵ	Relative CFO
$\widehat{\epsilon}_{(m)}$	Estimate of ϵ at time instant m
$\widehat{\epsilon}^i_{(m)}$	Estimate of ϵ at time instant m on the ith realization
$\widehat{\epsilon}_{(n,l)}$	Estimate of ϵ at time receiver processes sample n of symbol l
ζ	Timing offset in samples
η	Relative SFO
$\widehat{\eta}_{(n,l)}$	Estimate of η at time receiver processes sample n of symbol l
θ	Cummulative CFO phase
$\widehat{\theta}_{(i)}$	Estimate of θ at iteration i
$\widehat{\theta}_{(n,l)}$	Estimate of θ at time receiver processes sample n of symbol l
ϑ_k	Phase difference between samples of subcarrier k for adjacent symbols

$\bar{\kappa}$	NL-RLS conversion factor
λ	Forgetting factor
μ	Mean of a particular sample of the input to the adaptation algorithm
σ^2	Noise variance
τ	Channel multipath delay
ϕ	Cummulative SFO phase
$\widehat{\phi}_{(n,l)}$	Estimate of ϕ at time receiver processes sample n of symbol l
ψ	Phase of the decision error on a subcarrier
ΔT	Difference in sampling period between transmitter and receiver
Δf	Carrier frequency offset in Hertz
Δf_s	Inter-carrier spacing in Hertz
$\nabla f()$	Gradient vector of $f()$ with respect to the parameter vector
$*$	Complex conjugation
$Re\{\}$	Real part
$Im\{\}$	Imaginary part
$E\{\}$	Expectation operator
$tr[]$	Trace operator
$\langle\otimes\rangle_n$	nth element of the circular convolution of two N-point sequences
$[]^T$	Vector transpose
$[]^H$	Vector conjugate transpose

List of Abbreviations

ADC	Analog to digital converter
AWGN	Additive white gaussian noise
CIR	Channel impulse response
CFO	Carrier frequency offset
CFOCE-C	CFO and channel estimation and correction
CFOSFOCE-C	CFO, SFO and channel estimation and correction
CP	Cyclic prefix
CRLB	Cramer Rao lower bound
CRLS	Conventional recursive least squares
DAB	Digital Audio Broadcasting
DLL	Delay-locked loop
FIM	Fisher information matrix
FIR	Finite impulse response
FFT	Fast fourier transform
ICI	Inter-carrier interference
IFFT	Inverse fast fourier transform
ISI	Inter-symbol interference
LMS	Least mean squares
LS	Least squares
MIMO	Multiple-input, multiple-output
MSD	Mean square deviation
MSE	Mean square error
MMSE	Minimum mean squared error
NLMS	Normalized least mean squares
NL-RLS	Non-linear recursive least squares
OFDM	Orthogonal frequency division multiplexing
RLS	Recursive least squares

RMS	Root mean square
RFO	Residual frequency offset
SISO	Single-input, single output
SCA	Schmidl and Cox algorithm
SC-OFDM	Synchronous coherent OFDM
SFO	Sampling frequency offset
VDSL	Very-high-bit-rate digital subscriber lines
WLAN	Wireless local area network

Chapter 1

Introduction

1.1 Synchronization and Channel Estimation for Burst Mode OFDM

Orthogonal frequency division multiplexing (OFDM) is used extensively in wireless communications. The division of the transmission band into smaller subbands using the FFT/IFFT results in a flexible transmission scheme that can achieve high transmission rates by adaptively allocating information based on channel characteristics. This makes OFDM particularly robust to multipath fading, and also avoids complex equalization in the receiver. However, the performance of OFDM is highly sensitive to frequency synchronization errors at the receiver.

Receiver synchronization errors in OFDM cause inter-symbol interference (ISI) and inter-carrier interference (ICI) which degrade system performance by destroying the orthogonality between OFDM subcarriers. These synchronization errors are caused by carrier frequency offset (CFO), sampling frequency offset (SFO), and symbol timing offset. Performance degradation as a result of ISI and ICI becomes increasingly significant in high signal-to-noise ratio (SNR). In addition, synchronization errors can also adversely affect the results of channel estimation at the receiver. Imperfect channel estimates will introduce errors in frequency domain equalization that is traditionally employed in OFDM systems, thus further adding to performance degradation.

Synchronization and channel estimation for burst mode systems have attracted much research interest. Burst mode systems that operate in a slow fading channel environment assume a quasi-static model for the channel. This simplifies receiver structure and performance evaluation, since there is no need to consider time varying channel characteristics. It also requires that the burst length remains short, and that channel estimation and synchronization is repeated for each burst. As a result, the overhead of any training data used for these purposes must be kept to a minimum.

Synchronization and channel estimation for burst mode systems is performed using a preamble sequence which precedes the data. The correlation properties of this preamble sequence ensure that initial coarse synchronization can be performed without prior knowledge of the channel or the need to demodulate the received data. Correlation-based coarse synchronization techniques are well documented and discussed in [1] [2] [3]. When coarse synchronization has been performed and a sufficiently accurate estimate of the location of each OFDM symbol is obtained, the known data in the preamble can be used to perform channel estimation.

Coarse synchronization, however, is not sufficient to remove enough ICI to ensure reliable data transmission. Residual frequency offsets remain and must be removed by a procedure of fine synchronization. To improve correlation-based synchronization, fine synchronization methods generally make use of the data in the preamble sequence [4] [5] [6]. Synchronization methods which independently correct the effect of each synchronization parameter have limited effectiveness because of the interdependence between these parameters. As a result, independent correction of one type of synchronization error will be impeded by the presence of other synchronization errors. Furthermore, channel estimates made following coarse synchronization will contain errors due to the presence of CFO, SFO, and timing errors in the received training data, thus further degrading the performance of data-aided fine synchronization. For this reason, there is an advantage in performing joint estimation of these parameters, as demonstrated in [7] [8] [9].

A joint algorithm that estimates all of the synchronization offsets, as well as the channel parameters, has not been documented. This is due to the fact that the model for the received signal that accounts for all these effects is non-linear in the estimated parameters and an estimator for these parameters would have too high a complexity to be practical in a burst mode system. Instead, the algorithms in [7] [8] [9] consider only two of the distortions in synchronization and channel estimation. To avoid a non-linear estimation problem, these joint estimation algorithms approximate the effect of CFO and SFO as linear phase distortion in the frequency domain. This ignores all ICI caused by the frequency offsets, and reduces the effectiveness of using a joint approach since a suboptimal estimator solution will be achieved. In addition, correction will also be made using the linear phase model, which adds additional error.

A significant improvement in system performance can be expected if a non-linear estimation technique with reasonably low complexity is employed in the joint estimation and compensation problem. A technique that considers the effect of ICI should give significant gains at high SNR.

1.2 Research Objectives and Contributions

The main objective of this research is to develop a joint synchronization and channel estimation scheme for burst mode OFDM. As a key contribution, the non-linear recursive least squares (NL-RLS) adaptive algorithm is applied into development of two methods for joint synchronization and channel estimation. The first method performs joint CFO and channel estimation and compensation, while the second performs joint CFO, SFO, timing and channel estimation and compensation. Use of a non-linear adaptive algorithm allows for modeling of the effects of synchronization errors without approximations, while an RLS-type algorithm gives fast convergence in order to minimize overhead in terms of preamble length. Since estimation in both cases is performed in the time domain, performance of channel estimation is superior, and the algorithms are robust enough to decision errors to allow for decision feedback operation with no need for pilot tones. An additional contribution of this research is the derivation of the Cramer Rao lower bound (CRLB) for both the problems of jointly estimating the CFO and channel impulse response (CIR) as well as jointly estimating the CFO, SFO, and CIR. Finally, some analysis of stability and steady-state performance is also made.

1.3 Thesis Outline

The remainder of this thesis is organized as follows.

Chapter 2 gives background theory related to synchronization and channel estimation relevant to the development of a joint synchronization and channel estimation algorithm for burst mode OFDM systems. Several synchronization and channel estimation techniques presented in the literature are outlined. This chapter also presents the NL-RLS algorithm for estimation of unknown parameters in a non-linear system.

Chapter 3 presents the joint CFO and channel estimation and compensation (CFOCE-C) algorithm and evaluates its performance. The CRLB for a joint estimator of the CFO and channel is also derived. The effect of SFO on the CFOCE-C algorithm is evaluated.

Chapter 4 derives a data model for the effect of SFO and presents the joint CFO, SFO and channel estimation and compensation (CFOSFOCE-C) algorithm and evaluates its performance. The CRLB for the joint estimator of the CFO, SFO, and channel is also derived.

Chapter 5 gives the conclusion and provides suggested topics for future related research.

Chapter 2

Basics of Channel Estimation and Synchronization for OFDM

The transmission benefits of OFDM depend highly on the availability of adequate synchronization at the receiver. Channel estimation is also important to ensure accurate equalization and removal of the effects of channel distortion. In this chapter, the background information pertaining to the joint synchronization and channel estimation algorithms derived in Chapters 3 and 4 is discussed. In Section 2.1, OFDM transmission is presented and the concept of orthogonality is explained. The differences between burst mode systems and continuous mode systems relevant to the problem of synchronization and channel estimation are also outlined. Section 2.2 explains the multipath fading channel, which is assumed throughout this thesis. In Section 2.3, synchronization and channel estimation in OFDM is presented. Analytical expressions for the effects of these distortion in both time and frequency domains are given where applicable. Existing algorithms for synchronization and channel estimation in the literature will be outlined and the concept of a joint estimator for these parameters will be introduced. The burst format that is assumed in the simulations performed in this thesis is presented in this section. In Section 2.4, the non-linear RLS algorithm is presented as a means for solving the joint estimation problem.

2.1 OFDM

OFDM is currently being used in wireless and wireline communications because of its high transmission rate capabilities. The properties of the FFT/IFFT and the use of a cyclic prefix allow equalization by the receiver in the presence of multipath fading to be performed in the frequency domain using only a single tap (coefficient). This equalization requires knowledge of the frequency response (magnitude and phase) of the channel at specific frequencies which represent the OFDM subcarrier frequencies. The issues of estimation and synchronization are addressed differently in burst mode and continuous mode systems. In the former, channel estimation and synchronization must be repeated before each burst, whereas in the later, they are performed once and, if necessary, the estimates are adapted during data transmission.

2.1.1 OFDM Basics

In OFDM, data is modulated using multiple subcarriers so that each subcarrier sees a smaller portion of the frequency band, and hence a relatively flat portion of the channel frequency response. Although in theory, an infinite number of carriers is required to ensure flat fading on each subchannel, use of a cyclic prefix achieves this using any finite value of N. As a result, OFDM is rather insensitive to frequency selective fading, and is also highly adaptive due to its ability to load different data rates onto each of its subcarriers.

In a traditional OFDM system, a maximum of N complex values $X_{k,l}$ are each taken from an M-QAM constellation and are modulated by performing an IFFT to generate the lth set of OFDM time domain samples. The nth sample is given by

$$x_{n,l} = \frac{1}{N}\sum_{k=0}^{N-1} X_{k,l} e^{j\frac{2\pi kn}{N}}. \tag{2.1}$$

At the receiver, the received data subcarriers $Y_{k,l}$ are orthogonal when each $Y_{k,l}$ is a function of only $X_{k,l}$, the channel, and some additive noise. To ensure that orthogonality is maintained after distortion by a channel with impulse response of length v samples, a cyclic prefix of length $N_g \geq v-1$ and consisting of the last N_g samples of the IFFT is prepended to the lth set of samples described in equation 2.1 resulting in the lth transmitted OFDM symbol $s_l = [x_{N-N_g,l}, \ldots, x_{N-1,l}, x_{0,l}, \ldots, x_{N-1,l}]$. For passband transmission systems, this signal is then modulated to the band of interest by a carrier frequency f. At the receiver, the signal is first converted to baseband, the cyclic prefix is discarded and demodulation is performed with the FFT operation.

The purpose of the cyclic prefix is two-fold. Firstly, it removes any ISI at the receiver caused by the channel, since all symbol dispersion distorts only the samples in the cyclic prefix. For this reason, the cyclic prefix is often referred to as a guard interval. The second function of the cyclic prefix is the avoidance of ICI and the preservation of orthogonality in the presence of a frequency selective fading channel. Given a CIR of $\boldsymbol{h} = [h_0, h_1, \ldots, h_{v-1}]$, prepending a cyclic prefix causes the vector-channel representation for transmission of a symbol to be expressed in terms of an $N \times N$ circulant matrix as

$$\begin{bmatrix} y_{N-1,l} \\ y_{N-2,l} \\ \cdot \\ \cdot \\ y_{1,l} \\ y_{0,l} \end{bmatrix} = \begin{bmatrix} h_0 & h_1 & \ldots & h_{v-1} & 0 & \ldots & 0 \\ 0 & h_0 & h_1 & \ldots & h_{v-1} & \ldots & 0 \\ \ldots & & \ldots & & \ldots & & \ldots \\ h_{v-1} & 0 & \ldots & 0 & h_1 & \ldots & h_{v-2} \\ h_{v-2} & h_{v-1} & 0 & \ldots & 0 & h_1 & \ldots \\ \ldots & & \ldots & & \ldots & & \ldots \\ h_1 & h_2 & \ldots & h_{v-1} & 0 & \ldots & h_0 \end{bmatrix}_{N \times N} \begin{bmatrix} x_{N-1,l} \\ x_{N-2,l} \\ \cdot \\ \cdot \\ x_{1,l} \\ x_{0,l} \end{bmatrix} + \begin{bmatrix} w_{N-1,l} \\ w_{N-2,l} \\ \cdot \\ \cdot \\ w_{1,l} \\ w_{0,l} \end{bmatrix}. \tag{2.2}$$

Since the eigenvalue decomposition of a circulant matrix is obtained through the FFT and IFFT matrices [10], the frequency domain equivalent for OFDM transmission consists of N parallel subchannels, each represented by

$$Y_{k,l} = X_{k,l} H_k + W_{k,l} \quad ; \quad k = 0, 1, \ldots, N-1 \tag{2.3}$$

where H_k is the kth element of the FFT of $\boldsymbol{h}$, and $W_{k,l}$ is an AWGN sample. Equalization is performed using a single complex multiplication on each subcarrier, and hence each subchannel can be viewed as an AWGN or flat fading channel, regardless of the fact that a finite value of N was used. A typical OFDM system and its parallel channel equivalent are shown in the figures below. The transmitted symbols are distorted by a multipath fading channel $\boldsymbol{h}$, and AWGN is added at the receiver. Perfect synchronization is assumed.

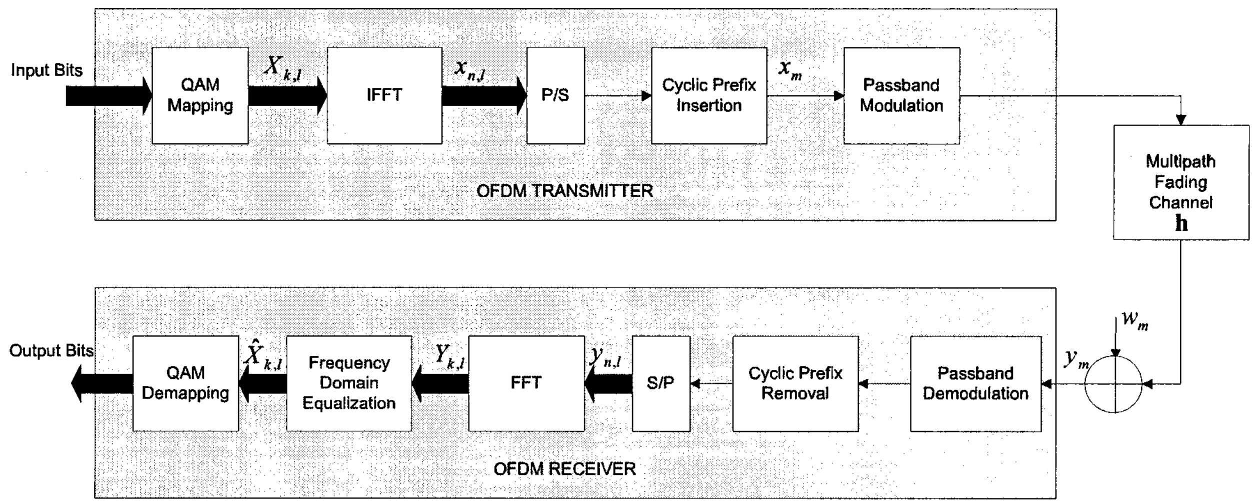

Fig. 2.1 Typical Passband OFDM System

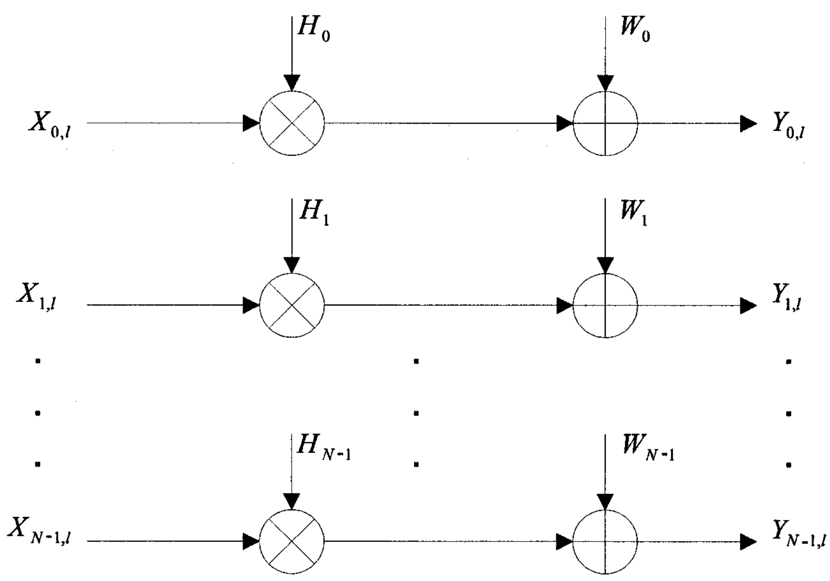

Fig. 2.2 Parallel Equivalent of OFDM System

2.1.2 Continuous Mode versus Burst Mode Transmission

OFDM systems can be divided into continuous mode systems and burst mode systems. Continuous mode systems first establish a link between the transmitter and receiver. Once a link is established, data transmission occurs in an uninterrupted fashion. Burst mode systems, on the other hand, transmit data in short packets or bursts, much like a traditional computer network. Each packet must be detected by the receiver for data demodulation to begin. Each burst will contain a portion of the overall data to be transmitted.

Continuous mode systems generally perform synchronization and channel estimation upon establishment of the link. In the case of mobile systems, channel information may be updated using periodically spaced training data. Blind estimation or decision-feedback estimation can also be employed. Synchronization is maintained using either training data or prefix-based estimation methods discussed in the next section. Typical continuous mode systems include Digital Audio Broadcasting (DAB) [11] and Very-high-bit-rate Digital Subscriber Lines (VDSL) [12].

Burst mode systems are more suitable for use in wireless networks. The channel and synchronization parameters are estimated from training data transmitted in the burst preamble. Properties of the channel, which are discussed in Section 2.2, require a small burst length. As a result, the choices of the synchronization and channel estimation methods are limited since the amount of training data becomes an important factor in the efficiency. Although minor adjustment of the estimates obtained using the preamble are sometimes made through the use of a small number of pilots distributed within the burst, insertion of these pilots further reduces data efficiency. Typical burst mode systems include HIPERLAN [13] and IEEE802.11a [14].

2.2 Time-Varying Multipath Channels

Signal transmission in wireless communications is affected by fading which can be caused by shadowing or multipath. Shadowing occurs when the signal is attenuated by an obstacle, while multipath is caused by multiple reflections of the transmitted signal reaching the receiver at different time instants. Because the effect of shadowing can be treated as an overall signal attenuation [15], only multipath is examined here.

In a multipath channel having obstacles creating signal reflections, each path traveled by the transmitted signal before it reaches the receiver can be associated with an attenuation and a delay. Changes in the surrounding environment cause these quantities to vary with time. As a result, the fading multipath channel is sometimes referred to as a double spread channel since the multiple delays will spread the transmitted signal in time, while the time varying characteristics of each path cause frequency spreading called Doppler spreading [16]. If it is further assumed that the propagation of the signal for different delays is uncorrelated, the time varying channel can be characterized by a two dimensional function called the scattering function $\mathcal{S}$ which measures the channel's power at a given delay and frequency offset. Further details concerning the scattering function are given in [16].

The Doppler spread of the channel B_d is the range of frequencies over which the time-averaged scattering function is non-zero. An important property of B_d is that it gives an indication of how rapidly the channel changes with time. A larger B_d indicates that the channel changes more rapidly, thus causing more frequency spreading. Channels are characterized as fast-fading when the Doppler spread is large compared to the signal bandwidth or slow-fading when the Doppler spread is small compared to the signal bandwidth [16].

The coherence bandwidth of the channel B_c is defined as the reciprocal of the time range over which the frequency-averaged scattering function is non-zero. When the bandwidth of the signal is larger than the coherence bandwidth, the transmitted signal undergoes a different attenuation at different frequency, thus exhibiting frequency-selective fading. Furthermore, the multipath components can be resolved from the received signal, so that the multipath channel can be characterized at the complex baseband as a linear time-varying system with CIR given by [17]

$$h(t;\tau) = \sum_{i=1}^{F} \alpha_i(t)\delta(\tau - \tau_i(t)) \tag{2.4}$$

where $\alpha_i(t)$ and $\tau_i(t)$ are the time varying complex attenuation and time varying delay of the ith path respectively. In burst mode systems, we can further assume, for purposes of receiver design, that the CIR does not changes within a burst and that α and τ_i are constant, randomly generated quantities. This can be assumed if the channel is slow fading. A FIR model for the channel in the digital domain can easily be obtained from Equation 2.4 and the sampling period of the received signal. Unless stated otherwise, the remainder of this thesis assumes a frequency selective slow-fading channel model.

2.3 Synchronization and Channel Estimation

The performance of the one tap equalizer in OFDM depends on the quality of channel estimation. Furthermore, synchronization must be performed prior to decoding in order for orthogonality to be maintained and for the full benefit of OFDM to be obtained. Synchronization errors in the receiver generally result in ICI which degrades the system performance.

2.3.1 Channel Estimation

Channel estimation can take place in the frequency domain (after the FFT at the receiver) or the time domain (prior to the FFT in the receiver). Frequency domain channel estimation is generally preferred because the parallel subchannel model described in Section 2.1.1 allows for a much simpler estimation on a subcarrier by subcarrier basis. The simplest and most common preamble-based channel estimation method use least-squares (LS) estimation based on S training symbols. The estimate of the channel frequency response in this case is

$$\widehat{H}_k = \sum_{l=0}^{S-1} \frac{Y_{k,l}}{\bar{X}_{k,l}} \tag{2.5}$$

where $\bar{X}_{k,l}$ is the complex element transmitted on the kth subcarrier of the lth training symbol.

For long bursts in which the channel can no longer be considered invariant over the burst, pilot tones are used to update the channel estimates. Studies of the various pilot organization and channel tracking methods are included in [18] [19] [20].

In time domain channel estimation, the CIR is estimated instead, and the FFT is used to obtain the channel frequency response required by the equalizer. The advantage of a time domain approach is the reduction in the number of parameters to be estimated. Since $v \ll N$, better performance is expected from a time domain estimator as opposed to a frequency domain estimator. Time domain channel estimation is discussed in [21] [22].

2.3.2 Symbol Timing Offsets

In burst mode transmission, symbol frame synchronization is required at the beginning of each burst. This requires a simple yet efficient method of detecting the start of a frame which has low overhead in terms of preamble or training symbols.

Symbol timing synchronization refers to estimating the correct position of the FFT window within the received set of samples. Timing is traditionally performed in two stages: a coarse synchronization which uses the auto-correlation properties of the preamble to detect the burst, and a fine synchronization which uses the cross-correlation of the received packet with a known training sequence [23]. This training sequence can be in time domain if the synchronization is done prior to any demodulation, or it can be in frequency domain if post-FFT synchronization is performed. The training data can be concentrated in a preamble, or dispersed into the data symbols as pilot subcarriers.

Despite two stages of symbol synchronization, timing offsets of several samples are still common [8]. These residual timing offsets can be accounted for in the estimate of the channel frequency response under certain conditions to be discussed in what follows.

Consider a symbol offset of ζ samples between the actual OFDM symbols and the estimated FFT window location. The effects of any frequency offsets are ignored for the moment. A negative value of the symbol offset signifies that the chosen FFT window is ζ samples early with respect to its actual position, while a positive value signifies that the chosen window is late. In the case where $-(N_g - v) \leq \zeta < 0$, with v being the length of the CIR, the FFT window selected for decoding contains all of the samples in the actual OFDM symbol in a circularly rotated order. Furthermore, due to the condition $N_g \geq v - 1$, ISI is avoided. By simple Fourier Transform properties, the received frequency domain samples after performing the FFT can be expressed as [6]

$$Y_{k,l} = X_{k,l} H_k e^{j\frac{2\pi\zeta k}{N}} + W_{k,l}. \tag{2.6}$$

In this first case, which is illustrated in Figure 2.3, orthogonality is maintained due to the presence of the cyclic prefix. The exponential term of Equation 2.6 can be incorporated into the estimated channel frequency response, resulting in the same error performance as would be expected for a case where $\zeta = 0$. In the time domain, the CIR is modified by insertion of ζ leading zeros. The only requirement to ensure that imperfect sampling results in received frequency domain samples given by Equation 2.6 and that the error performance is the same as for $\zeta = 0$ is for the effective CIR after insertion of ζ leading zeros to remain shorter than the cyclic prefix. Since the symbol offset is generally one or two samples, this requirement can be assumed to be satisfied [24].

On the other hand, if $\zeta > 0$, samples of the current OFDM symbol are lost and replaced with samples in the cyclic prefix of the following symbol, resulting in ISI as illustrated in Figure 2.4. This ISI induces a loss of orthogonality, or ICI. Both ISI and ICI appear in the expression for the received frequency domain samples, making this situation undesirable. In [6], this expression is given under the assumption of an AWGN channel as:

$$\begin{aligned} Y_{k,l} &= \frac{N-\zeta}{N} X_{k,l} e^{j\frac{2\pi\zeta k}{N}} + \frac{1}{N}\sum_{i=0}^{N-1} X_{i,l} \sum_{n=0}^{N-\zeta-1} e^{j2\pi\frac{i(n+\zeta)-nk}{N}} \\ &+ \frac{1}{N}\sum_{i=0}^{N-1} X_{k,l+1} \sum_{n=N-\zeta}^{N-1} e^{j2\pi\frac{i(n+\zeta-P)-nk}{N}} + W_{k,l} \end{aligned} \tag{2.7}$$

The case where $\zeta < -(N_g - v)$ will also have a form similar to Equation 2.7 and ISI will be incurred from the previous symbol instead. These results show that beginning the FFT window in the region $-(N_g - v) \leq \zeta \leq 0$ is equivalent, performance-wise, to having perfect symbol synchronization. This zone is known as the ISI-free portion of the cyclic prefix. This freedom in the choice of FFT window yields a set of multiple solutions to the joint channel and timing problem.

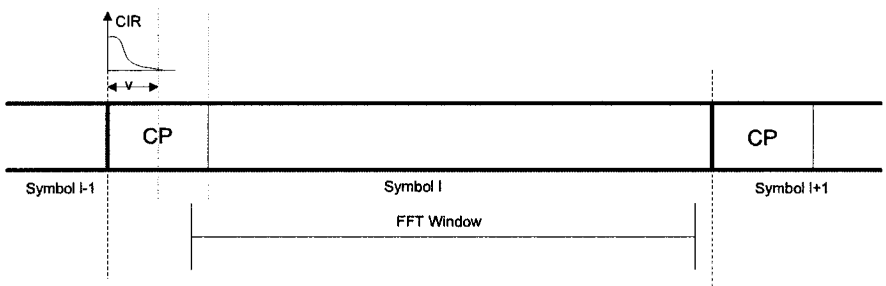

Fig. 2.3 FFT Window Location for no ISI

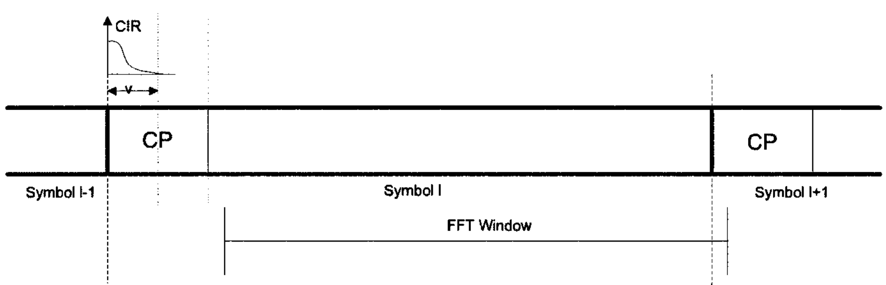

Fig. 2.4 FFT Window Location for ISI and ICI

Symbol synchronization is treated in [6] [8] [3] [25] [2]. In [2], symbol synchronization and CFO estimation are combined in an algorithm that exploits the use of two repeated time domain symbols. The correlation between the two symbols is used to detect the optimum FFT window location, and the change in phase between them is attributed to the CFO. The performance of this algorithm is improved in [6] using an iterative correction algorithm which is considerably expensive and ignores the effect of channel and other synchronization issues. The method of [3] generalizes symbol synchronization to variable preamble length. It also ignores channel and other synchronization issues. In

[25], a robust timing recovery scheme which also accounts for sampling frequency offsets is presented. Here, the effect of CFO is ignored. The author of [25] also distinguishes between guard-interval based techniques and pilot-based techniques for symbol synchronization. While guard interval based techniques do not require pilot carriers, they are based on autocorrelation and are hence less accurate. Pilot based techniques achieve a more accurate offset estimate but require an FFT window that already lies within the ISI-free portion of the cyclic prefix. For these reasons, guard interval based techniques are used for coarse symbol synchronization while pilot based techniques are used for fine symbol timing synchronization.

2.3.3 Carrier Frequency Offsets

A CFO occurs when the carrier frequencies of the passband modulated OFDM signal and the oscillator of the downconverter do not match exactly. This mismatch is attributed to either clock jitter or Doppler frequency shift caused by the channel [25]. Given an offset of Δf hertz caused by clock jitter only, the time domain effect of a CFO in the continuous and sampled domains is given by

$$\begin{aligned} y(t) &= e^{j2\pi\Delta f t}x(t) \\ y_n &= e^{j\frac{2\pi\epsilon n}{N}}x_n \end{aligned} \tag{2.8}$$

respectively, where x represents the useful signal before upconversion, y is the resulting signal after downconversion, $\epsilon = \Delta f/\Delta f_s$ is the relative CFO, and Δf_s is the intercarrier spacing. Equation 2.8 does not include the multipath fading channel. The effect of the channel in the analysis of CFO is generally ignored, as was noted in [26].

Doppler frequency shift occurs when there is a relative motion between the transmitter and receiver in a wireless system. The frequency range over which the shift occurs is the Doppler spread. In slow-moving mobile systems where burst-mode transmission is generally employed, the Doppler spread is generally small enough that the effect of Doppler frequency shift can be ignored. In most methods of CFO estimation for slow-moving mobile systems, the Doppler frequency spread is ignored. Some methods such as [24] use pilot tones to adjust for changes in the CFO. The use of pilot symbols reduces data efficiency and is limited in that it ignores any changes in channel and SFO.

For longer bursts, the effect of a Doppler frequency shift can be adequately modeled by either a time varying CIR or a time varying CFO. Use of a time varying CIR in modeling can improve the representation of the CFO in situations where the CFO changes significantly over one OFDM symbol interval. The use of an adaptive algorithm to estimate the CIR is therefore advantageous in this case of slow-moving mobile channels as well.

The time domain rotation in Equation 2.8 results in a frequency domain shift of the carriers relative to the frequency sampling point, as shown in Figure 2.5. Due to this shift, the modulated OFDM carriers will not be recovered at their peaks by FFT demodulation resulting in a loss of orthogonality. This loss of orthogonality results in an attenuation and phase rotation of the transmitted constellation as well as ICI caused by the sidelobes of other subcarriers. These effects are quantified in the expression for the received post-FFT samples [1]

$$Y_{k,l} = X_{k,l}H_k \frac{sin\pi\epsilon}{Nsin(\pi\epsilon/N)} e^{j\pi\epsilon(N-1)/N} + I_{k,l} + W_{k,l} \tag{2.9}$$

where the ICI term is given by

$$I_{k,l} = \sum_{l=0;l\neq k}^{N-1} X_l H_l \frac{sin(\pi(l+\epsilon-k))}{Nsin(\pi(l+\epsilon-k)/N)} e^{j\pi(l+\epsilon-k)(N-1)/N}. \tag{2.10}$$

The effect of CFO on the OFDM frequency spectrum and the system BER is studied in more detail in [27].

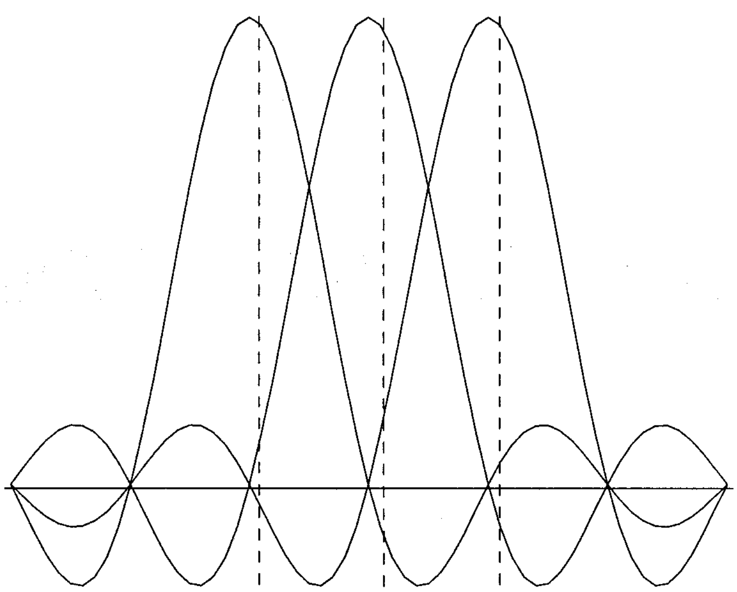

Fig. 2.5 Partial Plot of OFDM Symbol Spectrum

As was pointed out in [23] the frequency offset may be larger than the subcarrier spacing, resulting in an integer and fractional CFO. Integer offsets are best estimated by post-FFT methods, however, these methods tend to be adversely affected by ICI because they ignore its effect in order to simplify the expression in Equation 2.9. This is the case in the methods of [28] [29] [7].

A CFO correction algorithm capable of estimating both integer and fractional offsets was first presented in [1]. This technique employs the repetition of two identical OFDM symbols in the time domain, which allows for post-FFT CFO estimation even when ICI inhibits data demodulation. The effect of ISI discussed in Section 2.3.2 is, however, ignored and adequate removal of residual frequency offset requires several repetitions of the training symbol, resulting in a large preamble sequence and reduced packet efficiency. To remedy these issues, a synchronization method known as the Schmidl and Cox algorithm (SCA) is presented in [2] which addresses both timing and CFO. In [4], it is shown that the SCA can result in residual frequency offsets (RFO) which are large enough to cause a significant number of errors under certain conditions. A method of refining the estimates of the SCA is proposed which allows for reduction in the required preamble length. This method is, however, frequency domain based and ignores ICI caused by the RFO. It also assumes that phase differences between subsequent time-domain OFDM symbols are cause only by the RFO, thus ignoring the effects of a time-varying channel and possible SFO. The methods in [28] [29] [7] [30] are also frequency domain-based and ignore the effect of ICI. The effects of channel and SFO are also ignored in their analysis and simulations.

Based on the discussion in this section and Section 2.3.2, a method of estimating the residual timing and CFO to be used after the SCA can be beneficial to the performance of a burst-mode OFDM system. Combining this estimation with the estimation of the CIR removes the estimation error that would be incurred by ignoring the effects of the channel. It can also remove the need for several iterative steps of each estimation that may be required to achieve a certain estimator performance. Furthermore, if the estimation method is adaptive, small Doppler frequency shifts characteristic of slow-moving mobile systems with long burst durations can be accounted for. An estimation and correction method which addresses each of these issues is presented in Chapter 3.

2.3.4 Sampling Frequency Offsets

A SFO is caused by jitter in the receiver's sampling oscillator. Its effect is more difficult to quantify analytically because it must be coupled with the effect of clock drift which limits the use of a simple expression of the form of Equation 2.8 for CFO. Clock drift refers to the discrepancy between the transmit and receive symbol periods which causes a movement of the receiver's FFT window with respect to the actual data transmitted. As time progresses, the window may move out of the ISI-free region of the cyclic prefix discussed in Section 2.3.2. For this reason, SFO and symbol timing offsets are very closely related. This close relationship was exploited in the synchronization techniques discussed in [30] [25] [3] [7].

Given a relative sampling frequency offset of $\eta = \Delta T/T$ where ΔT is the difference in the sampling period between transmitter and receiver, and T is the actual sampling period, an expression for the received frequency domain samples in an AWGN channel distorted by a SFO was given in [5] as:

$$\begin{aligned} Y_{k,l} &= e^{-j\pi\frac{N-1}{N}\eta k}\frac{sin(\pi k\eta)}{Nsin(\pi k\eta/N)}X_{k,l} + W_{k,l} \\ &+\frac{1}{N}\sum_{i=0;i\neq k}^{N-1} X_{i,l}\frac{sin(\pi i\eta)}{sin\left[\frac{\pi}{N}\left[i(1+\eta)-k\right]\right]}e^{j\pi i\eta\frac{N-1}{N}}e^{-j\frac{\pi}{N}(i-k)}. \end{aligned} \tag{2.11}$$

This equation assumes sampling in the ISI-free portion of the cyclic prefix and ignores the phenomenon of clock drift. It also assumes perfect sampling phase synchronization at the start of each FFT window and so does not represent the effect on two consecutive OFDM symbols. Despite these restrictions, it is evident that, much like the case of CFO, SFO causes ICI in the received frequency domain samples. As in Equation 2.9, the received subcarrier undergoes an attenuation and phase rotation. In the case of SFO however, these effects are frequency dependent rather than fixed for every carrier.

The similarity in the frequency domain effect of CFO and SFO is exploited by many SFO estimation techniques. As in the case of CFO, these techniques are generally frequency domain based, and hence ignore the effect of ICI. The SFO estimation technique presented in [5] uses a preamble based technique but considers only the phase rotation caused by the SFO between subsequent repetitions of the training symbol in the preamble. Here, the effects of attenuation and ICI as well as the effects of the channel are ignored in the derivation. The same can be said about the technique in [3] which ignores any CFO and again uses the phase difference between training symbols in the preamble.

An expression showing the effect of SFO which is not restricted to only one OFDM symbol can be obtained if the received samples are modeled in time domain. Assuming an AWGN channel with ISI-free timing synchronization, this expression was given in [7] as

$$y_{n,l} = \frac{1}{N} \sum_{k=0}^{N-1} X_{k,l} e^{j\frac{2\pi k\eta}{N}(lN_s+N_g+n)} e^{j\frac{2\pi kn}{N}} + w_{n,l} \tag{2.12}$$

where $y_{n,l}$ is the received time domain data sample corresponding to symbol l and sample n of the chosen FFT window, N_s is the OFDM symbol length including the cyclic prefix. Equation 2.12 shows that, until the time when clock drift requires us to consider ISI, a SFO can be characterized by a linearly increasing phase rotation of the data transmitted on each subcarrier. This increase can also be used to explain the loss of orthogonality caused by a SFO, since the phase rotation changes within a single OFDM symbol. This linear relationship is exploited in [25] in which a DLL-based approach using early and late correlation values is used to track the SFO. In [7], the loss of orthogonality incurred by applying an FFT to Equation 2.12 is ignored in order to structure the problem as a linear problem to be able to apply the LS estimation method. A compensation scheme is not discussed.

2.3.5 Typical Burst Mode Preamble Structure for Synchronization and Channel Estimation

Figure 2.6 below shows a typical preamble which can be used for burst mode synchronization and channel estimation. This preamble is assumed in the simulations used to derive the results contained in later chapters of this thesis, and is exactly the structure of the burst used in the IEEE802.11a WLAN standard [14]

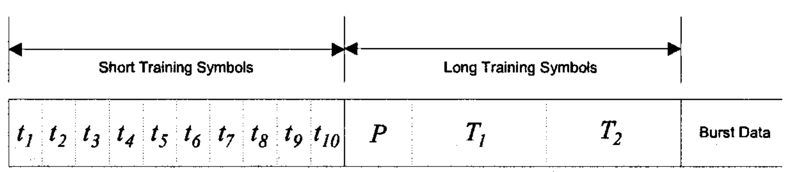

Fig. 2.6 Typical Preamble Structure

The short training symbols are each 16 samples long and identical to eachother. The long training symbols are each 64 samples long and also identical. A cyclic prefix (P) of 32 samples is added to enable demodulation of the long training symbols via the FFT.

The 16 sample and 64 sample sequences are designed in such a way that the correlation between subsequent samples is minimal. This is to ensure that the performance of correlation based synchronization methods described in the previous section is optimum.

The short training symbols are meant for coarse timing synchronization and coarse CFO estimation by means of the SCA algorithm in [2]. The long training sequence is meant for channel estimation and fine synchronization. The joint synchronization and channel estimation algorithms presented in this thesis will make use of the long training sequence, and will have an initial FFT window estimated from the SCA algorithm. The FFT window will be advanced by two samples following the SCA algorithm. This is sufficient to ensure an FFT window that is within the ISI-free portion of the cyclic prefix even at low SNR [24]. The CFO at the beginning of the long training sequence will be set manually.

The data portion of the burst contains OFDM symbols of $N_s = 80$ samples with $N_g = 16$ samples and an FFT size of 64. Only 52 of the carriers are loaded with data, and the other carriers are zeroed to form a frequency domain guard band. The organization of these carriers is based on [14]. Contrary to the IEEE802.11a standard which calls for the use of pilot subcarriers for channel and frequency offset tracking, these subcarriers are used for data in the algorithms introduced in this thesis since a decision directed approach is used instead.

2.3.6 Joint Estimation of Synchronization and Channel Parameters

It should be noted from the above discussion that complete synchronization requires several iterations between coarse and fine steps for each synchronization parameter because estimation of each parameter or correction of each distortion is limited by the presence of another distortion. Such an iterative procedure may represent too much overhead for a practical system, particularly when fine synchronization is considered.

In fine synchronization, a joint technique is desirable because considering the interrelation between variables in an optimization problem generally allows us to arrive at the solution with less overhead than an iterative approach. In our case, overhead could be computation resources, hardware resources, or data overhead in terms of preamble length or number of training pilots. A joint technique also improves performance because performance bounds which may be created by error propagation between iterations of a certain technique may be lifted by considering the joint effect of all the parameters at once. Finally, it is much simpler to derive an adaptive estimation algorithm when the technique employed considers the joint effect of most or all of the parameters to be estimated. An adaptive scheme is important in synchronization of burst mode systems because of the possibility of a non-negligible Doppler spread or a CIR which varies over the duration of a burst. Temperature variations may also affect the frequency offset parameters, especially for long bursts, which are desirable to improve data efficiency and ease the task of network layer protocols build on top of the burst.

The importance of jointly estimating synchronization and channel parameters has been realized of late. In [8] symbol timing and channel estimation is considered jointly in order to reduce the number of leading zeros in the impulse response and improve the estimate of the CIR. A pilot based scheme for joint symbol timing and SFO estimation is proposed in [3] which relates the phase difference between pilot subcarriers to both timing offset and SFO. CFO and SFO are considered jointly in [7]. Here, a LS estimation problem is derived by considering the phase rotation for a given frequency between two adjacent symbols. By examining Equations 2.9 and 2.11 this phase rotation can be jointly attributed to both CFO and SFO. Finally, in [9], the channel frequency response and the CFO is estimated jointly by a decision feedback two-dimensional NLMS tracking algorithm which treats the effect of CFO as a phase rotation of the received frequency domain sample with respect to the closest constellation point.

The difficulty which arises in estimation of any synchronization parameter by relating it to frequency domain rotation, whether this rotation is with respect to pilot carriers, decision symbols, or between carriers different carriers, is that the effect of ICI is ignored, and the estimation is suboptimal. Whereas a time domain model of the CFO and SFO would be more exact, such a model is non-linear and is avoided by joint synchronization methods in the literature. An alternative to ignoring the ICI would be to linearize the model used for estimation. If this technique is combined with an adaptive algorithm, the error incurred by linearization can be expected to disappear as the exact solution is approached.

2.4 The NL-RLS Adaptive Algorithm

The NL-RLS algorithm was first used in [31] for amplitude and delay estimation in CDMA systems. The derivation of the algorithm is reproduced here for the sake of completeness as well as to present a more general framework for non-linear estimation problems.

2.4.1 Estimation Error Linearization

The framework presented in this section considers adaptive non-linear estimation problems where the scalar estimation error at each time instant n can be expressed as

$$e_m = y_m - f(\boldsymbol{x}_m, \widehat{\boldsymbol{w}}_m), \tag{2.13}$$

where $\boldsymbol{x}_m$ is the system input vector at iteration m, $\widehat{\boldsymbol{w}}_m$ is the estimate of the unknown coefficient vector, $f()$ is a known non-linear function of $\boldsymbol{x}_m$ and $\widehat{\boldsymbol{w}}_m$ which best characterizes the system, and y_m is the observed noisy system output. In the case of a communication system, the system input vector $\boldsymbol{x}_m$ is obtained from either a training sequence or from demodulator decision feedback. The length of $\boldsymbol{x}_m$ will depend on the non-linear system $f()$ in question. The system will also determine what relationship, if any, exists between the vectors $\boldsymbol{x}_m$ and $\boldsymbol{x}_{m-1}$. For the remainder of this discussion, the elements of $\boldsymbol{x}_m$ will be assumed to come from the same input signal, namely $\boldsymbol{x}_m = \left[x_m, x_{m-1}, \ldots, x_{m-(\mathcal{M}-1)}\right]^T$.

Non-linear estimation techniques that minimize the error of Equation 2.13 in some sense have been explored in [32] [33] [34], however the complexity of such techniques limits their use in practice. The approach used in this thesis applies Taylor series approximation to convert the non-linear estimation problem characterized by the error in 2.13 into an approximate linear problem. This is done by expanding $f()$ into its Taylor series about the estimate of the system parameters at iteration $m-1$ and ignoring non-linear terms to obtain an approximate estimation error of

$$\begin{aligned} e_m &\approx y_m - \left\{f(\boldsymbol{x}_m, \widehat{\boldsymbol{w}}_{m-1}) + \boldsymbol{\nabla} f(\boldsymbol{x}_m, \widehat{\boldsymbol{w}}_{m-1})^T(\widehat{\boldsymbol{w}}_m - \widehat{\boldsymbol{w}}_{m-1})\right\} \\ &\approx \left\{y_m - f(\boldsymbol{x}_m, \widehat{\boldsymbol{w}}_{m-1}) + (\widehat{\boldsymbol{w}}^*_{m-1})^H \boldsymbol{\nabla} f(\boldsymbol{x}_m, \widehat{\boldsymbol{w}}_{m-1})\right\} - (\widehat{\boldsymbol{w}}^*_m)^H \boldsymbol{\nabla} f(\boldsymbol{x}_m, \widehat{\boldsymbol{w}}_{m-1}) \end{aligned} \tag{2.14}$$

where $\boldsymbol{\nabla} f(\boldsymbol{x}_m, \widehat{\boldsymbol{w}}_{m-1})$ is the gradient vector of the non-linear function with respect to the parameter vector $\widehat{\boldsymbol{w}}_{m-1}$. Equation 2.14 is of the form

$$\widetilde{e}_m = \widetilde{y}_m - \widehat{\boldsymbol{c}}_m^H \widetilde{\boldsymbol{x}}_m \tag{2.15}$$

with

$$\widetilde{y}_m \equiv y_m - f(\boldsymbol{x}_m, \widehat{\boldsymbol{w}}_{m-1}) + (\widehat{\boldsymbol{w}}^*_{m-1})^H \boldsymbol{\nabla} f(\boldsymbol{x}_m, \widehat{\boldsymbol{w}}_{m-1}) \tag{2.16}$$

$$\widetilde{\boldsymbol{x}}_m \equiv \boldsymbol{\nabla} f\left(\boldsymbol{x}_m, \widehat{\boldsymbol{w}}_{m-1}\right) \tag{2.17}$$

$$\widehat{\boldsymbol{c}}_m \equiv \widehat{\boldsymbol{w}}^*_m \tag{2.18}$$

Equation 2.15 is the error expression for the traditional finite impulse response (FIR) system estimation problem described in [35]. Provided $f()$ for the system is known and its gradient can be computed, linear estimation techniques can be applied to this equation to estimate or track the system parameters.

The figures below illustrate the difference between traditional adaptive linear estimation and adaptive non-linear estimation using Equations 2.15 to 2.18.

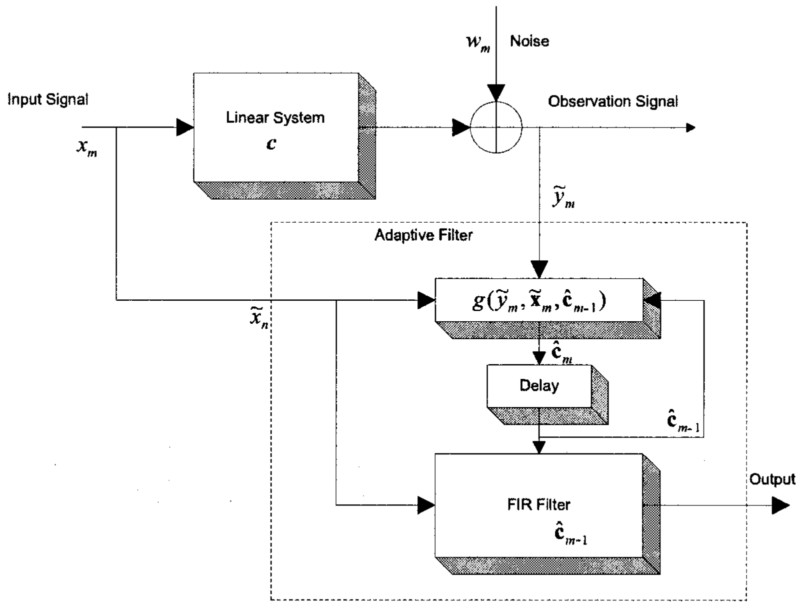

Fig. 2.7 Adaptive Linear Estimator

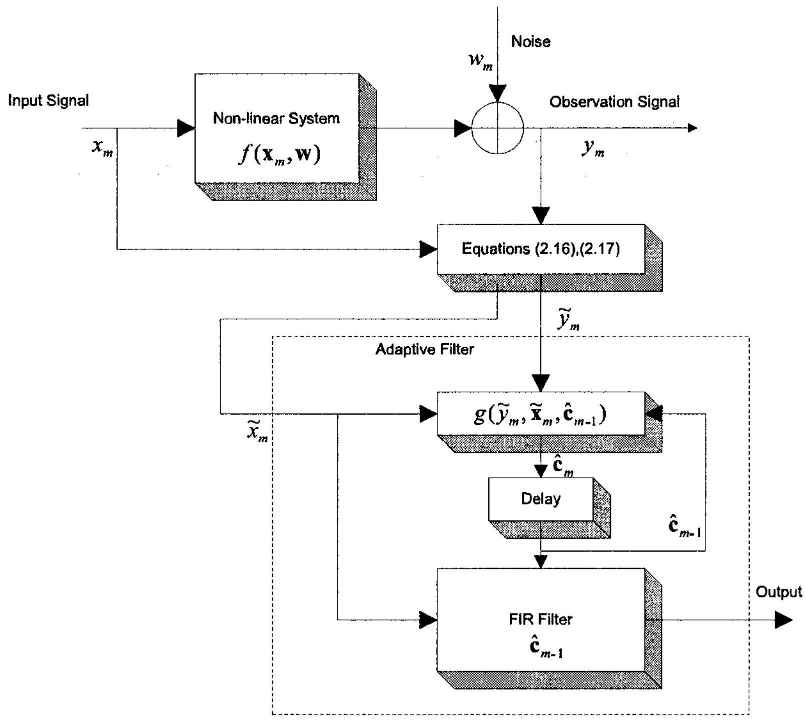

Fig. 2.8 Adaptive Non-Linear Estimator

The outputs of both FIR filters can be estimates of the input signal (detection), the desired signal (prediction), or the system parameters (system identification) depending on the application. In Figure 2.7 the adaptive filter has access to the noisy system output as observation, as well as the system input. The weight update function $g()$ computes the coefficients of the FIR filter $\widehat{\boldsymbol{c}}_m$ from the values of $\widetilde{\boldsymbol{x}}_m$, $\widetilde{y}_m$, and $\widehat{\boldsymbol{c}}_{m-1}$. This function is chosen based on the cost function to be minimized and hence on the algorithm used (LMS, RLS, etc).

In Figure 2.8 the same weight update function is used, with the inputs to $g()$ given by Equations 2.16 and 2.17. The algorithm illustrated in the figures is a-priori type since the computed coefficient vector is only used in filtering at the subsequent iteration. Derivation of an aposteriori type version of the algorithm is possible but is omitted here for the sake of simplicity.

2.4.2 The NL-RLS

The NL-RLS algorithm is obtained by using the conventional RLS (CRLS) of [35] as the update function $g()$. The algorithm is described in Table 2.1. In the remainder of this thesis, the variable $\widehat{\boldsymbol{w}}$ is referred to as the coefficient vector although its conjugate is the actual coefficient vector used in the traditional FIR filter notation, as shown in the table.

Initialization
$\widehat{\boldsymbol{c}}_{-1} = 0;\ \boldsymbol{P}_{-1} = \delta^{-1}\boldsymbol{I}$ $\delta =$ small positive constant
Adaptation gain computation
$\bar{\boldsymbol{g}}_m = \frac{1}{\lambda}\boldsymbol{P}_{m-1}\boldsymbol{\nabla} f(\boldsymbol{x}_m, \widehat{\boldsymbol{w}}_{m-1})$ $\bar{\kappa}_m = 1 + \bar{\boldsymbol{g}}_m^H \boldsymbol{\nabla} f(\boldsymbol{x}_m, \widehat{\boldsymbol{w}}_{m-1})$ $\boldsymbol{g}_m = \frac{1}{\bar{\kappa}_m}\bar{\boldsymbol{g}}_m$ $\boldsymbol{P}_m = \frac{1}{\lambda}\boldsymbol{P}_{m-1} - \boldsymbol{g}_m\bar{\boldsymbol{g}}_m^H$
Filtering
$e_m = y_m - f(\boldsymbol{x}_m, \widehat{\boldsymbol{w}}_{m-1})$ $\widehat{\boldsymbol{c}}_m = \widehat{\boldsymbol{c}}_{m-1} + \boldsymbol{g}_m e_m^*$ $\widehat{\boldsymbol{w}}_m = \widehat{\boldsymbol{c}}_m^*$

Table 2.1 NL-RLS Algorithm

2.4.3 Stability and Steady-State Performance

One of the strengths of the RLS is that, under the assumptions of a stationary environment and time-invariant optimum weight coefficient, the algorithm is stable regardless of the eigenvalue spread of the input vector correlation matrix [35]. This stability, in terms of convergence in the mean square, is proven mathematically in [36].

The effective input vector of the NL-RLS is given by Equation 2.17, and is dependent on the coefficient vector. The stability of the NL-RLS algorithm will therefore depend on the initial guess. The dependence of the input vector on the current coefficient vector also makes the derivation of a condition on stability very involved. In general, as the number of parameters being estimated increases, the condition on the initial guess required for stability becomes more restrictive, as the algorithm has more degrees of freedom in this case. The complex dependence of stability on the initial guess makes simulation-based stability analysis preferable.

Mean convergence of the CRLS is guaranteed for $\lambda = 1$ as soon as the number of samples exceeds the number of filter taps used [35]. For $\lambda < 1$ mean convergence is achieved only asymptotically. As a result, a CRLS estimator will have a bias in its estimate, which disappears only when steady-state is reached. This bias can affect the stability of the NL-RLS when it is used with $\lambda < 1$. For this reason, a forgetting factor as close to 1 as possible is required when using the NL-RLS in practice. Simulation results will be used to illustrate the behavior of the NL-RLS when applied to the joint estimation problem when the forgetting factor is not sufficiently close to 1.

In the steady-state, the CRLS has an excess mean square error (MSE), defined as

$$\mathcal{P}_{ex}(\infty) = E\left\{\left|y_\infty - \widehat{\boldsymbol{c}}_\infty^H \boldsymbol{x}_\infty\right|^2\right\} - \mathcal{P}_0, \tag{2.19}$$

that decreases as λ approaches 1 [35]. In Equation 2.19, $\mathcal{P}_O$ is the MSE when the optimum weight coefficients are used in estimating y. For $\lambda = 1$, the steady-state excess MSE is zero. In the case of the NL-RLS, the steady-state MSE cannot be assumed to be zero. Again, this is because of the dependence between the effective input vector and the weight coefficient that is introduced by the NL-RLS and which changes the steady-state analysis.

2.5 Chapter Summary

In this chapter, the OFDM burst mode synchronization and channel estimation problem was presented in detail. Based on the discussions, synchronization and channel estimation schemes for burst mode OFDM were shown to require low complexity, low training overhead, and good accuracy. As a result, a joint estimator for the problem becomes an attractive solution. To make such an estimator practical, the non-linearity in the joint signal model must be removed and an estimator with a low processing delay must be chosen. For these reasons, an adaptive non-linear estimator is chosen. The basic framework for this estimator in terms of the non-linear model of the received samples was derived. The CRLS was chosen as the weight update function to take advantage of its fast convergence. Using the NL-RLS, a joint synchronization and channel estimation algorithm can be derived in several ways.

Chapter 3

The Joint CFOCE-C Algorithm

Joint estimation of the CFO and channel parameters can be made to fit nicely into the framework of the NL-RLS of Section 2.4. In this chapter, a NL-RLS-based joint CFOCE-C algorithm that ignores the effect of SFO between the transmitter and receiver is presented. Some example applications where no SFO is present, or where the CFOCE-C algorithm could be applied in the presence of a SFO are presented in Section 3.1. The algorithm itself is derived in Section 3.2 by following a set of criteria that are expected to yield the best performance. These criteria are selected using the background presented in Chapter 2. In Section 3.3, the performance of the estimator, measured in terms of estimator variance as compared to the CRLB, is evaluated. Also, using the frame structure discussed in Section 2.3.5 the BER performance of the CFOCE-C is shown to be superior to two alternative methods of channel estimation and CFO correction. Finally, in Section 3.4, the stability and steady-state behavior of the estimator is analyzed in order to determine the allowable range of CFO over which the CFOCE-C shows the obtained BER improvement.

3.1 Applications of a Joint CFOCE-C Algorithm

Despite not treating the effects of SFO, an algorithm that jointly estimates and compensates for CFO and channel distortions may have a wide range of applications. Firstly, it can be used in systems where the SFO is negligible. In some burst mode systems, the burst may be short enough that the ICI caused by a SFO can be ignored. In this case, a simplified version of Equation 2.11 can be used for estimation and compensation. Pilot subcarriers, or the cyclic prefix correlation-based method can be employed in this case. The algorithm can also be employed in a system which already contains a SFO and symbol synchronization. As mentioned in Section 2.3, algorithms that perform this joint synchronization are common and quite advanced. The method presented in [25] itself, for instance, is used in many hardware implementations due to its robustness. Finally, to support high data rates, many systems proposed of late make use of cell synchronization where the base station and each of the mobiles derive their sampling clocks from the same source. One such system, the SC-OFDM system, is proposed in [37]. The joint CFOCE-C would prove useful in such systems to correct CFO and estimate the channel with low training overhead.

3.2 Derivation of the Estimator

Equation 2.13 gives a very general framework for a non-linear estimator in terms of observation samples, input samples, and the unknown coefficient vector being estimated. When applied to the problem of jointly estimating the CFO and channel, much leeway exists in the choice of y_n, $\boldsymbol{x}_n$ and $\widehat{\boldsymbol{w}}_n$ because the FFT/IFFT expressions can be included in the expression for the non-linear function $f()$. For this reason, in an OFDM system, y_n, $\boldsymbol{x}_n$ and $\widehat{\boldsymbol{w}}_n$ can each independently be time domain or frequency domain quantities. In fact, the vector $\widehat{\boldsymbol{w}}_n$ can in theory contain both time and frequency domain quantities simultaneously. The choices used for the joint CFOCE-C algorithm must first be discussed in terms of their motivation. The expression for $f()$ and the implementation of the estimator will follow from these choices and from the theory in Chapter 2.

3.2.1 Motivations for a Time Domain Approach

Three major issues arise when deriving a joint CFO and channel estimator from the NL-RLS. Firstly, the framework for the NL-RLS derived in Section 2.4 is general enough that both a time domain and frequency domain implementation is possible. In a time domain implementation, the observation samples y_n and the non-linear function $f()$ are time domain signals (taken prior to the FFT in the receiver). In a frequency domain implementation, the quantities are frequency domain signals (taken after the FFT at the receiver). Secondly, depending on whether the expression for the FFT or IFFT is included in $f()$, the coefficient vector $\widehat{\boldsymbol{w}}$ could contain quantities in the time domain or the frequency domain. In the time domain, the coefficient vector would contain the CIR and a parameter or parameters representing the exponential term in Equation 2.8. In the frequency domain, the coefficient vector would contain the channel frequency response and a parameter or parameters to represent the subcarrier rotation and attenuation caused by the CFO and expressed in Equation 2.9. Finally, an issue which is related to the choice of the domain of $f()$ and $\widehat{w}$ is the domain in which to compensate for the distortion caused by the channel and CFO.

The first and most obvious choice for the options mentioned above is in the way to perform compensation. We choose to perform CFO compensation in the time domain, and channel compensation in the frequency domain for several important reasons. Firstly, a frequency domain channel compensation maintains the traditionally accepted OFDM receiver structure which emphasizes the parallel channel model of Figure 2.2. It also avoids noise enhancement from channel equalization and imperfect compensation due to finite length of the filter representing the inverse of the CIR (which is generally infinite length). Compensation of the CFO in the time domain ensures that, assuming perfect knowledge of the CFO, orthogonality in the tones is restored prior to performing the FFT on the received frame. This will cause channel compensation to perform better since the ICI in Equation 2.9 will have already been removed completely (or partially in the case of imperfect knowledge of the CFO). Our method therefore has an immediate advantage over those proposed in [38] [5] [24] which ignore the ICI altogether. The alternative of removing the ICI in the frequency domain would be too complex for implementation because of the dependence on all the subcarriers in the expression for the ICI suffered by each tone. Although including all or part of the ICI as a parameter to be tracked itself is another alternative, this would greatly degrade the performance of the estimator due to the large increase in the number of parameters to be tracked.

Despite the use of frequency domain compensation for the channel, both the channel and CFO will be represented by time domain parameters in the coefficient vector. Since $v \ll N$, fewer parameters need to be estimated when describing the channel using its CIR than are needed when it is described using an N-point frequency response. This should lead to more accurate characterization of the system and better performance. Also, a time domain characterization is preferred since, as mentioned in Section 2.4, stability of the NL-RLS depends on the number of parameters estimated. The drawback of estimating the impulse response is the need for an FFT to convert from a time domain CIR to a frequency response required for frequency domain equalization, as well as an IFFT required for conversions of the frequency domain decisions to the time domain in the estimator model. However, it will be shown in Section 3.2.3 that the FFT and IFFT are required only once per frame and not once per sample. A hardware implementation could therefore share this additional FFT/IFFT module with the FFT module in the demodulation path of the receiver through a pipelining operation.

Finally, the choice of a time domain implementation over a frequency domain implementation is made for both performance and complexity considerations. The strength of any adaptive estimator depends on the amount of new information it sees as observations, or equivalently, on the number of iterations it performs [35]. In the time domain, due the presence of the cyclic prefix, the estimator will benefit from the use of $N_s = N + N_g$ iterations as opposed to less than N iterations in the frequency domain (assuming some tones are used as a frequency domain guard band as is the case in [14]). In addition, since the input signal used consists of decisions on each tone, an error signal e_n generated by comparison with time domain observations will reduce the chance of instability caused by decision errors because a decision error is first redistributed over the entire frame by means of the IFFT before it used in the estimator. The reduction of the impact of decision feedback errors on estimator performance resulting from a time domain approach is explored in more details in Section 3.3.3. Also, given the importance of the choice of representing the channel by its CIR, a time domain error signal avoids having the FFT function in the expression for $f()$, thus simplifying the generation of both $f()$ and its gradient expressions in the estimator.

3.2.2 Non-Linear Function Development

By following the above motivations, the non-linear function will estimate time domain observation samples and will be a function of time domain arguments. Assuming perfect carrier phase between the transmitter and receiver at the start of transmission, the minimum mean squared error (MMSE) estimate of the observations will be given by

$$\widehat{y}_i = e^{j\frac{j2\pi i}{N}\widehat{\epsilon}_{(i-1)}} \sum_{r=0}^{v-1} \widehat{h}_{r_{(i-1)}} x_{i-r}; \quad i = 0, 1, \ldots \tag{3.1}$$

where x_i is the transmitted signal after addition of the cyclic prefix and i is the absolute time index. The cost function we attempt to minimize by applying the NL-RLS to Equation 3.1 is the total squared error from the start of adaptation,

$$C_{\mathcal{M}}\left(\widehat{h}_0, \widehat{h}_1, \ldots, \widehat{h}_{v-1}, \widehat{\epsilon}\right) = \sum_{i=0}^{\mathcal{M}-1} \left| y_i - e^{j\frac{2\pi i}{N}\widehat{\epsilon}} \sum_{r=0}^{v-1} \widehat{h}_r x_{i-r} \right|^2. \tag{3.2}$$

There are two main flaws with the direct application of equation 3.1 in the NL-RLS. Firstly, we have assumed that the carrier phases are initially synchronized, as is done in [39]. This cannot be guaranteed in a practical system where the two clocks function independently. More importantly, using expression 3.1 for $f()$ in the NL-RLS results in a gradient having magnitude that increases without bound, since

$$\frac{\partial \widehat{y}_i}{\partial \hat{\epsilon}} = j\frac{2\pi i}{N}\widehat{y}_i \tag{3.3}$$

This increase will eventually cause instability in the NL-RLS and must be avoided. Both of these flaws can be remedied by modifying the expression for $\widehat{y}_i$ to include a parameter (θ) modeling the cumulative phase of the CFO, which increases by $\frac{2\pi\epsilon}{N}$ at each iteration. This parameter is part of the coefficient vector $\widehat{\boldsymbol{w}}$ and its update proceeds in two stages.

1. The estimate of the parameter θ is first updated by the NL-RLS algorithm at each sample instant so that the carrier phase offset is tracked. This makes the algorithm more robust to phase noise as well.

2. Following this update, the new value of $\widehat{\theta}$ will be increased using the deterministic update rule given by
$$\widehat{\theta}_{(i)} = \widehat{\theta}_{(i)} + \frac{2\pi}{N}\hat{\epsilon}_{(i)} \tag{3.4}$$
before it is used for estimation of $\widehat{y}_{i+1}$ and in generation of $\widehat{\boldsymbol{w}}_{(i+1)}$.

In steady-state, $\widehat{\theta}_{(i)}$ will converge to a linearly increasing quantity that is governed by Equation 3.4.

With the introduction of the parameter θ, the coefficient vector, estimate of the observation variable, and cost function at iteration i are given by the set of equations below

$$\widehat{\boldsymbol{w}}_{(i)} = \left[\ \widehat{h}_{0_{(i)}}, \widehat{h}_{1_{(i)}}, .., \widehat{h}_{v-1_{(i)}}, \hat{\epsilon}_{(i)}, \widehat{\theta}_{(i)}\ \right]^T \tag{3.5}$$

$$\widehat{y}_i = f(\boldsymbol{x}_i, \widehat{\boldsymbol{w}}) = e^{j\left(\hat{\theta}+\frac{2\pi}{N}\hat{\epsilon}\right)}\sum_{r=0}^{v-1}\widehat{h}_r x_{i-r} \tag{3.6}$$

$$C_M\left(\widehat{h}_{0_{(M)}}, \widehat{h}_{1_{(M)}}, \ldots, \widehat{h}_{v-1_{(M)}}, \hat{\epsilon}_{(M)}, \widehat{\theta}_{(M)}\right) = \sum_{i=0}^{M}\left|y_i - e^{j\left(\hat{\theta}+\frac{2\pi}{N}\hat{\epsilon}_{(M)}\right)}\sum_{r=0}^{v-1}\widehat{h}_{r_{(M)}}x_{i-r}\right|^2 \tag{3.7}$$

Computation of the gradient vector of the function in equation 3.6 can be found in appendix A.

3.2.3 Estimator Implementation

Figure 3.1 below shows a block diagram of a receiver containing the joint CFOCE-C algorithm to track and compensate for the CFO and CIR.

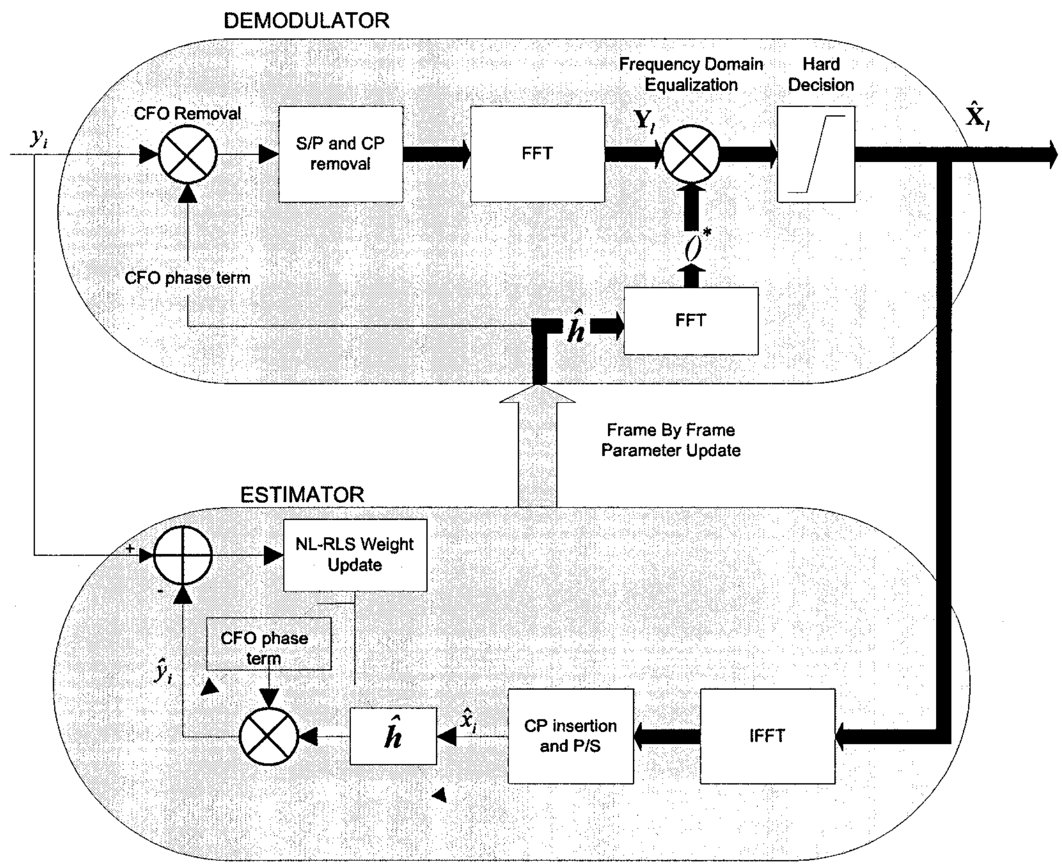

Fig. 3.1 OFDM Demodulator with the CFOCE-C Algorithm

The demodulator module performs CFO removal and frequency domain equalization using the CFO and channel estimates provided by the estimator module. These estimates are updated at the beginning of each OFDM symbol so that the demodulator can process the input in the traditional symbol-by-symbol fashion. The estimator, on the other hand, functions on a sample-by-sample basis. Estimates of the CFO and CIR are updated using the NL-RLS update rule at the arrival of each observation sample y_i. It should be noted that for a linear problem, the estimator could function in a symbol-by-symbol fashion, using least squares estimation for instance. However, the strength of sample-by-sample estimator update is that it allows for a practical non-linear estimator, since a multivariable Taylor series expansion would result in an estimator with a much more complex implementation. Figure 3.1 depicts decision feedback operation. If the data bursts contain a preamble, the input symbols to the estimator during this preamble will be the known preamble sequence instead.

3.3 Performance Evaluation of the Estimator

The performance of the CFOCE-C algorithm is evaluated both analytically and by simulation. The CRLB is computed analytically to serve as a reference for the variance of a joint estimator for the problem. The effect of decision feedback errors is also investigated analytically. A more practical evaluation is done through simulation on a system with preamble and data structure described in Section 2.3.5. Comparison with other methods is used in order to confirm the effectiveness of the joint time domain approach adopted by the CFOCE-C algorithm. Details concerning the simulation environment are first described in Section 3.3.1.

3.3.1 Simulation Details

The joint CFOCE-C algorithm is evaluated by simulation using the IEEE802.11a burst format and specifications [14]. Although the algorithm is general enough to perform qualitatively the same on any burst mode system with CIR length limited to the length of the cyclic prefix, simulations on this platform serve as a practical reference in comparing with other methods presented in the literature.

All simulations in this thesis have been performed with 64-QAM modulation on all tones, the maximum allowed by the IEEE802.11a standard, in order to simulate maximum rate transmission. Both AWGN and exponentially decaying Rayleigh fading channel are tested. An exponentially decaying Rayleigh fading channel has a continuous impulse response of the form in Equation 2.4 with each α_i having uniformly distributed phase, and Rayleigh distributed magnitude. The variance of the Rayleigh random variables for each path is obtained from the exponential function [40]

$$\sigma_i^2 = \sigma_o^2 e^{-iT/T_{RMS}} \tag{3.8}$$

$$\sigma_o^2 = 1 - e^{-T/T_{RMS}} \tag{3.9}$$

where T_{RMS} is termed the RMS delay spread of the channel. For the Rayleigh channel used in our simulations, an RMS delay spread of $T_{RMS} = 25ns$ is used, as suggested in [40]. This is a typical channel for indoor environments. No coding of bits is performed, and BER curves are plotted at typical uncoded BER values. A burst length of 225 OFDM symbols is employed in each case. A range of signal-to-noise ratios (SNR's) were used in the simulations where applicable. Throughout this thesis, the SNR is defined using the symbol energy at the transmitter, denoted E_s. This allows for a fair representation of results obtained in an exponentially decaying Rayleigh fading channel where the channel may attenuate the signal considerably for a number of realizations. Performance results which assume an exponentially decaying Rayleigh fading channels can therefore be expected to be considerably worse than those which assume an AWGN channel.

A CFO with desired magnitude is introduced into the received frame before any receiver processing is performed. This could represent the result of coarse CFO correction by the SCA algorithm. Before application of the joint CFOCE-C algorithm, coarse and fine timing synchronization are performed to simulate a practical system. Coarse timing synchronization is performed using the correlation method introduced in [2]. Fine timing synchronization is achieved using cross-correlation with the long training symbols in the preamble. Finally, an advancement of the FFT window of two samples ensures that the start of the FFT window occurs inside the ISI free region despite possible timing errors. As a result, residual timing errors after this point can then be accounted for by an estimated CIR with leading zeros.

The joint CFOCE-C algorithm employs decision feedback throughout the data portion of the burst. For this reason, the four pilot tones normally used for fine synchronization during the burst carry ordinary data instead. These tones are, however, employed as pilots when simulation results of pilot-based methods are presented.

3.3.2 CRLB for the Joint Estimator

The quality of an unbiased estimator for a set of parameters is given by the variance of the estimator as compared to the best estimator for the problem, whose variance is given by the CRLB [41]. The NL-RLS given in chapter 2 was shown to be asymptotically unbiased in [31]. The performance of the joint estimator was evaluated by comparing its variance to the CRLB. For an estimator applied in burst mode systems, the behavior of the estimator variance with time is of greater importance than its variance for different SNRs. For this reason, the value of the CRLB at each sample of the burst is desired.

For a joint estimator, the Fisher information matrix (FIM) must be derived to obtain the CRLB for each of the estimated parameters [41]. The parameters estimated in the case of the joint CFOCE-C algorithm are the CIR and the CFO parameter ϵ. Since it is used as an aid to ensure stability, the parameter θ is not included in the model for deriving the FIM and the model containing the linearly increasing phase term of

Equation 3.1 is employed instead. The derivation of the FIM and the CRLB is given in detail in Appendix B.

The variance of the CFO and CIR are estimated by an averaging process given by:

$$\begin{aligned} var\left(\widehat{\epsilon}_{(m)}\right) &= \frac{1}{R}\sum_{i=1}^{R}\left|\widehat{\epsilon}^{i}_{(m)} - \epsilon\right|^2 \\ var\left(\widehat{\boldsymbol{h}}_{(m)}\right) &= \frac{1}{R}\sum_{i=1}^{R}\|\widehat{\boldsymbol{h}}^{i}_{(m)} - \boldsymbol{h}\|^2 \end{aligned} \tag{3.10}$$

where $\widehat{\boldsymbol{h}}^{i}_{(m)}$ and $\widehat{\epsilon}^{i}_{(m)}$ are the estimates of the CIR and CFO respectively at time instant m that are obtained for the ith realization. The averaging is performed over R packets having identical transmit data and CIR realizations. This is because the CRLB, and hence the minimum variance of an estimator, will depend on the transmit data and CIR, as shown in Appendix B. An R of 1000 was employed in the simulations. A random realization for the transmit data sequence and the CIR was used. It should be noted in this case that the variance is computed with respect to the known values of the CIR and CFO, and not with respect to the mean for the realizations. This ensures that a bias in the estimator is displayed in the variance plotted variance curves.

Figures 3.2 and 3.3 show the variance of the estimator for different starting values of the CFO. Simulations were performed for a single realization of a Rayleigh channel with SNR of 30dB. Similar trends were obtained for an AWGN channels and different SNRs.

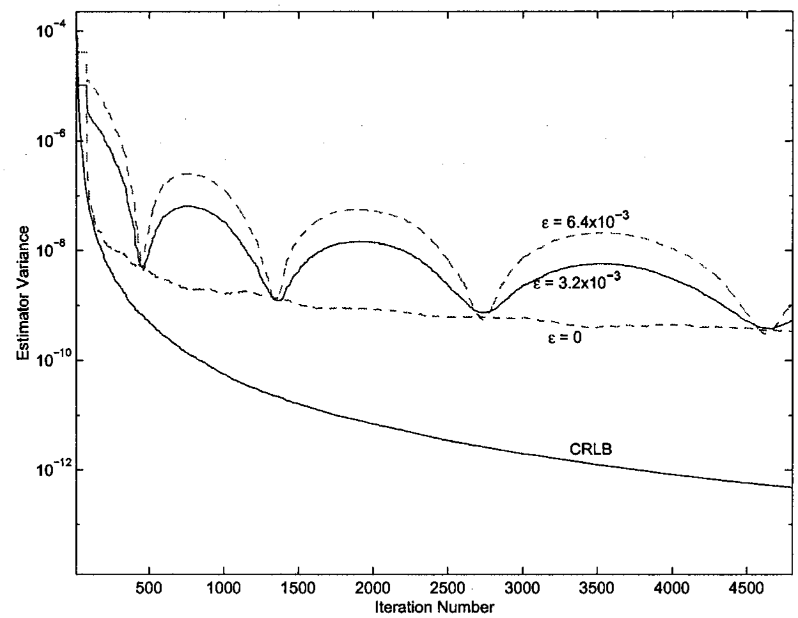

Fig. 3.2 CFO Variance versus Time for Different Starting CFO

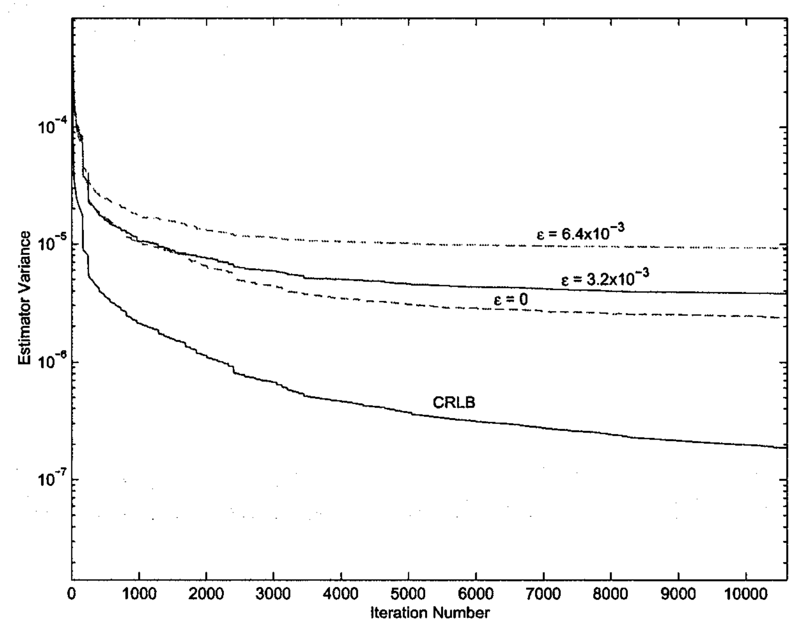

Fig. 3.3 CIR Variance versus Time for Different Starting CFO

The above figures show that the estimator converges very rapidly to an efficient estimator defined in [41], as was expected from the use of an RLS-type algorithm. The increased gap in variance with time compared to the CRLB is a result of the approximation of the optimal search direction that is introduced by the NL-RLS algorithm.

However, use of decision feedback during the data portion, which begins after iteration 160, results in a considerable reduction of the estimator variance and consequently an improvement in system performance as discussed in Section 3.3.4.

A larger value of CFO to be estimated causes oscillations in the CFO estimate variance. These oscillations arise due to the introduction of θ into the tracking algorithm. This parameter causes the CFOCE-C algorithm to behave much like a DLL in tracking of the CFO. The increase in variance is attributed to a small time varying bias in the estimate which is typical of the operation of a DLL, and which is visible in the variance plots due to the variance definition of Equation 3.10. Oscillation increase in size as the size of the CFO to be estimated increases, as is expected. A discussion of the effects of CFO size on performance is included in Section 3.4.

The effect of varying λ on the goodness of the estimator is shown in figures 3.4 and 3.5.

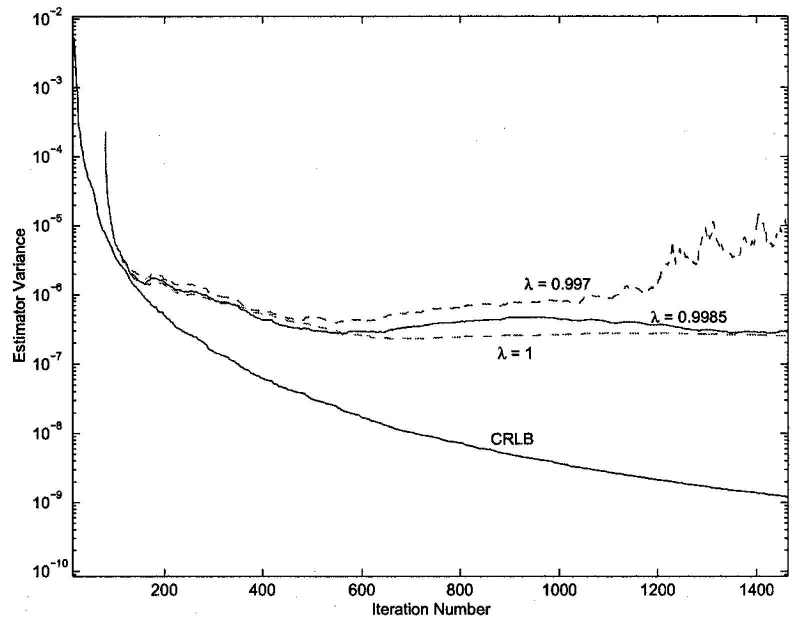

Fig. 3.4 CFO Variance versus Time for Different λ

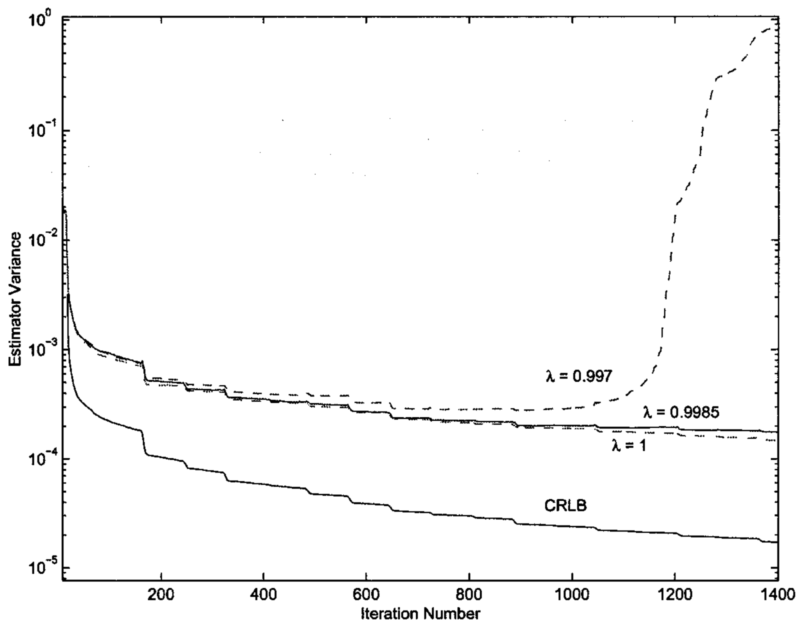

Fig. 3.5 CIR Variance versus Time for Different λ

From the above figures, it can be observed that exponentially decaying memory has an adverse effect on the stability of the NL-RLS. This is due to the bias introduced into the CRLS estimates and was mentioned in Section 2.4.3. This bias should disappear in the estimator as time progresses (as was noted in the proof of an asymptotically unbiased estimator in [31]), however, its presence has adverse effects on the stability of the NL-RLS. For values of λ close enough to 1, the bias is in fact visible in the variance curves. For the NL-RLS, this bias affects stability, as it will cause the search direction of the algorithm to deviate too much from the optimal search direction. As a result, long data bursts will require a value of $\lambda \approx 1$ to ensure stability. Although $\lambda = 1$ shows the best estimator performance in the above figures, it should be noted that this value should be avoided in practice. It was shown in [42] that the CRLS is numerically unstable under the effect of finite-word-length when $\lambda = 1$. For this reason, a practical implementation of the CFOCE-C algorithm should use a value of λ as close as possible to, but not equal to, unity.

3.3.3 Effect of Decision Feedback Errors

It was mentioned in Section 3.2.1 that a time domain estimator will perform better in the presence of decision errors than a frequency domain estimator because the IFFT will redistribute an error over the entire symbol. This redistribution eliminates the short term bias of the noise caused by a decision error. The removal of this bias is explained analytically by statistical arguments in what follows.

Consider a decision error with value $Ae^{j\psi}$ affecting any one of the N tones in the demodulated symbol with equal probability. The decision feedback symbol can be viewed as the desired symbol perturbed by some noise vector $\boldsymbol{D}$. For one particular realization in which the error occurs on the kth subcarrier, the estimated set of transmitted frequency samples will have the form

$$\widehat{\boldsymbol{X}} = \boldsymbol{X} + \boldsymbol{D} = \begin{bmatrix} X_0 \\ X_1 \\ \cdot \\ \cdot \\ \cdot \\ X_{N-1} \end{bmatrix} + \begin{bmatrix} 0 \\ \cdot \\ 0 \\ Ae^{j\psi} \\ \cdot \\ 0 \end{bmatrix}. \tag{3.11}$$

Two parameters of interest in analyzing the effect of this noise on the adaptive algorithm are the variance of the noise (or equivalently, the SNR at the input of the adaptation algorithm for a particular sample) and the mean value of one sample taken over the set of N possible realizations that corresponds to an error at each of the subcarriers. A noise with non-zero statistical mean will cause a bias in the input signal being used as a reference by the adaptation algorithm, which in turn will result in a bias in the coefficients being estimated. Such a bias will introduce additional decision errors due to inaccurate demodulation and is of special concern in an algorithm such as the NL-RLS because it can be large enough to cause instability, as was shown in Section 3.3.2.

In a frequency domain implementation, the decision feedback symbol itself is used directly as the input to the estimator. From Equation 3.11, the SNR seen by the adaptation algorithm is

$$SNR_{FREQ} = \frac{NE\left\{|X_i|^2\right\}}{A^2} \tag{3.12}$$

where $E\left\{|X_i|^2\right\}$ is assumed to be the same for all subcarriers. The mean value for any particular sample of the input is given by:

$$\mu_{FREQ} = E\left\{X_i\right\} + \frac{A}{N}e^{j\psi} \tag{3.13}$$

since each realization of the error vector has equal probability. A bias term is therefore introduced by the decision feedback error. This bias is in fact a temporary bias, since the quantity $\frac{A}{N}e^{j\psi}$ itself will have zero mean if enough errors occur at the same subcarrier.

However, this temporary bias is of interest because in a short time window, it may cause instability in the algorithm. In this case, the error must be considered as a deterministic quantity, since the algorithm's behavior depends on the statistics of the input signal over a finite time window.

In a time domain implementation, $\widehat{\boldsymbol{X}}$ is first passed through an IFFT before being used as input to the adaptation algorithm. This modified time domain input can be expressed as

$$\widehat{\boldsymbol{x}} = \boldsymbol{x} + \boldsymbol{d} = \begin{bmatrix} x_0 \\ x_1 \\ \cdot \\ \cdot \\ \cdot \\ x_{N-1} \end{bmatrix} + \frac{A}{N} e^{j\psi} \begin{bmatrix} e^{j\frac{2\pi k(0)}{N}} \\ e^{j\frac{2\pi k(1)}{N}} \\ \cdot \\ \cdot \\ \cdot \\ e^{j\frac{2\pi k(N-1)}{N}} \end{bmatrix} \tag{3.14}$$

where k is the tone position of the decision error and is assumed uniformly distributed over the integers in $[0, N-1]$. In terms of the frequency domain transmit power, the SNR in this case is the same as the frequency domain implementation and is given by

$$SNR_{TIME} = \frac{NE\left\{|X_i|^2\right\}}{A^2} \tag{3.15}$$

while the mean is given by the expression

$$\mu_{TIME} = E\left\{x_i\right\} + \begin{Bmatrix} \frac{A}{N} e^{j\psi} & if \quad l = 0 \\ 0 & if \quad l \neq 0 \end{Bmatrix} \tag{3.16}$$

which results due to a well-known property for a sum of exponentials. The $k = 0$ case in Equation 3.16 can be made to have probability zero if we consider the inclusion of frequency domain guard bands [14] in which case, an error can never occur for this tone. As a result, while the SNR at the input of the estimator is unchanged, the bias in the noise caused by a decision error is eliminated by using a time domain approach. Effectively, the IFFT will distribute a single decision error in the input over the entire symbol with phases evenly distributed around the unit circle, and thus the estimator will remain unbiased in the short term in the presence of decision feedback errors. Lack of a bias avoids any possible instabilities in the NL-RLS, but also reduces deviation in the coefficient vector with respect its optimal value.

A more intrinsic way of viewing the benefit of having the adaptation algorithm after the IFFT is obtained from an error performance surface view for the tracking algorithm. A single decision error in the frequency domain would cause a significant shift in the estimated coefficient vector compared to the optimum point. If this estimate is redistributed via the IFFT, the estimate of the coefficient vector will more likely move randomly and with smaller amplitude around the optimum value.

It also follows from the summary of the NL-RLS in Section 2.4.2 that the input vector of the adaptive algorithm is actually the gradient of non-linear function at the given transmit vector $\boldsymbol{x}$ rather than $\boldsymbol{x}$ itself. This further complicates the analysis of the effect of decision errors on the NL-RLS. Simulation is used in the next section to show the advantage of a time domain approach in a more exact fashion.

3.3.4 Performance in a Practical System

Although estimator variance is a universally accepted measure for the performance of an estimation algorithm, system performance is much more important because it contains a practical element, and because it accounts for the effectiveness of the compensation scheme. Compensation of the CFO in the time domain by the CFOCE-C algorithm is expected to have performance benefits over frequency domain compensation used in [38] [28] [9]. The main goal in the performance simulations is to evaluate the advantage in BER of

1. performing joint estimation of the CFO and channel, and
2. performing estimation of the CFO and channel in the time domain, as well as compensation of the CFO in the frequency domain

The CFOCE-C method is compared with two benchmark methods to quantify the BER gain of each of these. The first method, described in detail in [24] performs correlation-based CFO estimation and LS channel estimation using the long training sequence. Phase tracking is performed using four pilot tones. As mentioned in [24], this method is common in low complexity implementations of an IEEE802.11a receiver. The second method, presented in [9], performs joint estimation of CFO and channel in decision directed mode of operation, much like the CFOCE-C method. However, the estimated parameters as well as the error variable of the adaptive algorithm are all in the frequency domain rather than the time domain. The LMS is the adaptive algorithm used in this case.

Figures 3.6 and 3.7 show the BER performance of the three methods being compared for an AWGN and exponentially decaying Rayleigh fading channel respectively.

In each case, it has been assumed that an effective coarse CFO synchronization has been performed to reduce the CFO to 100Hz.

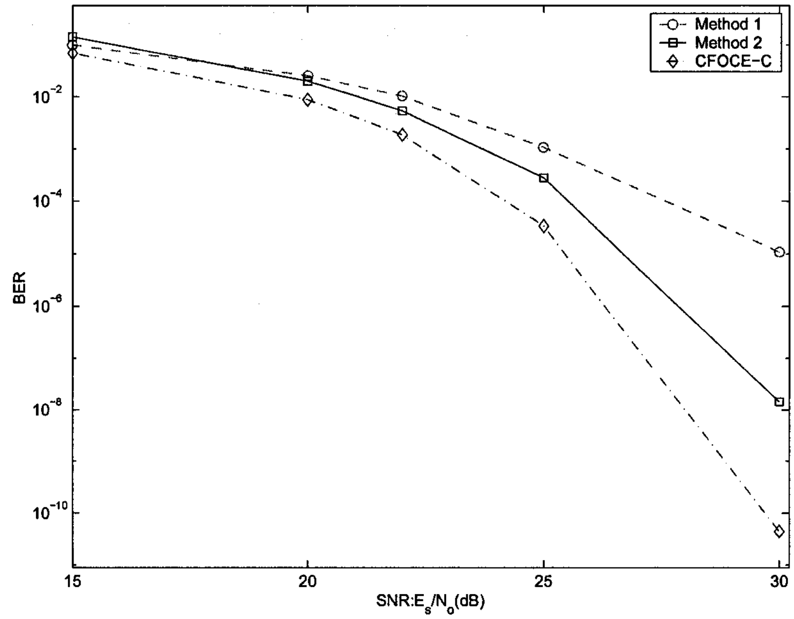

Fig. 3.6 BER versus SNR for Different Estimation Methods in AWGN Channel

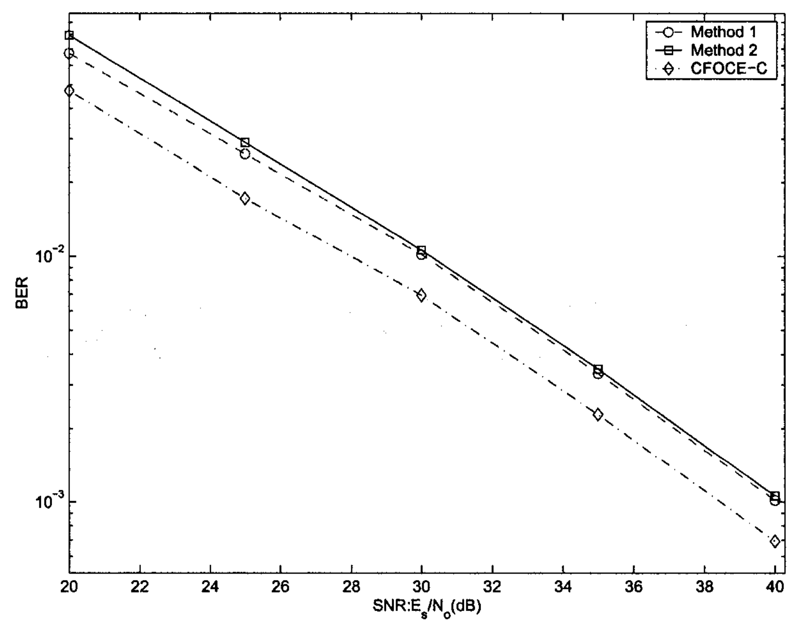

Fig. 3.7 BER versus SNR for Different Estimation Methods in Rayleigh Channel

Both of the above figures show a gain of at least 2dB over a wide range of SNR obtained using the CFOCE-C method. Several other observations can also be made. Firstly, the degradation of the CFOCE-C method at low SNR attributed to decision feedback errors is slightly lower than in the case of Method 2 due the use of a decision feedback signal being employed after the IFFT. The CFOCE-C method still outperforms Method 1, which does not employ any decision feedback, even at considerably low SNR. Finally, at high SNR, the gain of the CFOCE-C method increases with respect to both Method 1 and Method 2. This is most visible in Figure 3.6 and can be attributed to time domain modeling and correction of the CFO, which causes ICI that is dominant over AWGN at these large SNRs. At uncoded BERs typical of an uncoded system, the gain of the CFOCE-C over Method 2 is of 3dB for an AWGN channel. Reversal of the performance curves of Method 1 and Method 2 for the Rayleigh channel is attributed to an approximation of the channel in the model derived in [9].

Figure 3.8 below further shows the robustness of the CFOCE-C method to decision feedback errors, which was examined briefly in Section 3.3.3 The BER is plotted for the normal operation of the CFOCE-CE as well as an ideal feedback implementation, where the reference input to the estimator is obtained from the actual input used at the transmitter, rather than the estimated input after decision feedback. The minimal degradation of the decision feedback implementation compared to the ideal feedback implementation at low SNR confirms the advantage of a time domain approach to estimation. Similar results are observed for a Rayleigh fading environment.

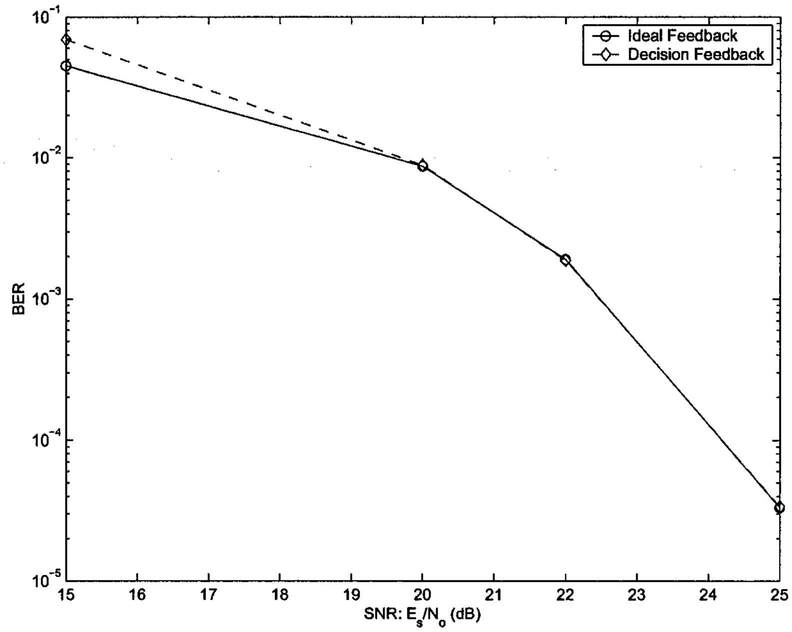

Fig. 3.8 BER versus SNR for For Ideal Feedback and Decision Feedback NL-RLS in AWGN Channel

3.3.5 Effect of Sampling Frequency Offsets

As mentioned in Section 2.3.4, SFO causes a frequency dependant attenuation and phase rotation. This attenuation and phase rotation also increases with time. The effect of SFO on the performance of a channel and CFO estimation scheme depends on how well the model can incorporate the frequency dependant attenuation and phase rotation by representing it as a time varying channel. The CFOCE-C method represents the CIR in the time domain, which allows little room for representation of a frequency dependant, time-varying distortion. Method 2 outlined in [9] represents the channel in the frequency domain, which allows for the effect of SFO to be incorporated into the channel estimates of each subcarrier. Since method 1 in [24] tracks only a frequency independent phase shift to correct for the CFO, it is most susceptible to a small SFO.

Simulations were performed in an AWGN channel with a relatively short burst length of 20000 bits. A SFO of 200Hz ($\eta = 10^{-5}$), which is within the allowable clock jitter specified in [14], is simulated using the method explained in the next chapter. The BER curves for each of the methods under these conditions is shown in Figure 3.9 below.

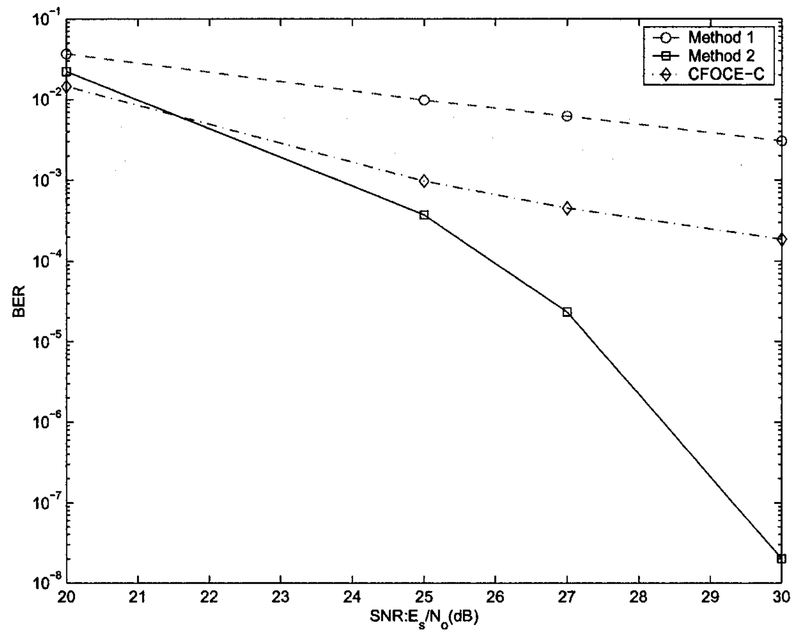

Fig. 3.9 BER versus SNR for Different Estimation Methods in AWGN with SFO

While the CFOCE-C method remains more robust than Method 1, the degradation compared to no CFO is significant enough to require modification of the model used to derive the CFOCE-C to account for SFO. This observation, as well as the benefit of maintaining a time domain approach, is used as a motivation for deriving the CFOSFOCE-C method of chapter 4.

3.4 Stability and Steady-State Analysis

The analysis of stability and convergence of an adaptive algorithm is performed by examining the properties of the weight error correlation matrix [36]. Such a matrix is difficult to derive for the NL-RLS without introducing unreasonable assumptions due to the dependence of the effective input vector on the weight vector, as mentioned in Section 2.4.3. This interdependence also introduces the possibility of instability. Simulation is therefore a better alternative for evaluating the convergence and steady-state behavior of the CFOCE-C algorithm.

A method of deriving an initial guess which guarantees stability for a large range of CFO is of interest. Given that we deal with burst mode transmission, this initial guess should be derived from the preamble. A possible choice for the initial guess would be a block LS estimate using the preamble data. This choice has two major disadvantages.

Firstly, it requires a matrix inversion in the case of a variable preamble. Secondly, it will not ensure stability by itself because, although a good estimate of the coefficient vector will be ensured, an estimate of the RLS inverse-correlation matrix is still unavailable. As a result, the initial search directions generated by the NL-RLS may cause instability.

An improved initial guess procedure is described in this section. In this procedure, the CRLS is first employed to ensure rapid convergence of the channel estimate and to obtain an initial guess of the RLS-correlation matrix. As a result, the channel estimates must account for the CFO during the initial convergence phase.

3.4.1 Initial Guess Procedure

Figure 3.10 below illustrates the procedure for deriving the initial guess of the coefficient vector and RLS inverse-correlation matrix.

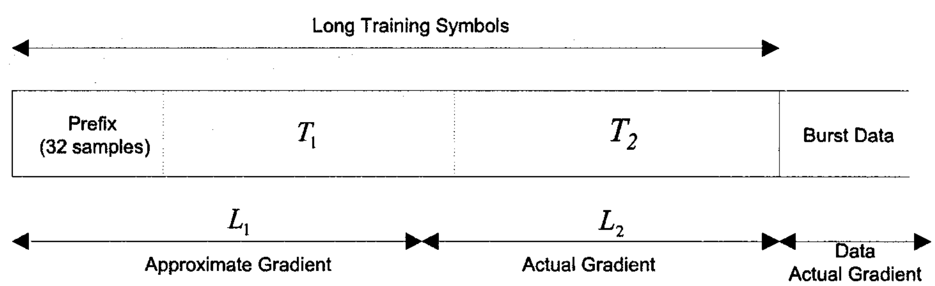

Fig. 3.10 Initial Guess Procedure Applied to the IEEE802.11a Preamble

The NL-RLS algorithm is first applied to the preamble with the known training symbols as input. The initial guess of the coefficient vector and RLS inverse-correlation matrix are as specified in the initialization portion of Table 2.1. In order to ensure convergence, adaptation of only the CIR coefficients is allowed by setting the last two elements of the gradient vector of Equation C.3 to zero over the first L_1 samples of the long training sequence. This is an approximation of the actual gradient vector. Since the estimate of y_n under this condition is now a linear function of the estimated coefficients, the algorithm is effectively the CRLS, which is guaranteed to converge for any initial guess. The CFOCE-C algorithm as described in the previous sections is then enabled during the next L_2 samples, as well as for the data portion of the burst. Decision feedback mode is enabled at the start of the data portion.

It should be obvious from the above description that stability of the algorithm will be affected by two factors. Firstly, a large enough value of L_1 is require to obtain good enough initial guesses of the coefficient vector and the RLS inverse-correlation matrix before the NL-RLS algorithm is started. The second issue is the size of CFO that must be estimated. During the first L_1 samples, since the CFO term in Equation 3.1 is ignored in estimation, the CIR estimates must account for the effect of a CFO as well. This effect is actually a time-varying phase rotation of the CIR. The effective channel to be estimated during this phase is the time-varying channel defined by

$$\boldsymbol{h}_{(i),eff} = \begin{cases} e^{j\frac{2\pi\epsilon i}{N}}\boldsymbol{h} & 0 < i < L_1 \\ e^{j\frac{2\pi\epsilon(L_1-1)}{N}}\boldsymbol{h} & i \geq L_1 \end{cases} \tag{3.17}$$

If the CFO to be estimated is too large, the effective CIR over the first L_1 samples will change too quickly for the RLS with $\lambda \approx 1$ to track the channel adequately. Each of these factors is considered by both analysis and simulation.

It should be noted that the NL-RLS is not limited to use in a problem where it can be transformed to a CRLS by setting some of the gradient elements to zero. In more general problems, an alternate method of obtaining a good enough initial guess of the coefficient vector and correlation matrix must be derived.

3.4.2 Transient Analysis of the NL-RLS in the Preamble

Since the effective channel to be estimated during the first L_1 samples of the long training sequence changes with time, analytical evaluation of the performance of the NL-RLS during these samples can be done in a method similar to the tracking performance analysis of the CRLS found in [43]. Some minor changes need to be made to the analysis in [43] for it to apply to the time varying channel given in Equation 3.17. Effectively, the channel model used in the analysis is not Markov as it is in [43]. Instead, the model which results from Equation 3.17 is illustrated in the figure below.

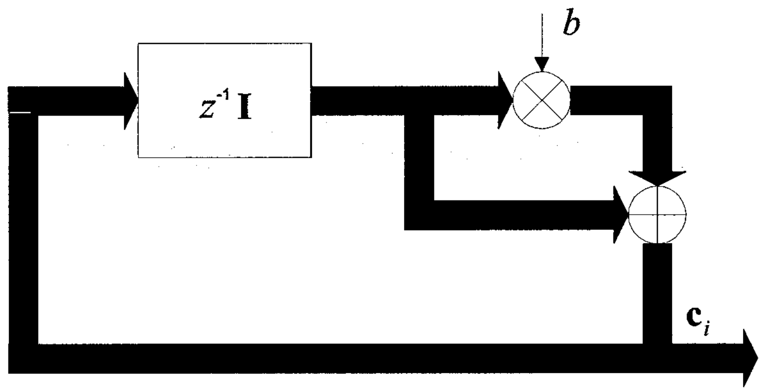

Fig. 3.11 First Order Channel Model for L_1 Preamble Samples

Figure 3.11 shows a deterministic update rule for the coefficient vector to be tracked that is given by

$$\boldsymbol{c}_i = \boldsymbol{c}_{i-1} + b\boldsymbol{c}_{i-1} \tag{3.18}$$

where

$$\boldsymbol{c}_i \equiv \boldsymbol{h}^*_{(i),eff} \tag{3.19}$$

$$b = e^{j\frac{2\pi\epsilon}{N}} - 1 \tag{3.20}$$

It should be noted that rather than modeling the effect of the CFO as a multiplying constant a of [43], the effect of the CFO is instead modeled as an additive term. This is because [43] requires $a \approx 1$, which is not the case for the exponential term, which varies around the unit circle with time. Unlike in [43] the disturbance vector $b\boldsymbol{c}_{i-1}$ is deterministic and need not be uncorrelated with the coefficient vector. The correlation matrix of the disturbance vector is

$$E\left\{(b\boldsymbol{c}_{i-1})(b\boldsymbol{c}_{i-1})^H\right\} = |b|^2\boldsymbol{h}\boldsymbol{h}^H \tag{3.21}$$

As a result, the correlation matrix $\boldsymbol{K}$ of the weight error vector $\boldsymbol{e}_i = \widehat{\boldsymbol{c}}_i - \boldsymbol{c}_i$ is given by

$$\boldsymbol{K}_i \approx \frac{1-\lambda}{2}\sigma^2\boldsymbol{R}^{-1} + \frac{1 - cos\left(\frac{2\pi\epsilon}{N}\right)}{(1-\lambda)}\boldsymbol{h}\boldsymbol{h}^H \tag{3.22}$$

where $\boldsymbol{R}$ is the correlation matrix of the input vector $\boldsymbol{x}$, σ^2 is the variance of the noise, and it was assumed that $\lambda \approx 1$ but $\lambda \neq 1$ [43]. This last assumption is reasonable, given the discussion in section 3.3.2 which treats the selection of λ. In deriving Equation 3.22 it is assumed that i is large. As a result, the approximation becomes better for the last of the L_1 samples, assuming L_1 is large enough. Also assumed is the independence of $\boldsymbol{c}_{i-1}$ and $\boldsymbol{x}_i$ which follows from the independence of the CIR and the transmitted time-domain OFDM symbol.

From the correlation, the mean square deviation (MSD) of the coefficient vector is obtained by taking the trace of the matrix in Equation 3.22. As in the case of the CRLS tracking a Markov channel model, the MSD for the NL-RLS with simplified gradient has an estimation variance term contributed by the matrix $\boldsymbol{R}$ and a lag variance term:

$$\mathcal{D}_i \approx \frac{1-\lambda}{2}\sigma^2 tr\left[\boldsymbol{R}^{-1}\right] + \frac{1-cos\left(\frac{2\pi\epsilon}{N}\right)}{(1-\lambda)}\|\boldsymbol{h}\|^2; \lambda \neq 1 \tag{3.23}$$

Provided L_1 is sufficiently large, the MSD of the channel estimates will approach the expression in Equation 3.23. The two contributions in equation 3.23 vary in proportion to $(1-\lambda)$ and $(1-\lambda)^{-1}$ which indicates the presence of a optimal value of the forgetting factor as was derived in [43]. However, since ϵ is orders of magnitude less than λ, the lag variance term tends not to contribute and the optimal value of λ is very close to one, as was found in Section 3.3.2. For large initial CFO, the minimum MSD that can be achieved over the first L_1 samples increases, and an alternative optimum value of λ that is CFO dependant is required.

3.4.3 Effect of Preamble Length on Stability and Steady-State Performance

Stability and steady-state behavior is evaluated from the MSD at the end of a burst of 225 OFDM symbols, in which case steady-state is assumed. The MSD in this case is defined as

$$MSD = \frac{1}{R}\sum_{i=1}^{R} \|\widehat{\dot{\boldsymbol{w}}}^{(i)} - \dot{\boldsymbol{w}}\|^2 \tag{3.24}$$

where $\widehat{\dot{\boldsymbol{w}}}^{(i)}$ is the estimate of the coefficient vector excluding the parameter θ at the steady-state for the ith realization, and $R = 1000$ realizations were used as in the case of variance computation in Section 3.3.2. Also consistent with variance computation is the exclusion of θ required to measure the performance of the estimator. The CFOCE-C is deemed stable if the MSD is considerably smaller (at least 3 decades) than the squared norm of the vector $\dot{\boldsymbol{w}}$, which is approximately 1 in both AWGN and Rayleigh channels. To determine the required length L_1 that ensures stability as well as the value that results in the best estimator performance, the MSD at the end of the burst is plotted for different values of L_1 in Figure 3.12 below.

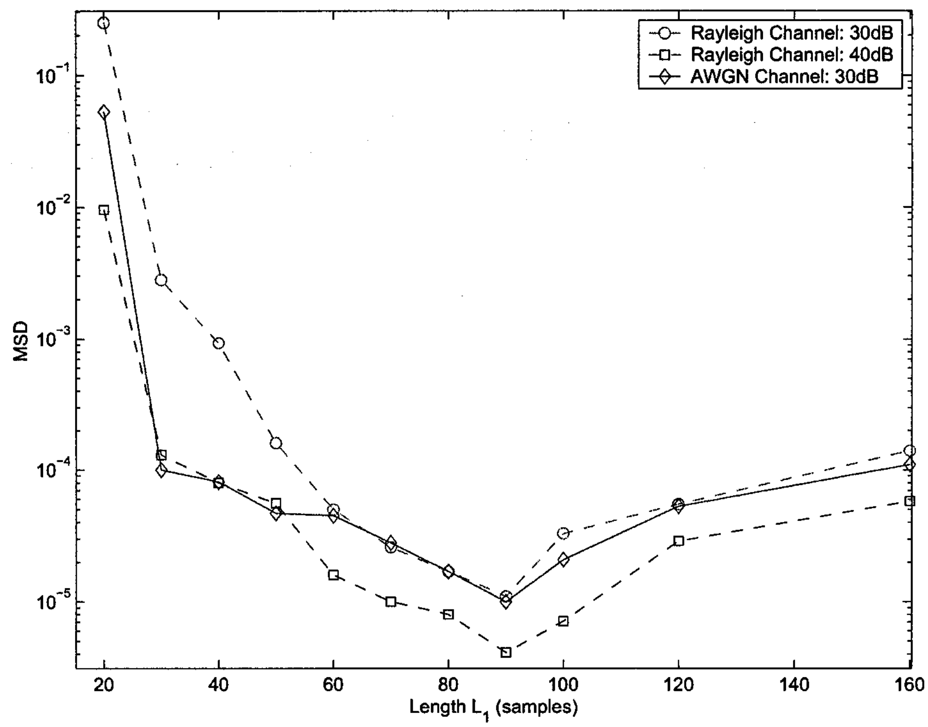

Fig. 3.12 Steady-state MSD versus Length L_1 for Different Channels

Stability is reached when marginal changes in the value of L_1 make only small changes in MSD. This indicates the absence of any unstable realizations which produce a high MSD for that iteration and affect the size of the quantity computed in Equation 3.24. From the figure this occurs for $L_1 \approx 30$ for AWGN and Rayleigh channel at 40dB and at $L_1 \approx 60$ for Rayleigh channel at 30dB. Furthermore, an optimal value of $L_1 \approx 90$ is observed for each of these three channels. Values larger than $L_1 \approx 90$, although they produce a stable result, suffer from a slightly higher steady-state MSD because of fewer samples used to refine the estimate of the initial guess and the inverse correlation matrix when the exact gradient is used. It should be noted from the discussion of Section 3.4.2 that the value of the CFO has no effect on the optimum L_1 provided the algorithm can track the time varying channel produced by this CFO during the L_1 samples. A CFO of $\epsilon = 3.2 \times 10^{-3}$ was chosen for the simulations in Figure 3.12, which is shown to be sufficient for stability in Section 3.4.4 that follows.

The following conclusions can also be made from Figure 3.12. Firstly, it should be noted that stability is maintained even when $L_1 = 160$, in which case the refinement of the coefficient vector and inverse correlation matrix that occurs when the exact gradient is used is performed only in the data portion of the burst. The importance of this observation is that the minimum value of L_1 could be used as the length of the preamble itself and acceptable performance can be expected. A preamble of 60 samples for the CFOCE-C is therefore sufficient in each of the above channels. Secondly, the steady-state MSD for a stable CFOCE-C algorithm is independent of the length of the CIR, as it remains the same for both AWGN and Rayleigh channels with the same SNR. This is expected, since in each case the algorithm tracks the same number of CIR parameters. The value of L_1 required for stability is lower in the case of an AWGN channel than a Rayleigh fading channel, owing to the closeness of the initial guess to the AWGN CIR. Therefore, the channel type affects the required preamble length, but not the final performance of the estimator with a sufficient preamble. Finally, higher SNR results both in a lower steady-state MSD as well as a lower minimum L_1 to achieve stability.

3.4.4 Effect of CFO on Stability and Steady-State Performance

Following the results of Section 3.4.3 a value of $L_1 = 90$ is used to determine the range of CFO in which the CFOCE-C can be employed reliably. The results are summarized in Figure 3.13.

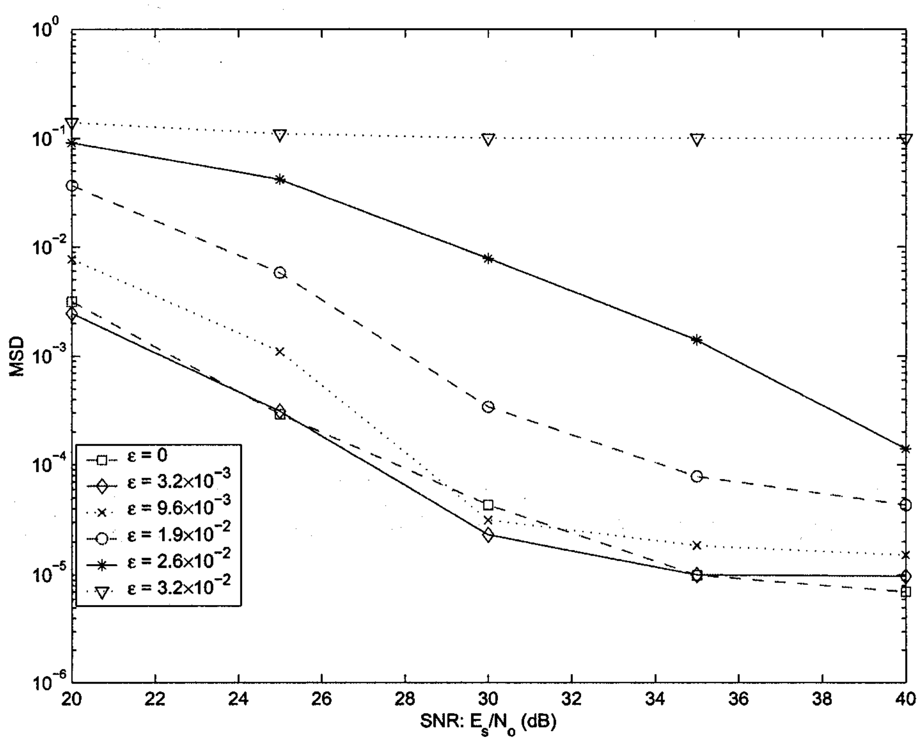

Fig. 3.13 Steady-state MSD versus SNR for Different CFO

Comparable steady-state performance is obtained for values of ϵ up to 10^{-2} approximately. For this range of CFO, the BER performance of the CFOCE-C should be as given in Section 3.3.4 where the CFO used was 3.2×10^{-4}. Beyond 10^{-2}, the performance of the estimation algorithm begins to degrade with increase in the CFO and some realizations become unstable. Stability is lost for a significant number of realizations for values of ϵ beyond 3×10^{-2}. Therefore, to ensure operation at a point which is far enough from instability, the CFOCE-C requires a CFO of less than $\epsilon = 10^{-2}$.

3.5 Chapter Summary

The joint CFOCE-C algorithm derived in this chapter was shown to maintain a relatively low estimator variance and to provide a gain of at least 2dB over a large range of SNR compared to the better of the two alternative methods presented in this chapter. This gain can be expected for a starting CFO of up to $\epsilon = 10^{-2}$. Simulation results were used to show the sensitivity of the CFOCE-C algorithm to a SFO. As a result, a modification to the CFOCE-C which estimates the SFO as well is necessary.

Chapter 4

Joint CFOSFOCE-C Algorithm

When the sampling clocks of the transmitter and receiver are not synchronized, the receiver must estimate and compensate for SFO to ensure that performance is not degraded as the length of the burst increases. For long bursts and/or large frequency offsets, an FFT window adjustment is also required to maintain proper timing and avoid ISI. In this chapter, a joint algorithm that performs CFO, SFO and channel estimation using the NL-RLS, and compensates for the distortions digitally, is presented. This algorithm can also inherently adjust the FFT window based on the information it tracks. A model for simulating the effect of SFO in the receiver that will serve in evaluation of the algorithm by simulation is first derived in Section 4.1. More importantly, the model shows that even in the presence of a multipath fading channel, the effect of a SFO can be modeled as a frequency dependent phase rotation followed by a linear convolution by a modified CIR. In Section 4.2 the joint algorithm is derived based on the observations in Section 4.1 and implementation details are given. Section 4.3 shows that the CFOSFOCE-C algorithm outperforms an alternative joint synchronization algorithm in terms of system BER.

4.1 Sampling Frequency Offset Modeling

The effect of CFO and SFO on the received time domain samples in an OFDM system is given in [7] and [5], however, both assume an AWGN channel. In order to derive a NL-RLS-based joint estimator for these frequency offsets which also considers the effect of a multipath fading channel, an expression for the received samples involving the effect of the channel is first derived here. Furthermore, in order to simulate the effect of a SFO using digital simulation tools, an interpolation and resampling of the received samples is generally required. This operation will introduce distortion into the received signal, making it difficult to assess the performance of the estimation algorithm. For this reason, a digital model for the effect of SFO that does not involve resampling is of interest and follows from the model of the received samples that is derived in this section. Modeling the SFO using this method requires some synchronization assumptions to be made, but these assumptions are shown to be practical. The derivation presented in this section uses the resampling technique of [7], however, the technique is applied to a general multipath fading channel and further analysis is made here to obtain a time domain model.

The figure below shows an OFDM system with the analog front-ends of both the transmitter and receiver.

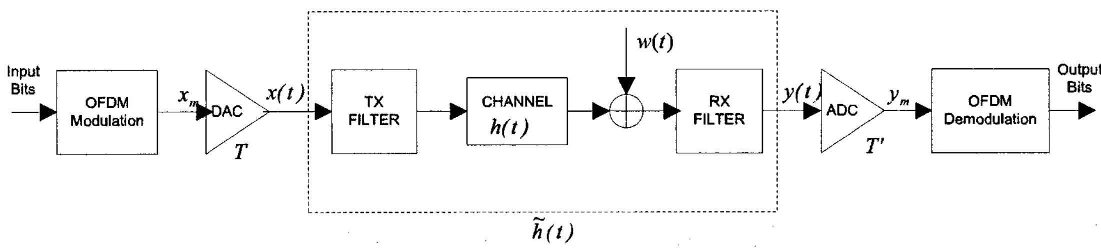

Fig. 4.1 Source of SFO in an OFDM System

The channel $h(t)$ is a multipath fading channel with path gains that are assumed invariant over the transmission burst interval. The analog impulse response for this channel was given in chapter 2. It is further assumed in our model that the bandwidths of the transmit and receive analog filters are large enough that the overall sampled impulse response has a negligible amount of energy outside the length of the cyclic prefix. In this case, the overall impulse response $\tilde{h}(t)$ is limited to a maximum length of N_g samples, or N_gT' seconds. Finally, the bandwidth of the receive filter should be considerably larger than the signal bandwidth so that the noise $w(t)$ remains approximately white at the sampling stage of the analog-to-digital converter (ADC).

To adopt a time domain approach, the interference between time domain samples at the receiver prior to demodulation is first examined. With the assumption of a large enough cyclic prefix, ISI between OFDM symbols does not occur and only interference between samples of the same OFDM symbol exists. For the first $v-1$ data samples of y_n, the interference involves samples in the cyclic prefix, while for all other samples, the interference is caused purely by the preceding data samples of the transmit signal. In the later case, the received signal can be expressed as a linear convolution of the data symbol with an FIR channel. Using this fact and adjusting for the first case, the received time domain data samples (after removal of the cyclic prefix) for the l^{th} received OFDM symbol can be expressed in terms of the transmitted tones as

$$y_{n,l} = \begin{cases} \sum_{i=0}^{v-1} \widetilde{\alpha}_i e^{j2\pi\Delta f(t_{n,l}-iT')} \frac{1}{N} \sum_{k=0}^{N-1} X_{k,l} e^{j\frac{2\pi k}{NT}(t_{n,l}-iT'-(lN_s+N_g)T)} + \beta_n + w_{n,l} & 0 \leq n \leq v-1 \\ \sum_{i=0}^{v-1} \widetilde{\alpha}_i e^{j2\pi\Delta f(t_{n,l}-iT')} \frac{1}{N} \sum_{k=0}^{N-1} X_{k,l} e^{j\frac{2\pi k}{NT}(t_{n,l}-iT'-(lN_s+N_g)T)} + w_{n,l} & n \geq v, \end{cases} \tag{4.1}$$

where $t_{n,l}$ is the sampling time for the n^{th} sample of the l^{th} OFDM symbol defined by

$$t_{n,l} = (lN_s + N_g + n)\, T'; 0 \leq n \leq N-1, \tag{4.2}$$

T, T' are the transmitter and receiver sampling clock periods respectively and β_n is an additional interference term defined as

$$\begin{aligned} \beta_n &= \sum_{i=n+1}^{v-1} \widetilde{\alpha}_i \left(e^{j2\pi\Delta f(t_{0,l}-iT')} \frac{1}{N} \sum_{k=0}^{N-1} X_{k,l} e^{j\frac{2\pi k}{NT}(t_{N-i,l}-(lN_s+N_g)T)} \right) \\ &\quad - \sum_{i=n+1}^{v-1} \widetilde{\alpha}_i \left(e^{j2\pi\Delta f(t_{n,l}-iT')} \frac{1}{N} \sum_{k=0}^{N-1} X_{k,l} e^{j\frac{2\pi k}{NT}(t_{n,l}-iT'-(lN_s+N_g)T)} \right). \end{aligned} \tag{4.3}$$

In Equation 4.1 it has been assumed that there is no timing offset between the transmitted and received symbols. A timing offset can be accounted for in this equation by modifying $t_{n,l}$ appropriately, provided the receiver begins OFDM symbol sampling in the ISI-free portion of the cyclic prefix. If this is not the case, the model given in Equation 4.1 is incomplete and the effect of ISI must be included.

Ignoring the additional interference term, and making the substitutions $\Delta f = \frac{\epsilon}{N(1+\eta)T}$ and $T' = (1+\eta)T$ into equation 4.1 the received samples can be simplified as shown below.

$$\begin{aligned} y_{n,l} &= \sum_{i=0}^{v-1} \widetilde{\alpha}_i e^{j\frac{2\pi\epsilon}{N}(lN_s+N_g+n-i)} \frac{1}{N} \sum_{k=0}^{N-1} X_{k,l} e^{j\frac{2\pi k}{NT}\{(lN_s+N_g+n-i)T'-(lN_s+N_g)T\}} \\ &= e^{j\frac{2\pi\epsilon}{N}(lN_s+N_g+n)} \frac{1}{N} \sum_{k=0}^{N-1} X_{k,l} e^{j\frac{2\pi k}{NT}\{(lN_s+N_g+n)T'-(lN_s+N_g)T\}} \\ &\quad \cdot \left\{ \sum_{i=0}^{v-1} \widetilde{\alpha}_i e^{-j\frac{2\pi\epsilon i}{N}} e^{-j\frac{2\pi k i}{N}(1+\eta)} \right\} + w_{n,l}. \end{aligned} \tag{4.4}$$

Since both ϵ and η are assumed to be small, the bracketed summation term in equation 4.4 can be approximated as a modified frequency response defined as

$$\begin{aligned}\bar{H}_k &\equiv \sum_{i=0}^{v-1}\left\{\widetilde{\alpha}_i e^{-j\frac{2\pi\epsilon i}{N}} e^{-j\frac{2\pi i\eta(N/2)}{N}}\right\} e^{-j\frac{2\pi ki}{N}} \\ &= \sum_{i=0}^{v-1}\bar{h}_i e^{-j\frac{2\pi ki}{N}} = FFT\left(\bar{\boldsymbol{h}}\right).\end{aligned} \tag{4.5}$$

In Equation 4.5 the dependence on k in the last exponential of the expression for $\bar{h}_i$ is removed by assuming $k = N/2$. This will minimize the maximum error in any of the values of $\bar{H}_k$ and will result in a negligible error in the expression for $y_{n,l}$. Using this approximation, the joint effect of CFO and SFO can be incorporated into the time domain CIR, which is of interest since our estimator operates in time domain.

What remains is to characterize any changes in the transmitter required to generate received samples given by Equation 4.1. Substitution of the expression of Equation 4.5 into Equation 4.4 and performing additional simplification yields the following two equivalent expressions for the received data samples

$$\begin{aligned}y_{n,l} &= e^{j\frac{2\pi\epsilon}{N}(lN_s+N_g+n)}\frac{1}{N}\sum_{k=0}^{N-1}\bar{H}_k X_{k,l} e^{j\frac{2\pi kn}{N}} e^{j\frac{2\pi k}{N}(lN_s+N_g+n)\eta} + \bar{\beta}_n + a_n \\ &= e^{j\frac{2\pi\epsilon}{N}(lN_s+N_g+n)}\left\langle\left\{\frac{1}{N}\sum_{k=0}^{N-1}X_{k,l}e^{j\frac{2\pi km}{N}} e^{j\frac{2\pi k}{N}(lN_s+N_g+m)\eta}\right\}_{m=0,1,\ldots,N-1} \otimes \bar{\boldsymbol{h}}\right\rangle_n + \bar{\beta}_n + w_{n,l}\end{aligned} \tag{4.6}$$

where the interference term is accounted for by the variable $\bar{\beta}_n$ whose value is given by

$$\bar{\beta}_n = \begin{cases}\beta_n & 0 \leq n \leq v-1 \\ 0 & n \geq v.\end{cases} \tag{4.7}$$

Aside from the exponential term inside the summation, Equation 4.6 has the exact form of a received signal under CFO and channel distortion only. This additional exponential term therefore represents exactly the loss of orthogonality in the transmit signal caused by a SFO. In order to simulate this loss of orthogonality without the need for resampling the transmit data, the extra exponential term can be incorporated into the

IFFT at the transmitter, resulting in a modified IFFT definition. This modified IFFT will generate the transmitted data samples according to the equation

$$x_{n,l} = \sum_{k=0}^{N-1} X_{k,l} e^{j\frac{2\pi kn}{N}} e^{j\frac{2\pi k}{N}(lN_s+N_g+n)\eta}. \tag{4.8}$$

The cyclic prefix will consist of the last P samples of the modified IFFT output so that the circular convolution of Equation 4.6 occurs in the data samples when the prefixed OFDM symbols are linearly convolved with the modified CIR of Equation 4.5.

In addition to providing a transmitter model which can incorporate the effect of a SFO in the received time domain samples, Equation 4.6 can now serve as the starting point for the derivation of the joint CFOSFOCE-C algorithm. The derivation of the algorithm in Section 4.2 uses this equation.

Finally, as was mentioned, Equation 4.8 accurately describes the effective transmitter seen at a receiver suffering from SFO only in the case that the receiver samples in the ISI-free region of the cyclic prefix. For instance, for an AWGN channel and a receiver with an OFDM window that is initially perfectly aligned with the transmit data, a circular shift of N_g samples is allowable in one direction, while in the other direction, a shift of one sample will result in ISI that is not accounted for by the transmitter model. In order to include the effect of ISI at the receiver, the transmitter must be able to simulate the effect of a clock drift. This is accomplished by an adjustment of the transmit OFDM window by the insertion or removal of a time domain sample. In this way, the stream of time domain samples will appear shifted at the receiver. In order to maintain data consistency, samples will always be added to or dropped from the cyclic prefix. When a sample is added, the prefix length for that particular OFDM symbol is $N_g + 1$ and when a sample is removed, the prefix length for that symbol is $N_g - 1$. The value of $m = lN_s + N_g + n$ in Equation 4.8 is then reduced by the appropriate amount at the start of the data portion of this modified OFDM symbol in order to account for the change in the transmit window. As opposed to tracking n and l, the value of m is tracked by the transmitter to obtain better granularity during this change.

The condition for a modification in the length of the prefix for a given symbol is that the last sample of the previous symbol satisfies

$$|m| > 1 \tag{4.9}$$

In this case, adjustment to the prefix is made, and the value of m is modified according to

$$m_{new} = m_{old} - \left\lfloor \frac{1}{|\eta|} \right\rfloor \tag{4.10}$$

Since changes in the transmit window can only occur at OFDM symbol boundaries, the value of $m = lN_s + N_g + n$ may momentarily have an absolute value larger than one. In this case, ISI will not be simulated by the transmitter when the receiver's OFDM window matches the data exactly. For this reason, the receiver being used with this transmit model must always sample the OFDM symbol early (begin the window inside the cyclic prefix) by at least one sample in order for the transmit and receive pair to always simulate the true effects of a SFO. Although this may seem to be an impractical assumption, the practice of early sampling in the receiver is already common, since it is used as a protection mechanism against ISI caused by imperfect receiver timing [24]. In addition, if this assumption is not used, the consistency of the transmit model is only affected for one OFDM symbol.

The figure below shows a practical OFDM transmitter and a transmitter modified so that it can model the effect of SFO without any oversampling.

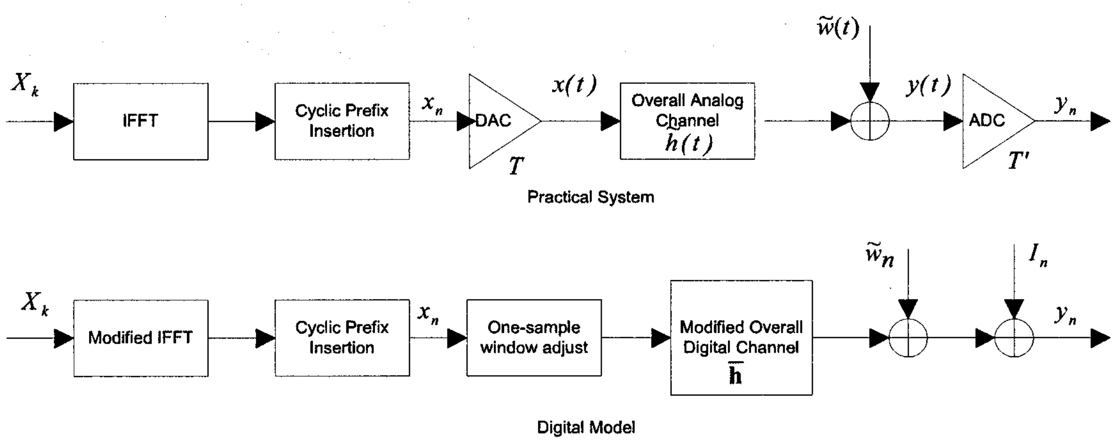

Fig. 4.2 Digital Model of an OFDM Transmitter with SFO

As mentioned, the window adjustment in the transmitter is used to maintain a consistent simulation model by causing ISI in the case of an FFT window drift. This window adjustment is independent of the one performed by the receiver described in the next section, which is performed exclusively for ISI avoidance.

Consistent with Equation 4.6, the interference $\bar{\beta}_n$ is added as noise at the receiver. The effect of this interference, nonetheless, is minimal, and its effect is ignored in the derivation of the estimator in Section 4.2. To confirm this, if η is sufficiently small, and since the sampling period T' is generally in the nanosecond range [13] [14], then

$e^{j2\pi\Delta f(t_{0,l}-iT')} \approx e^{j2\pi\Delta f(t_{n,l}-iT')}$ and the interference term can be approximated as

$$\beta_n \approx \sum_{i=n+1}^{v-1} \widetilde{\alpha}_i e^{j2\pi\Delta f(t_{0,l}-iT')} \left(IFFT\left\{\mathbf{X}_l\right\}_{N-i} - IFFT\left\{\mathbf{X}_l\right\}_n \right). \tag{4.11}$$

From the limits of the summation in Equation 4.11 we see that only the first few samples of the frame are affected by the interference since the path gains $\widetilde{\alpha}_i$ tend to die off rapidly. Since the behavior of the estimator over the entire symbol of N samples is desired, we can ignore the effect of the interference on the first sample at the receiver. This interference is nonetheless added in the transmitter, since it is part of the effect of the SFO and must be simulated.

4.2 Derivation of the Estimator

Derivation of the joint CFOSFOCE-C algorithm follows the same strategy as the derivation of the joint CFOCE-C algorithm. The same motivations of Section 3.2.1 are followed with a slight modification due to the fact that a SFO cannot be modeled purely in the time domain in a simple manner. This modification results in a more complicated design, since the cost function must include the expression for the IFFT in order for estimation error computation to be performed in the time domain. The increase in complexity results in the need for introduction of a damping mechanism in the tracking of the SFO parameters to avoid oscillations in the received tone constellations. Generation of the initial guess for this joint estimator is the similar to the method discussed in Section 3.3.1, and is outlined in this section.

4.2.1 Non-Linear Function Development

A SFO is difficult to represent in the time domain due to the presence of fractional offsets. In the time domain, the effect of the offset can only be expressed in terms of an interpolated version of the transmit signal, and the interpolating function will change with time due to clock drift. In the frequency domain, a SFO is much more easily modeled by multiplication in the IFFT definition of the transmitted value on each subcarrier by a complex exponential whose phase increases linearly with time. This is analogous to how a CFO, which is a frequency domain phenomenon, is modeled by multiplication of the received time domain samples by a complex exponential with linearly increasing phase.

An expression for the received time domain sample when affected by CFO, SFO, channel distortion, and possible timing offsets was given in Equation 4.6. In this expression the SFO is modeled in the frequency domain as required. In addition, this expression treats SFO and timing offsets in the same manner, so that a timing offset caused by clock drift can also be tracked in the joint estimator. The assumptions needed to ensure that Equation 4.6 provides a correct model for the received time samples under synchronization errors and channel distortion are:

1. Clock drift must never cause the beginning of the FFT window to leave the ISI free portion of the cyclic prefix. This is because the transmitter model in Section 4.1 does not account for ISI-induced ICI. This requirement will be ensured by an FFT window adjustment to be explained in what follows.

2. The interference samples given in Equations 4.7 and 4.3 must have little or no effect on the estimator. This can be assumed, since only the first 2-3 samples of the interference are non-negligible and the estimator has the remainder of the frame to recover from their effect.

3. The assumptions about the channel frequency response and the transmit and receive filters made in Section 4.1 hold.

Under these three assumptions, the estimator can be designed using the data model of Equation 4.6 to serve as the non-linear function $f()$.

As in the case of the estimator derived in the case of perfect sampling clock synchronization, a gradient vector with an unbounded magnitude is avoided by introducing the parameter θ to account for the cumulative CFO, and an additional parameter ϕ to account for the cumulative SFO. These parameters also account for initial phase offset in each of the respective clocks. The resulting coefficient vector being estimated is

$$\widehat{\boldsymbol{w}}_{(n,l)} = \left[\ \widehat{h}_{0_{(n,l)}}, \widehat{h}_{1_{(n,l)}}, ..\widehat{h}_{v-1_{(n,l)}}, \widehat{\epsilon}_{(n,l)}, \widehat{\theta}_{(n,l)}, \widehat{\eta}_{(n,l)}, \widehat{\phi}_{(n,l)}\ \right]^T \tag{4.12}$$

where the subscript (n,l) indicates the estimate of the coefficient vector at the computation of the estimate of the observation $y_{n,l}$. The non-linear function estimating the received samples now becomes:

$$\begin{aligned} \widehat{y}_{n,l} &= f(\dot{\boldsymbol{x}}_{m_{n,l}}, \widehat{\boldsymbol{w}}) \\ &= e^{j(\hat{\theta}+\frac{2\pi\hat{\epsilon}}{N})} \left\langle \dot{\boldsymbol{x}}_{m_{n,l}} \otimes \widehat{\bar{\boldsymbol{h}}} \right\rangle_n \end{aligned} \tag{4.13}$$

where

$$\dot{\boldsymbol{x}}_{m_n,l} \equiv \left\{ \frac{1}{N} \sum_{k=0}^{N-1} X_{k,l} e^{j\frac{2\pi ki}{N}} e^{j\frac{2\pi k}{N}(\hat{\eta}+\hat{\phi})} \right\}_{i=0,1,\ldots,N-1}, \tag{4.14}$$

$X_{k,l}$ is the transmitted complex element for the kth tone of the lth OFDM symbol, and $\langle \otimes \rangle_n$ represents the nth element of the convolution of the two N point sequences. Because the channel must be represented in time domain and the effect of the SFO in frequency domain, the IFFT expression and the circular convolution must be included into the expression for the received samples. It is further noticed that the presence of a circular convolution as opposed to linear convolution forces us to estimate only the data portion of the received samples, and hence the cyclic prefix cannot be used as input to the estimator, as it was in the CFOCE-C algorithm. The gradient vector of the non-linear function in Equation 4.13 is given in Appendix C.

4.2.2 Receiver Implementation

A receiver that accounts for SFO will require an FFT window adjustment. In the demodulator, FFT window adjustment occurs at the beginning of every frame in which the following inequality holds

$$\left|\widehat{\phi}\right| > 1 \tag{4.15}$$

By performing window adjustment, we prevent sampling clock drift from moving the current FFT window out of the ISI-free portion of the cyclic prefix where the estimator's model in Equation 4.13 would no longer apply due to the presence of ISI-induced ICI. In practice, the receiver should remain in the ISI-free region to avoid degradation of performance from ICI.

When the inequality in Equation 4.15 holds, the cumulative parameters must be updated to reflect the change in the location of the FFT window. As a result, the following operations must be performed to ensure proper adjustment of the FFT window.

1. If $\widehat{\phi}$ is positive, a cyclic prefix of $N_g - 1$ is assumed for the current symbol in order to advance the FFT window by one sample. If $\widehat{\phi}$ is negative, a cyclic prefix of $N_g + 1$ samples is assumed for the current symbol in order to delay the window by one sample.

2. If $\widehat{\phi}$ is positive, $\widehat{\phi}$ is decreased by 1 before it is used to demodulate the current frame, and serve as the current estimate in the estimator module. If $\widehat{\phi}$ is negative, $\widehat{\phi}$ is increased by 1 instead.

3. If $\widehat{\phi}$ is positive, $(2\pi\hat{\epsilon})/N$ is subtracted from the value of $\widehat{\theta}$ before $\widehat{\theta}$ is used in CFO removal in the current symbol and update in the estimator block. If $\widehat{\phi}$ is negative, $(2\pi\hat{\epsilon})/N$ is added to $\widehat{\theta}$.

Figure 4.3 below shows a block diagram of a demodulator that uses the joint CFOSFOCE-C algorithm.

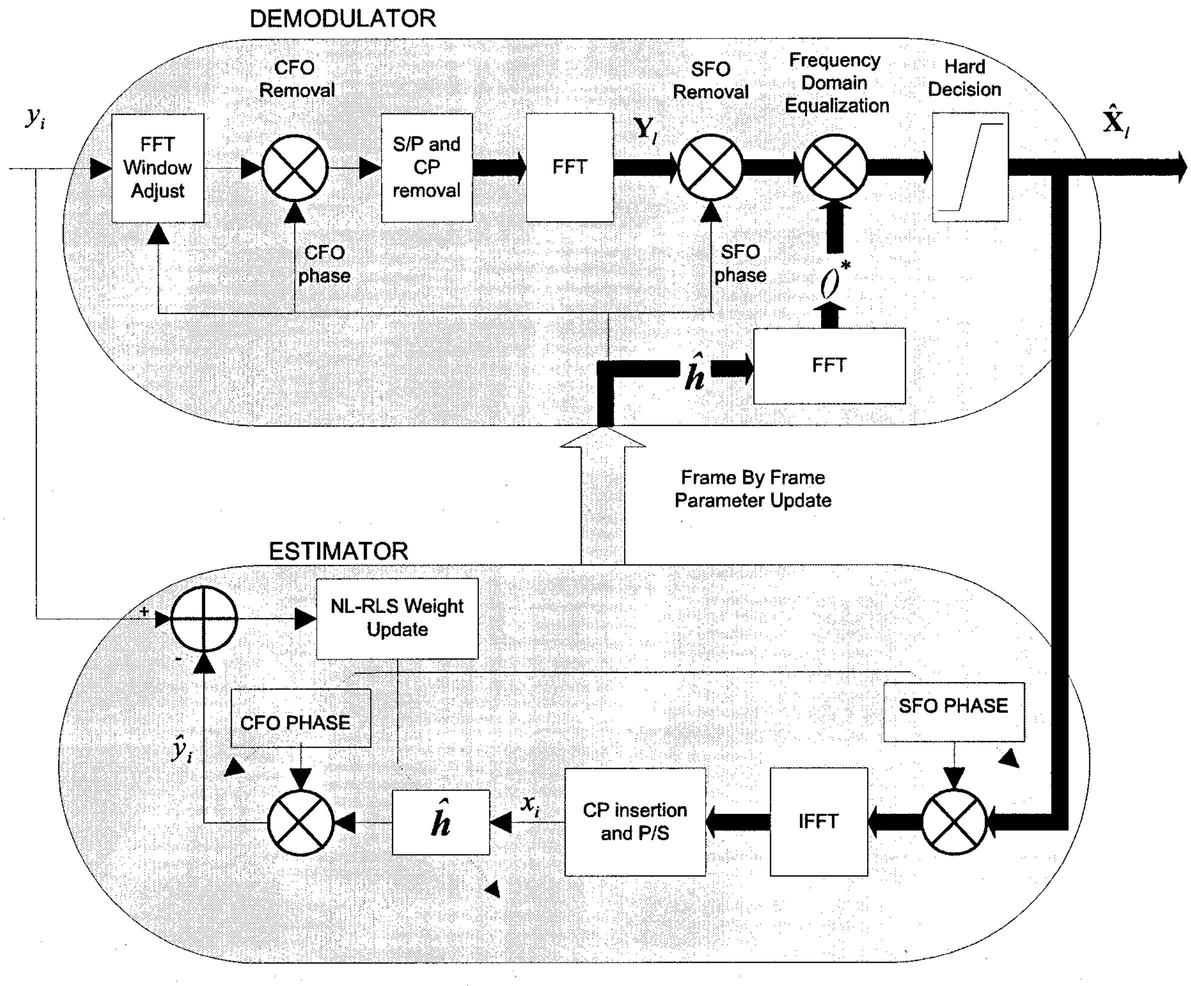

Fig. 4.3 OFDM Demodulator with the joint CFOSFOCE-C Algorithm

In the demodulator, FFT window adjustment occurs at the beginning of every frame in which inequality 4.15 is satisfied. The CFO is corrected in the time domain as in the case of the CFOCE-C algorithm.

In the frequency domain, a multiplication of the tones by $e^{-j\frac{2\pi k}{N}\hat{\phi}(N/2,l)}$ to correct for the CFO is added to the frequency domain equalization. This does not remove the ICI cause by SFO completely, however. Ideally, since $\widehat{\phi}$ increases linearly within a single OFDM symbol, the IFFT definition would have to be modified to remove the SFO correctly. However, since this would introduce considerable overhead in the receiver, and since η is assumed small, a fixed value of $\widehat{\phi}$ is assumed over a symbol. This fixed value is chosen to be the value that $\widehat{\phi}$ would have in the middle of the current frame in order to minimize the error that this simplifying assumption causes. For small values of N typical of burst-mode systems such as IEEE802.11a, this approximate removal of the effect of SFO is sufficient. For systems with larger FFT sizes, a method for correcting the SFO on a sample-by-sample basis is preferable. This is reserved for future study as mentioned in Chapter 5.

The estimator block functions on a sample-by-sample basis as in the case of the CFOCE-C algorithm. Although the expression for $\widehat{y}_{n,l}$ involves a circular convolution, linear convolution following the addition of the cyclic prefix to the transmit sequence is used to generate $\widehat{y}_{n,l}$ for simplified implementation, since the two methods are in fact equivalent. As a result, the portion of the estimator which generates $\widehat{y}_{n,l}$ is again an FIR filter, as in the case of the CFOCE-C algorithm, making it simple to change the taps of this filter at the generation of each new coefficient vector. The error used as input to the NL-RLS is generated only for the time domain samples corresponding to the data portion of the OFDM symbol.

The details of the receiver used in simulation of the estimator are identical to those described in Section 3.3.1 except for generation of the initial guess. To generate the initial guess within the preamble, the all-zero coefficient vector is first used. For the first long training symbol, the gradient for the CFO and SFO parameters is set to zero. For the second long training symbol, the gradient with respect to η and ϕ only are forced to zero, which allows adaptation of the CFO parameters and refinement of the channel. Finally, when the data phase begins, the gradient as computed in Appendix C is used.

4.2.3 Timing Parameter Damping

The receiver described in the previous section can be shown by simulation to have timing adjustments in the frequency domain that are too sensitive to the error used in the NL-RLS update. This sensitivity results from the combination of having the IFFT in the non-linear description of the system, and using the same value of $\widehat{\phi}$ to perform SFO compensation for all samples in the same OFDM symbol. The observable consequence of this sensitivity is that the estimate of the SFO parameters, although unbiased, varies widely around the actual value. In the receiver, this translates into an underdamped oscillation of each received subcarrier constellation.

To reduce the amplitude of these oscillations, a damping mechanism was introduced into the estimator. This mechanism was implemented using two modifications to the joint CFOSFOCE-C algorithm. Firstly, the estimator is made to track larger values of the timing parameters by modifying the gradient expressions so that the unknowns being estimated are $\Gamma\widehat{\eta}$ and $\Gamma\widehat{\phi}$. This is described in Appendix D. Secondly, the change in $\Gamma\widehat{\eta}$ computed by the NL-RLS at each iteration was reduced by dividing it by a factor of Ω. The values of Γ and Ω which produced the best damping over a wide range of SFO's was $\Gamma = 1000$ and $\Omega = 100$. These values are used in the performance evaluation of the estimator.

4.3 Performance Evaluation of the Estimator

The CRLB is derived for the new signal model presented in this chapter that accounts for a SFO. In addition, the BER performance of a receiver based on this joint estimator is compared with another representative method to evaluate the impact of the two main contributions of the estimator, namely the joint estimation and the time domain modeling of all synchronization and channel parameters.

4.3.1 CRLB for the Joint Estimator

The derivation of the elements of the FIM and the CRLB for the joint estimator is presented in Appendix E. Figures 4.4, 4.5 and 4.6 below show the variance of the estimators of the CFO, SFO and CIR respectively for an exponentially decaying Rayleigh fading channel with SNR of 35dB. The variance of each is compared to the CRLB. Both the CFO and SFO variance show oscillation since the estimates tend to be unbiased at these instances, owing to the introduction of θ and ϕ in tracking the CFO and SFO. The approximated compensation for the SFO, and the introduction of damping also contributes to making the variance of these quantities considerably higher than the CRLB. Despite oscillations in the frequency offset variance, the channel estimation remains very close to the CRLB throughout the duration of the packet.

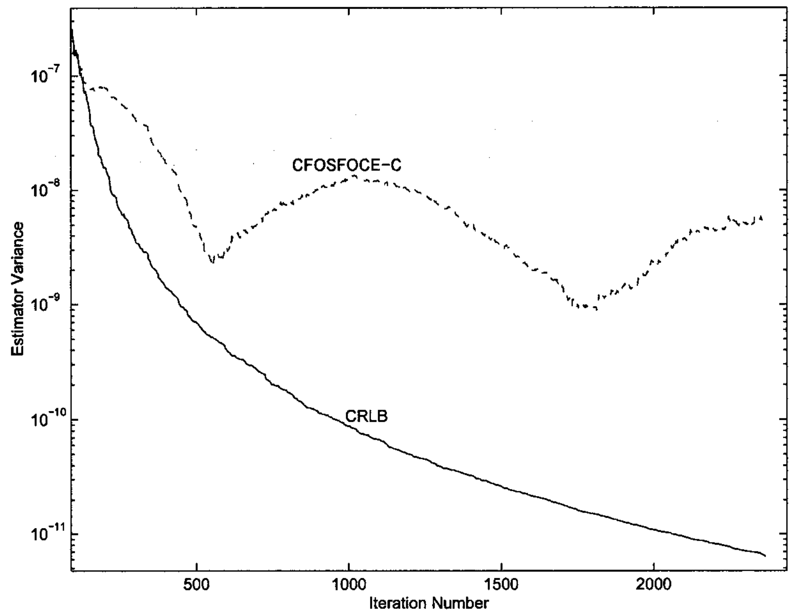

Fig. 4.4 CFO Variance versus Time

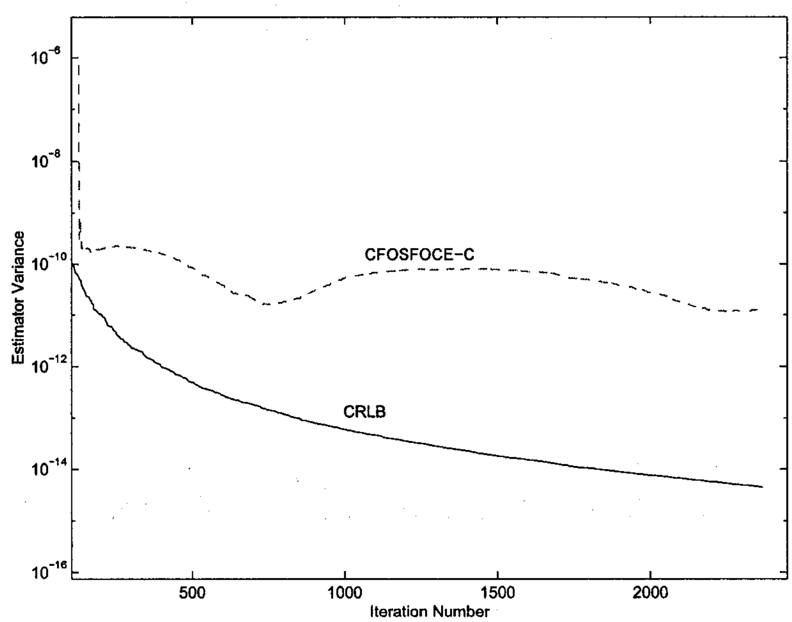

Fig. 4.5 SFO Variance versus Time

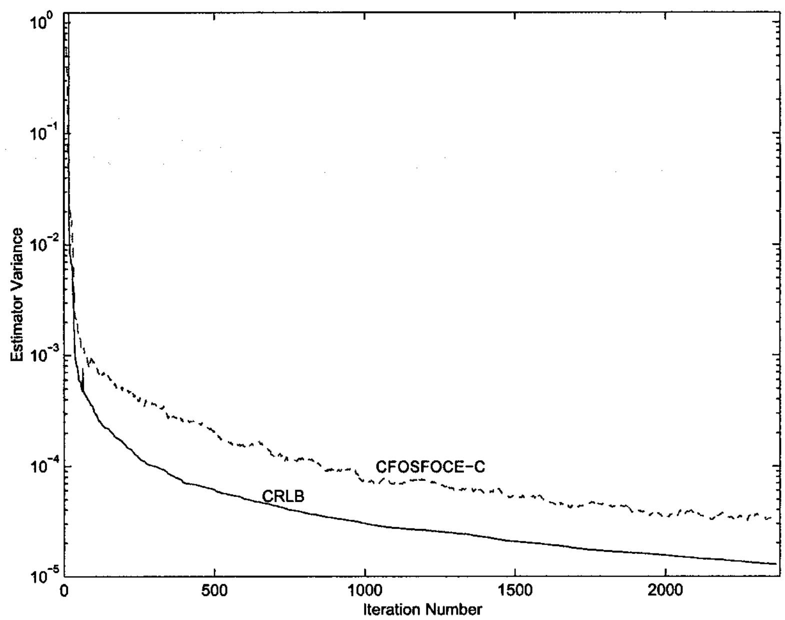

Fig. 4.6 CIR Variance versus Time

4.3.2 Performance in a Practical System

The CFO and SFO estimates from the CFOSFOCE-C method tend to have a large variance when compared to the CRLB due to the use of tracking. Use of tracking is required in order to use the NL-RLS to estimate the frequency offsets using a time domain model. Despite this large variance, the performance of the joint CFOSFOCE-C method remains superior to existing joint estimation methods which consider the effects of CFO and SFO in the frequency domain only. The CFOSFOCE-C also has the distinct advantage that it can inherently track drifts in the optimal position of the FFT window.

The gain of utilizing a time domain model is evaluated by comparing the CFOSFOCE-C method to a two-dimensional least squares joint estimate of the CFO and SFO presented in [7]. This method, referred to in the remainder of this thesis as Method 3, models the effect of the CFO and SFO in frequency domain, but simplifies the model to ignore ICI in order to make the estimation problem linear. Estimation is done by assuming that the phase difference between the kth tones of two adjacent symbols can be expressed as

$$\vartheta_k \approx \frac{2\pi\epsilon N_s}{N} + \frac{2\pi\eta N_s k}{N} \tag{4.16}$$

Although frequency offset correction is not discussed in [7], since the model considers only the frequency domain compensation by rotation will be the method of correction assumed. Finally, since [7] does not discuss channel estimation, and given the low variance of the channel estimates by the CFOSFOCE-C method observed in Section 4.3.1, perfect channel knowledge is assumed when simulating Method 3.

Figures 4.7 and 4.8 show the BER performance of the CFOSFOCE-C method and Method 3 described above for both AWGN and exponentially decaying Rayleigh fading channels with CFO of 3.2×10^{-3} and SFO of 5×10^{-5}. These values of the frequency offset represent approximately 3 times the allowable tolerance of the oscillator clocks in an IEEE802.11 system as specified in [14]. The given SFO is also sufficient to produce a one sample drift in the FFT window so that the window tracking portion of the algorithm is also tested.

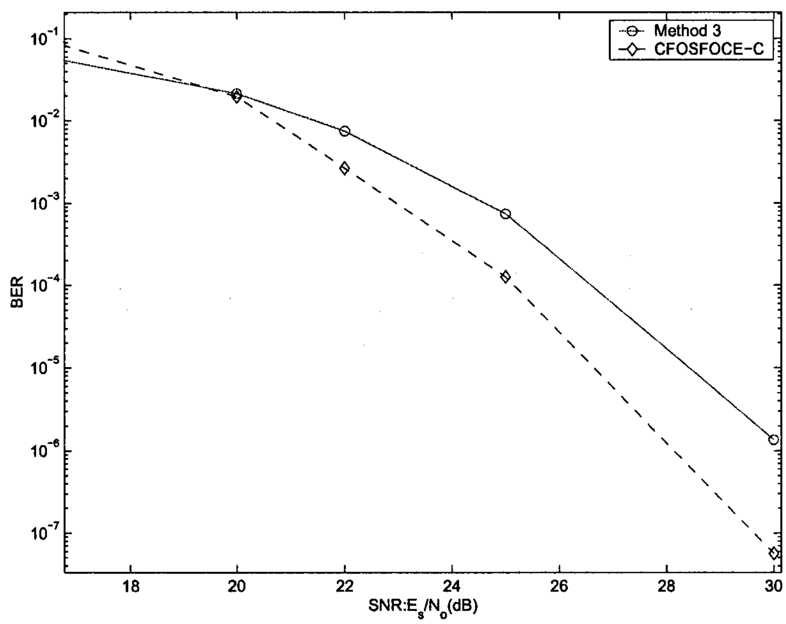

Fig. 4.7 BER versus SNR for Different Estimation Methods in AWGN with SFO

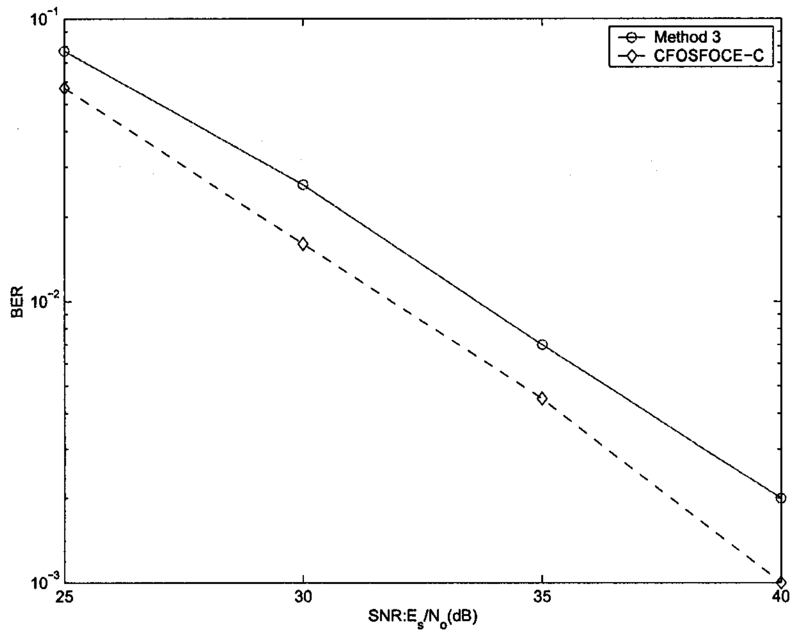

Fig. 4.8 BER versus SNR for Different Estimation Methods in Rayleigh Channel with SFO

Even in the case where perfect channel knowledge is available to Method 3, the CFOSFOCE-C method shows a gain of at least 1.5 dB for BERs below 10^{-3} in an AWGN channel, where ICI is the dominant distortion. The gain increases for larger SNR as expected. A gain of at least 1.5 dB is maintained for an exponentially decaying Rayleigh fading channel as well. This gain shows the improvement of the CFOSFOCE-C algorithm despite ignoring initial samples of interference in the signal model derived in Section 4.1 as well as the approximate compensation scheme discussed in Section 4.2.2.

4.4 Chapter Summary

In this chapter, the CFOCE-C of Chapter 3 was modified in order to account for the effects of SFO and clock drift. The resulting CFOSFOCE-C algorithm exhibits relatively low estimator variance for an FFT size of 64, considering the approximate compensation scheme used. The algorithm also shows a 1.5 dB gain in performance over the joint algorithm presented in [7] for both AWGN and exponentially decaying Rayleigh fading channels for practical values of CFO and SFO.

Chapter 5

Conclusion

The aim of this research was to develop a joint synchronization and channel estimation algorithm for burst mode OFDM. It was shown using analysis and simulation that a joint approach is superior to performing independent synchronization and channel estimation, and that a time domain estimation algorithm is superior to a frequency domain estimation algorithm due to improved estimator performance and increased robustness to decision feedback errors.

This chapter provides a summary of this thesis and suggests topics for future research.

5.1 Thesis Summary

The topic of synchronization and channel estimation in OFDM is presented in Chapter 1. The importance of synchronization in burst mode OFDM systems is outlined, and the problems related to performing synchronization and channel estimation separately are explained. The benefit of developing a joint algorithm for synchronization and channel estimation is given. The main objective and contributions of the thesis are also discussed.

Given the objective in Chapter 1, the background required to understand the importance of and difficulties in developing a joint synchronization and channel estimation algorithm for burst mode OFDM is presented in Chapter 2. The relationship between orthogonality and frequency domain equalization is demonstrated to show the impact of inaccurate synchronization on channel estimation. Well known mathematical expressions for the effect of synchronization offsets are presented in order to explain traditional synchronization techniques in the literature. The NL-RLS is introduced as the tool for development of a joint synchronization and channel estimation scheme which addresses the shortcomings of traditional joint methods.

In Chapter 3, the NL-RLS is used in the derivation of the joint CFOCE-C algorithm. We see that such a technique can have several applications in burst mode systems. Simulation results show that the algorithm provides a low variance estimate of the CIR, as well as a sufficiently low variance estimate of the CFO when the tracking nature of the algorithm is taken into consideration. Simulation also shows the advantage of a joint approach to synchronization and channel estimation in the presence of only CFO. The time domain approach utilized by the CFOCE-C is shown to be better that a frequency domain approach, primarily due to the reduced number of parameters estimated, and the robustness to decision feedback errors. A method for obtaining the initial guess for the CFOCE-C is presented, and the requirements on the preamble sequence length, and the CFO supported are given. The CFOCE-C maintains a 2dB gain over the best of the two methods presented in this section for an initial CFO of up to 10^{-2}.

In Chapter 4 the sensitivity of the CFOCE-C to SFO is addressed by derivation of the CFOSFOCE-C algorithm, which takes into account SFO as well as FFT window drift cause by SFO. Simulation results are obtained by using a simulation model for the effect of SFO that is also derived in this chapter. These results show a performance gain of at least 2dB over a joint estimation algorithm which uses a linear estimation model. The CFOSFOCE-C algorithm is also shown to have low CIR estimate variance with respect to the CRLB, while the CFO and SFO variances are considerably low when the nature of the algorithm is considered.

5.2 Future Research Work

The joint synchronization and channel estimation schemes developed in this thesis are promising for use in burst mode OFDM systems. Some suggestions for future research in the context of the work presented in this thesis are listed below.

- This thesis presents only a limited analysis of stability and steady state performance due to the difficulty in deriving the correlation matrix of the weight error vector. This complexity arises due to the dependence of the input vector to the CRLS (which is the actually the gradient of the non-linear function) and the current estimate of the weight vector. Further work can be done to overcome this difficulty and characterize the convergence and steady state behavior of the CFOCE-C algorithm more precisely. An analysis of the convergence and steady state behavior of the CFOSFOCE-C can then also be performed.

- The RLS algorithm is known to be unstable under finite precision arithmetic. A study of the stability of the NL-RLS, and of the joint synchronization and channel estimation algorithms presented in this thesis under finite precision arithmetic would be beneficial in order to allow application of these algorithms in a practical system. For a software-based implementation of the NL-RLS, such an analysis is not necessary and the results obtained in this thesis are valid.

- This thesis deals with burst mode systems, in which case the channel parameters and frequency offsets are assumed fixed for a single burst. The effects on the presented algorithms of variations in the channel and frequency offsets during the bursts is beyond the scope of this thesis. However, this analysis could be beneficial in the development of joint synchronization and channel estimation techniques for continuous mode systems.

- Along these lines, the feasibility of switching from NL-RLS to a non-linear version of the LMS once convergence is achieved can be evaluated. An LMS-type algorithm during the data phase of the burst may equip the CFOCE-C and CFOSFOCE-C algorithms with better tracking ability, as noted in [44]. Again, such an analysis would be beneficial in the study of synchronization and channel estimation for burst mode systems, but is unnecessary for analyzing burst mode systems.

- Compensation for the SFO in Chapter 4 was done by assuming the same phase rotation for all samples in the same OFDM symbol. In other words, while estimation considers the sample-by-sample effect of the SFO, SFO correction is performed only on a symbol-by-symbol basis, not a sample-by-sample basis, thus ignoring the effect of SFO within one symbol. Although this compensation is acceptable for small FFT sizes which are typical of most burst mode systems currently being used, the ICI for larger FFT sizes could be considerable. A modification of CFOSFOCE-C which compensates for this effect without adding too much complexity is desirable. Such a modification could be desirable for future high data rate applications that may use a larger FFT size.

- Both the CFOCE-C and CFOSFOCE-C algorithms have been developed for single-input, single-output (SISO) systems. Extension of these algorithms to a multi-input, multi-output (MIMO) system would require future work. Particularly, if joint detection is performed in a MIMO system, each receive antenna would have a different CIR estimate, but the same frequency offsets estimates. An extension of these algorithm to MIMO systems would have immediate applications in

IEEE802.16 [45] which specifies the use of multiple input single output synchronization and channel estimation using a single preamble.

Appendix A

Gradient Expressions for Joint CFOCE-C Method

The non-linear function for estimating the received sample y_n at time n is

$$f(\boldsymbol{x}_i, \widehat{\boldsymbol{w}}) = e^{j\left(\hat{\theta}+\frac{2\pi}{N}\hat{\epsilon}\right)} \sum_{r=0}^{v-1} \hat{h}_r x_{i-r} \quad ; i = 0, 1, \ldots, \mathcal{M} - 1. \tag{A.1}$$

The gradient vector consists of the vector of partial derivatives of the non-linear function with respect to each of the variables. The partial derivatives are given below.

$$\boldsymbol{\nabla} f(\boldsymbol{x}_i, \widehat{\boldsymbol{w}}) = \left[\begin{array}{cccc} \frac{\partial f(\boldsymbol{x}_i, \hat{\boldsymbol{w}})}{\partial \hat{h}_0}, .., & \frac{\partial f(\boldsymbol{x}_i, \hat{\boldsymbol{w}})}{\partial \hat{h}_{v-1}}, & \frac{\partial f(\boldsymbol{x}_i, \hat{\boldsymbol{w}})}{\partial \hat{\epsilon}}, & \frac{\partial f(\boldsymbol{x}_i, \hat{\boldsymbol{w}})}{\partial \hat{\theta}} \end{array} \right]^T \tag{A.2}$$

$$\frac{\partial f(\boldsymbol{x}_i, \widehat{\boldsymbol{w}})}{\partial \hat{h}_p} = e^{j\left(\hat{\theta}+\frac{2\pi}{N}\hat{\epsilon}\right)} x_{i-p} \quad ; p = 0, 1, \ldots, v - 1 \tag{A.3}$$

$$\frac{\partial f(\boldsymbol{x}_i, \widehat{\boldsymbol{w}})}{\partial \hat{\epsilon}} = j\frac{2\pi}{N} e^{j\left(\hat{\theta}+\frac{2\pi}{N}\hat{\epsilon}\right)} \sum_{r=0}^{v-1} \hat{h}_r x_{i-r} \tag{A.4}$$

$$\frac{\partial f(\boldsymbol{x}_i, \widehat{\boldsymbol{w}})}{\partial \hat{\theta}} = j e^{j\left(\hat{\theta}+\frac{2\pi}{N}\hat{\epsilon}\right)} \sum_{r=0}^{v-1} \hat{h}_i x_{i-r} \tag{A.5}$$

Appendix B

CRLB Derivation for Joint CFOCE-C Method

The data model for the received time domain samples (before removal of the cyclic prefix) used to derive the CRLB for the estimator is

$$y_i = e^{j\left(\theta_0 + \frac{2\pi\epsilon}{N}(i+1)\right)} \sum_{r=0}^{v-1} h_r x_{i-r} + w_i; \quad i = 0, 1, \ldots, \mathcal{M}-1 \tag{B.1}$$

The noise samples ω_i are complex independant Gaussian with variance σ^2 so the likelihood function is given by

$$\begin{aligned} L &= p\left(y_0, y_1, \ldots, y_{\mathcal{M}-1} \mid \epsilon, \theta_0, \boldsymbol{h}\right) \\ &= \frac{1}{\left(\pi\sigma^2\right)^{\mathcal{M}}} exp\left\{ -\frac{1}{\sigma^2} \sum_{i=0}^{\mathcal{M}-1} \left| y_i - e^{j\left(\theta_0 + \frac{2\pi\epsilon}{N}(i+1)\right)} \sum_{r=0}^{v-1} h_r x_{i-r} \right|^2 \right\} \end{aligned} \tag{B.2}$$

The second order partial derivatives of the log of the likelihood function in equation B.2 are given below.

$$\frac{\partial^2 ln(L)}{\partial \epsilon^2} = -\frac{2}{\sigma^2}\left(\frac{2\pi}{N}\right)^2 \sum_{i=0}^{\mathcal{M}-1} (i+1)^2 Re\left\{ y_i^* e^{j\left(\theta_0 + \frac{2\pi\epsilon}{N}(i+1)\right)} \sum_{r=0}^{v-1} h_r x_{i-r} \right\} \tag{B.3}$$

$$\frac{\partial^2 ln(L)}{\partial\epsilon\partial\theta_0} = -\frac{2}{\sigma^2}\left(\frac{2\pi}{N}\right)\sum_{i=0}^{\mathcal{M}-1}(i+1)Re\left\{y_i^* e^{j\left(\theta_0+\frac{2\pi\epsilon}{N}(i+1)\right)}\sum_{r=0}^{v-1}h_r x_{i-r}\right\} \tag{B.4}$$

$$\frac{\partial^2 ln(L)}{\partial\theta_0^2} = -\frac{2}{\sigma^2}\sum_{i=0}^{\mathcal{M}-1}Re\left\{y_i^* e^{j\left(\theta_0+\frac{2\pi\epsilon}{N}(i+1)\right)}\sum_{r=0}^{v-1}h_r x_{i-r}\right\} \tag{B.5}$$

$$\frac{\partial^2 ln(L)}{\partial Re\{h_q\}\partial\theta_0} = -\frac{2}{\sigma^2}\sum_{i=0}^{\mathcal{M}-1}Im\left\{y_i^* e^{j\left(\theta_0+\frac{2\pi\epsilon}{N}(i+1)\right)}x_{i-q}\right\} \tag{B.6}$$

$$\frac{\partial^2 ln(L)}{\partial Re\{h_q\}\partial\epsilon} = -\frac{2}{\sigma^2}\left(\frac{2\pi}{N}\right)\sum_{i=0}^{\mathcal{M}-1}(i+1)Im\left\{y_i^* e^{j\left(\theta_0+\frac{2\pi\epsilon}{N}(i+1)\right)}x_{i-q}\right\} \tag{B.7}$$

$$\frac{\partial^2 ln(L)}{\partial Im\{h_q\}\partial\theta_0} = -\frac{2}{\sigma^2}\sum_{i=0}^{\mathcal{M}-1}Re\left\{y_i^* e^{j\left(\theta_0+\frac{2\pi\epsilon}{N}(i+1)\right)}x_{i-q}\right\} \tag{B.8}$$

$$\frac{\partial^2 ln(L)}{\partial Im\{h_q\}\partial\epsilon} = -\frac{2}{\sigma^2}\left(\frac{2\pi}{N}\right)\sum_{i=0}^{\mathcal{M}-1}(i+1)Re\left\{y_i^* e^{j\left(\theta_0+\frac{2\pi\epsilon}{N}(i+1)\right)}x_{i-q}\right\} \tag{B.9}$$

$$\frac{\partial^2 ln(L)}{\partial Re\{h_q\}^2} = -\frac{2}{\sigma^2}\sum_{i=0}^{\mathcal{M}-1}|x_{i-q}|^2 \tag{B.10}$$

$$\frac{\partial^2 ln(L)}{\partial Im\{h_q\}^2} = -\frac{2}{\sigma^2}\sum_{i=0}^{\mathcal{M}-1}|x_{i-q}|^2 \tag{B.11}$$

$$\frac{\partial^2 ln(L)}{\partial Re\{h_q\}\partial Im\{h_q\}} = 0 \tag{B.12}$$

$$\frac{\partial^2 ln(L)}{\partial Re\{h_q\}\partial Re\{h_p\}_{q\neq p}} = -\frac{2}{\sigma^2}\sum_{i=0}^{\mathcal{M}-1}Re\left\{x_{i-q}x_{i-p}^*\right\} \tag{B.13}$$

$$\frac{\partial^2 ln(L)}{\partial Im\{h_q\}\partial Im\{h_p\}_{q\neq p}} = -\frac{2}{\sigma^2}\sum_{i=0}^{\mathcal{M}-1}Re\left\{x_{i-q}x_{i-p}^*\right\} \tag{B.14}$$

$$\frac{\partial^2 ln(L)}{\partial Re\{h_q\}\partial Im\{h_p\}_{q\neq p}} = -\frac{2}{\sigma^2}\sum_{i=0}^{\mathcal{M}-1}Im\left\{x_{i-q}x_{i-p}^*\right\} \tag{B.15}$$

The elements of the FIM are obtained by taking expectation of the above second order partial derivatives. The entries the negatives of the expectations given below.

$$E\left\{\frac{\partial^2 ln(L)}{\partial \epsilon^2}\right\} = -\frac{2}{\sigma^2}\left(\frac{2\pi}{N}\right)^2 \sum_{i=0}^{\mathcal{M}-1}\left\{(i+1)^2\left|\sum_{r=0}^{v-1} h_r x_{i-r}\right|^2\right\} \tag{B.16}$$

$$E\left\{\frac{\partial^2 ln(L)}{\partial \epsilon \partial \theta_0}\right\} = -\frac{2}{\sigma^2}\left(\frac{2\pi}{N}\right) \sum_{i=0}^{\mathcal{M}-1}\left\{(i+1)\left|\sum_{r=0}^{v-1} h_r x_{i-r}\right|^2\right\} \tag{B.17}$$

$$E\left\{\frac{\partial^2 ln(L)}{\partial \theta_0^2}\right\} = -\frac{2}{\sigma^2} \sum_{i=0}^{\mathcal{M}-1}\left\{\left|\sum_{r=0}^{v-1} h_r x_{i-r}\right|^2\right\} \tag{B.18}$$

$$E\left\{\frac{\partial^2 ln(L)}{\partial Re\{h_q\} \partial \theta_0}\right\} = -\frac{2}{\sigma^2} \sum_{i=0}^{\mathcal{M}-1} Im\left\{x_{i-q}\sum_{r=0}^{v-1} h_r^* x_{i-r}^*\right\} \tag{B.19}$$

$$E\left\{\frac{\partial^2 ln(L)}{\partial Re\{h_q\} \partial \epsilon}\right\} = -\frac{2}{\sigma^2}\left(\frac{2\pi}{N}\right) \sum_{i=0}^{\mathcal{M}-1}(i+1) Im\left\{x_{i-q}\sum_{r=0}^{v-1} h_r^* x_{i-r}^*\right\} \tag{B.20}$$

$$E\left\{\frac{\partial^2 ln(L)}{\partial Im\{h_q\} \partial \theta_0}\right\} = -\frac{2}{\sigma^2} \sum_{i=0}^{\mathcal{M}-1} Re\left\{x_{i-q}\sum_{r=0}^{v-1} h_r^* x_{i-r}^*\right\} \tag{B.21}$$

$$E\left\{\frac{\partial^2 ln(L)}{\partial Im\{h_q\} \partial \epsilon}\right\} = -\frac{2}{\sigma^2}\left(\frac{2\pi}{N}\right) \sum_{i=0}^{\mathcal{M}-1}(i+1) Re\left\{x_{i-q}\sum_{r=0}^{v-1} h_r^* x_{i-r}^*\right\} \tag{B.22}$$

$$E\left\{\frac{\partial^2 ln(L)}{\partial Re\{h_q\}^2}\right\} = -\frac{2}{\sigma^2} \sum_{i=0}^{\mathcal{M}-1} |x_{i-q}|^2 \tag{B.23}$$

$$E\left\{\frac{\partial^2 ln(L)}{\partial Im\{h_q\}^2}\right\} = -\frac{2}{\sigma^2} \sum_{i=0}^{\mathcal{M}-1} |x_{i-q}|^2 \tag{B.24}$$

$$E\left\{\frac{\partial^2 ln(L)}{\partial Re\{h_q\} \partial Im\{h_q\}}\right\} = 0 \tag{B.25}$$

$$E\left\{\frac{\partial^2 ln(L)}{\partial Re\{h_q\} \partial Re\{h_p\}_{q \neq p}}\right\} = -\frac{2}{\sigma^2} \sum_{i=0}^{\mathcal{M}-1} Re\left\{x_{i-q} x_{i-p}^*\right\} \tag{B.26}$$

$$E\left\{\frac{\partial^2 ln(L)}{\partial Im\{h_q\} \partial Im\{h_p\}_{q \neq p}}\right\} = -\frac{2}{\sigma^2} \sum_{i=0}^{\mathcal{M}-1} Re\left\{x_{i-q} x_{i-p}^*\right\} \tag{B.27}$$

$$E\left\{\frac{\partial^2 ln(L)}{\partial Re\{h_q\} \partial Im\{h_p\}_{q \neq p}}\right\} = -\frac{2}{\sigma^2} \sum_{i=0}^{\mathcal{M}-1} Im\left\{x_{i-q} x_{i-p}^*\right\} \tag{B.28}$$

Appendix C

Gradient Expressions for Joint CFOSFOCE-C Method

The non-linear function for estimating the received data samples (after removal of the cyclic prefix) is given by

$$f(\dot{\boldsymbol{x}}_{m_{n,l}}, \widehat{\boldsymbol{w}}) = e^{j\left(\hat{\theta}+\frac{2\pi}{N}\hat{\epsilon}\right)} \left\langle \dot{\boldsymbol{x}}_{m_{n,l}} \otimes \bar{\boldsymbol{h}} \right\rangle_n \tag{C.1}$$

where

$$\dot{\boldsymbol{x}}_{m_{n,l}} \equiv \left\{ \frac{1}{N} \sum_{k=0}^{N-1} X_{k,l} e^{j\frac{2\pi k i}{N}} e^{j\frac{2\pi k}{N}(\hat{\eta}+\hat{\phi})} \right\}_{i=0,1,\ldots,N-1} \tag{C.2}$$

The gradient vector of the non-linear expression with respect to the coefficient vector is given below.

$$\boldsymbol{\nabla} f(\dot{\boldsymbol{x}}_{m_{n,l}}, \widehat{\boldsymbol{w}}) = \begin{bmatrix} \frac{\partial f(\dot{\boldsymbol{x}}_{m_{n,l}}, \hat{\boldsymbol{w}})}{\partial \hat{\bar{h}}_0} \\ \frac{\partial f(\dot{\boldsymbol{x}}_{m_{n,l}}, \hat{\boldsymbol{w}})}{\partial \hat{\bar{h}}_1} \\ \cdot \\ \cdot \\ \frac{\partial f(\dot{\boldsymbol{x}}_{m_{n,l}}, \hat{\boldsymbol{w}})}{\partial \hat{\bar{h}}_{v-1}} \\ \frac{\partial f(\dot{\boldsymbol{x}}_{m_{n,l}}, \hat{\boldsymbol{w}})}{\partial \hat{\epsilon}} \\ \frac{\partial f(\boldsymbol{x}_{m_{n,l}}, \hat{\boldsymbol{w}})}{\partial \hat{\theta}} \\ \frac{\partial f(\boldsymbol{x}_{m_{n,l}}, \hat{\boldsymbol{w}})}{\partial \hat{\eta}} \\ \frac{\partial f(\boldsymbol{x}_{m_{n,l}}, \hat{\boldsymbol{w}})}{\partial \hat{\phi}} \end{bmatrix} \tag{C.3}$$

$$\frac{\partial f(\dot{\boldsymbol{x}}_{m_{n,l}}, \hat{\boldsymbol{w}})}{\partial \hat{\bar{h}}_p} = e^{j\left(\hat{\theta}+\frac{2\pi}{N}\hat{\epsilon}\right)} \frac{\partial \left\langle \dot{\boldsymbol{x}}_{m_{n,l}} \otimes \bar{\boldsymbol{h}} \right\rangle_n}{\partial \bar{h}_p} \equiv e^{j\left(\hat{\theta}+\frac{2\pi}{N}\hat{\epsilon}\right)} \dot{x}^p_{m_{n,l}} \quad ; p = 0, 1, \ldots, v-1 \tag{C.4}$$

$$\frac{\partial f(\dot{\boldsymbol{x}}_{m_{n,l}}, \widehat{\boldsymbol{w}})}{\partial \hat{\epsilon}} = j\frac{2\pi}{N} e^{j\left(\hat{\theta}+\frac{2\pi}{N}\hat{\epsilon}\right)} \left\langle \dot{\boldsymbol{x}}_{m_{n,l}} \otimes \bar{\boldsymbol{h}} \right\rangle_n \tag{C.5}$$

$$\frac{\partial f(\dot{\boldsymbol{x}}_{m_{n,l}}, \widehat{\boldsymbol{w}})}{\partial \hat{\theta}} = j e^{j\left(\hat{\theta}+\frac{2\pi}{N}\hat{\epsilon}\right)} \left\langle \dot{\boldsymbol{x}}_{m_{n,l}} \otimes \bar{\boldsymbol{h}} \right\rangle_n \tag{C.6}$$

$$\frac{\partial f(\dot{\boldsymbol{x}}_{m_{n,l}}, \widehat{\boldsymbol{w}})}{\partial \hat{\eta}} = e^{j\left(\hat{\theta}+\frac{2\pi}{N}\hat{\epsilon}\right)} \left\langle \left\{ \frac{1}{N} \sum_{k=0}^{N-1} j\frac{2\pi k}{N} X_{k,l} e^{j\frac{2\pi k i}{N}} e^{j\frac{2\pi k}{N}(\eta+\phi)} \right\}_{i=0,1,\ldots,N-1} \otimes \bar{\boldsymbol{h}} \right\rangle_n \tag{C.7}$$

$$\frac{\partial f(\dot{\boldsymbol{x}}_{m_{n,l}}, \widehat{\boldsymbol{w}})}{\partial \hat{\phi}} = e^{j\left(\hat{\theta}+\frac{2\pi}{N}\hat{\epsilon}\right)} \left\langle \left\{ \frac{1}{N} \sum_{k=0}^{N-1} j\frac{2\pi k}{N} X_{k,l} e^{j\frac{2\pi k i}{N}} e^{j\frac{2\pi k}{N}(\eta+\phi)} \right\}_{i=0,1,\ldots,N-1} \otimes \bar{\boldsymbol{h}} \right\rangle_n \tag{C.8}$$

Appendix D

Gradient Expressions for Joint CFOSFOCE-C Method with Damped Implentation

When damping descibed in section 4.2.3 is applied, the non-linear expression for estimating the received samples is given by equation C.1 with the modification given below:

$$\dot{\boldsymbol{x}}_{m_{n,l}} \equiv \left\{ \frac{1}{N} \sum_{k=0}^{N-1} X_{k,l} e^{j\frac{2\pi k i}{N}} e^{j\frac{2\pi k}{N}(\frac{\hat{\eta}'}{\Gamma}+\frac{\hat{\phi}'}{\Gamma})} \right\}_{i=0,1,\ldots,N-1} \tag{D.1}$$

where

$$\widehat{\eta}' = \Gamma\widehat{\eta} \tag{D.2}$$

$$\widehat{\phi}' = \Gamma\widehat{\phi} \tag{D.3}$$

The coefficent vector being tracked in this case is

$$\widehat{\boldsymbol{w}}_{(i)} = \left[\; \widehat{h}_{0_{(i)}}, \widehat{h}_{1_{(i)}}, .., \widehat{h}_{v-1_{(i)}}, \widehat{\epsilon}_{(i)}, \widehat{\theta}_{(i)}, \widehat{\eta}'_i, \widehat{\phi}'_i \; \right]^T \tag{D.4}$$

The gradient vector of the non-linear expression with respect to this modified coefficient vector is given below.

$$\nabla f(\dot{\boldsymbol{x}}_{m_{n,l}}, \widehat{\boldsymbol{w}}) = \begin{bmatrix} \frac{\partial f(\dot{\boldsymbol{x}}_{m_{n,l}}, \hat{\boldsymbol{w}})}{\partial \hat{\bar{h}}_0} \\ \frac{\partial f(\dot{\boldsymbol{x}}_{m_{n,l}}, \hat{\boldsymbol{w}})}{\partial \hat{\bar{h}}_1} \\ \cdot \\ \cdot \\ \frac{\partial f(\dot{\boldsymbol{x}}_{m_{n,l}}, \hat{\boldsymbol{w}})}{\partial \hat{\bar{h}}_{v-1}} \\ \frac{\partial f(\dot{\boldsymbol{x}}_{m_{n,l}}, \hat{\boldsymbol{w}})}{\partial \hat{\epsilon}} \\ \frac{\partial f(\boldsymbol{x}_{m_{n,l}}, \hat{\boldsymbol{w}})}{\partial \hat{\theta}} \\ \frac{\partial f(\boldsymbol{x}_{m_{n,l}}, \hat{\boldsymbol{w}})}{\partial \hat{\eta}'} \\ \frac{\partial f(\boldsymbol{x}_{m_{n,l}}, \hat{\boldsymbol{w}})}{\partial \hat{\phi}'} \end{bmatrix} \tag{D.5}$$

$$\frac{\partial f(\dot{\boldsymbol{x}}_{m_{n,l}}, \hat{\boldsymbol{w}})}{\partial \hat{\bar{h}}_p} = e^{j\left(\hat{\theta}+\frac{2\pi}{N}\hat{\epsilon}\right)} \frac{\partial \left\langle \dot{\boldsymbol{x}}_{m_{n,l}} \otimes \bar{\boldsymbol{h}} \right\rangle_n}{\partial \bar{h}_p} \equiv e^{j\left(\hat{\theta}+\frac{2\pi}{N}\hat{\epsilon}\right)} \dot{x}^p_{m_{n,l}} \quad ; p = 0, 1, \ldots, v-1 \tag{D.6}$$

$$\frac{\partial f(\dot{\boldsymbol{x}}_{m_{n,l}}, \widehat{\boldsymbol{w}})}{\partial \hat{\epsilon}} = j\frac{2\pi}{N} e^{j\left(\hat{\theta}+\frac{2\pi}{N}\hat{\epsilon}\right)} \left\langle \dot{\boldsymbol{x}}_{m_{n,l}} \otimes \bar{\boldsymbol{h}} \right\rangle_n \tag{D.7}$$

$$\frac{\partial f(\dot{\boldsymbol{x}}_{m_{n,l}}, \widehat{\boldsymbol{w}})}{\partial \hat{\theta}} = j e^{j\left(\hat{\theta}+\frac{2\pi}{N}\hat{\epsilon}\right)} \left\langle \dot{\boldsymbol{x}}_{m_{n,l}} \otimes \bar{\boldsymbol{h}} \right\rangle_n \tag{D.8}$$

$$\frac{\partial f(\dot{\boldsymbol{x}}_{m_{n,l}}, \widehat{\boldsymbol{w}})}{\partial \hat{\eta}'} = e^{j\left(\hat{\theta}+\frac{2\pi}{N}\hat{\epsilon}\right)} \left\langle \left\{ \frac{1}{N} \sum_{k=0}^{N-1} j \frac{2\pi k}{\Gamma N} X_{k,l} e^{j\frac{2\pi k i}{N}} e^{j\frac{2\pi k}{N}(\eta+\phi)} \right\}_{i=0,1,\ldots,N-1} \otimes \bar{\boldsymbol{h}} \right\rangle_n \tag{D.9}$$

$$\frac{\partial f(\dot{\boldsymbol{x}}_{m_{n,l}}, \widehat{\boldsymbol{w}})}{\partial \hat{\phi}'} = e^{j\left(\hat{\theta}+\frac{2\pi}{N}\hat{\epsilon}\right)} \left\langle \left\{ \frac{1}{N} \sum_{k=0}^{N-1} j \frac{2\pi k}{\Gamma N} X_{k,l} e^{j\frac{2\pi k i}{N}} e^{j\frac{2\pi k}{N}(\eta+\phi)} \right\}_{i=0,1,\ldots,N-1} \otimes \bar{\boldsymbol{h}} \right\rangle_n \tag{D.10}$$

Appendix E

CRLB Derivation for Joint CFOSFOCE-C Method

The data model for the received data samples (after removal of the cyclic prefix) used to derive the CRLB for the estimator is

$$\begin{aligned} y_{n,l} &= e^{j\left(\theta_0+\frac{2\pi\epsilon}{N}(m_{n,l}+1)\right)} \left\langle \left\{ \frac{1}{N}\sum_{k=0}^{N-1} X_{k,l} e^{j\frac{2\pi k i}{N}} e^{j\frac{2\pi k}{N}(\eta(m_{0,l}+i+1)+\phi_0)} \right\}_{i=0,1,\ldots,N-1} \otimes \bar{\boldsymbol{h}} \right\rangle_n + w_{m_{n,l}} \\ &= e^{j\left(\theta_0+\frac{2\pi\epsilon}{N}(m_{n,l}+1)\right)} \left\langle \dot{\boldsymbol{x}}_{m_{n,l}} \otimes \bar{\boldsymbol{h}} \right\rangle_n + w_{m_{n,l}} \end{aligned} \tag{E.1}$$

where, for simplification purposes, the following symbol has been introduced to represent the sequence involved in the convolution with the channel.

$$\dot{\boldsymbol{x}}_{m_{n,l}} \equiv \left\{ \frac{1}{N}\sum_{k=0}^{N-1} X_{k,l} e^{j\frac{2\pi k i}{N}} e^{j\frac{2\pi k}{N}(\eta(m_{0,l}+i+1)+\phi_0)} \right\}_{i=0,1,\ldots,N-1} \tag{E.2}$$

The allowable values of $m_{n,l}$ in equations E.1 and E.2 are given by the expression

$$m_{n,l} = \left\{m^1, m^2, \ldots, m^{\mathcal{M}}\right\} = \left\{lN_s + N_g + n \mid n\epsilon\left[0, N-1\right], l\epsilon\mathcal{N}\right\}. \tag{E.3}$$

The following symbols related to the sequence $\dot{\boldsymbol{x}}_{m_{n,l}}$ will also be of use in simplifying future expressions.

$$\frac{\partial \dot{\boldsymbol{x}}_{m_{n,l}}}{\partial \eta} \equiv \left\{ \frac{1}{N} \sum_{k=0}^{N-1} j \left(\frac{2\pi k}{N} \right) (m_{0,l} + i + 1) X_{k,l} e^{j\frac{2\pi k i}{N}} e^{j\frac{2\pi k}{N}(\eta(m_{0,l}+i+1)+\phi_0)} \right\}_{i=0,1,\ldots,N-1} \tag{E.4}$$

$$\frac{\partial \dot{\boldsymbol{x}}_{m_{n,l}}}{\partial \phi_0} \equiv \left\{ \frac{1}{N} \sum_{k=0}^{N-1} j \left(\frac{2\pi k}{N} \right) X_{k,l} e^{j\frac{2\pi k i}{N}} e^{j\frac{2\pi k}{N}(\eta(m_{0,l}+i+1)+\phi_0)} \right\}_{i=0,1,\ldots,N-1} \tag{E.5}$$

Given that the noise samples $\omega_{m_{n,l}}$ are complex, independant Gaussian samples with variance σ^2, the likelihood of the received samples is

$$\begin{aligned} L &= p\left(y_{m^1}, y_{m^2}, \ldots, y_{m^{\mathcal{M}}} \mid \epsilon, \theta_0, \eta, \phi_0, \bar{\boldsymbol{h}}\right) \\ &= \frac{1}{(\pi\sigma^2)^{\mathcal{M}}} exp \left\{ -\frac{1}{\sigma^2} \sum_{m_{n,l}=m^1}^{m_{\mathcal{M}}} \left| y_{n,l} - e^{j(\theta_0 + \frac{2\pi\epsilon}{N}(m_{n,l}+1))} \left\langle \dot{\boldsymbol{x}}_{m_{n,l}} \otimes \bar{\boldsymbol{h}} \right\rangle_n \right|^2 \right\} \end{aligned} \tag{E.6}$$

The second order partial derivatives of the log of the likelihood function in equation E.6 are given below.

$$\frac{\partial^2 ln(L)}{\partial Re\{\bar{h}_q\}^2} = -\frac{2}{\sigma^2} \sum_{m_{n,l}=m^1}^{m^{\mathcal{M}}} |\dot{x}^q_{m_{n,l}}|^2 \tag{E.7}$$

$$\frac{\partial^2 ln(L)}{\partial Im\{\bar{h}_q\}^2} = -\frac{2}{\sigma^2} \sum_{m_{n,l}=m^1}^{m^{\mathcal{M}}} |\dot{x}^q_{m_{n,l}}|^2 \tag{E.8}$$

$$\frac{\partial^2 ln(L)}{\partial Re\{\bar{h}_q\} Re\{\bar{h}_p\}}_{q \neq p} = -\frac{2}{\sigma^2} \sum_{m_{n,l}=m^1}^{m^{\mathcal{M}}} Re\{\dot{x}^q_{m_{n,l}} (\dot{x}^p_{m_{n,l}})^*\} \tag{E.9}$$

$$\frac{\partial^2 ln(L)}{\partial Im\{\bar{h}_q\} Im\{\bar{h}_p\}}_{q \neq p} = -\frac{2}{\sigma^2} \sum_{m_{n,l}=m^1}^{m^{\mathcal{M}}} Re\{\dot{x}^q_{m_{n,l}} (\dot{x}^p_{m_{n,l}})^*\} \tag{E.10}$$

$$\frac{\partial^2 ln(L)}{\partial Re\{\bar{h}_q\} Im\{\bar{h}_p\}}_{q \neq p} = -\frac{2}{\sigma^2} \sum_{m_{n,l}=m^1}^{m^{\mathcal{M}}} Im\{\dot{x}^q_{m_{n,l}} (\dot{x}^p_{m_{n,l}})^*\} \tag{E.11}$$

$$\frac{\partial^2 ln(L)}{\partial Re\{\bar{h}_q\} Im\{\bar{h}_q\}} = 0 \tag{E.12}$$

$$\frac{\partial^2 ln(L)}{\partial \epsilon^2} = -\frac{2}{\sigma^2} \sum_{m_{n,l}=m^1}^{m^{\mathcal{M}}} Re\left\{ \left(\frac{2\pi}{N}\right)^2 (m_{n,l}+1)^2 y_{n,l}^* \left\langle \dot{\boldsymbol{x}}_{m_{n,l}} \otimes \bar{\boldsymbol{h}} \right\rangle_n \right\} \tag{E.13}$$

$$\frac{\partial^2 ln(L)}{\partial \theta_0^2} = -\frac{2}{\sigma^2} \sum_{m_{n,l}=m^1}^{m^{\mathcal{M}}} Re\left\{ y_{n,l}^* \left\langle \dot{\boldsymbol{x}}_{m_{n,l}} \otimes \bar{\boldsymbol{h}} \right\rangle_n \right\} \tag{E.14}$$

$$\frac{\partial^2 ln(L)}{\partial \epsilon \partial \theta_0} = -\frac{2}{\sigma^2} \sum_{m_{n,l}=m^1}^{m^{\mathcal{M}}} Re\left\{ \left(\frac{2\pi}{N}\right) (m_{n,l}+1) y_{n,l}^* \left\langle \dot{\boldsymbol{x}}_{m_{n,l}} \otimes \bar{\boldsymbol{h}} \right\rangle_n \right\} \tag{E.15}$$

$$\begin{aligned} \frac{\partial^2 ln(L)}{\partial \eta^2} \quad &= -\frac{2}{\sigma^2} \sum_{m_{n,l}=m^1}^{m^{\mathcal{M}}} Re\left\{ -y_{n,l}^* \left\langle \frac{\partial^2 \dot{\boldsymbol{x}}_{m_{n,l}}}{\partial \eta^2} \otimes \bar{\boldsymbol{h}} \right\rangle_n \right\} \\ &+ Re\left\{ \left\langle \frac{\partial^2 \dot{\boldsymbol{x}}_{m_{n,l}}}{\partial \eta^2} \otimes \bar{\boldsymbol{h}} \right\rangle_n \left\langle \dot{\boldsymbol{x}}_{m_{n,l}}^* \otimes \bar{\boldsymbol{h}}^* \right\rangle_n \right\} \\ &+ Re\left\{ \left\langle \frac{\partial \dot{\boldsymbol{x}}_{m_{n,l}}}{\partial \eta} \otimes \bar{\boldsymbol{h}} \right\rangle_n \left\langle \frac{\partial \dot{\boldsymbol{x}}_{m_{n,l}}^*}{\partial \eta} \otimes \bar{\boldsymbol{h}}^* \right\rangle_n \right\} \end{aligned} \tag{E.16}$$

$$\begin{aligned} \frac{\partial^2 ln(L)}{\partial \phi_0^2} \quad &= -\frac{2}{\sigma^2} \sum_{m_{n,l}=m^1}^{m^{\mathcal{M}}} Re\left\{ -y_{n,l}^* \left\langle \frac{\partial^2 \dot{\boldsymbol{x}}_{m_{n,l}}}{\partial \phi_0^2} \otimes \bar{\boldsymbol{h}} \right\rangle_n \right\} \\ &+ Re\left\{ \left\langle \frac{\partial^2 \dot{\boldsymbol{x}}_{m_{n,l}}}{\partial \phi_0^2} \otimes \bar{\boldsymbol{h}} \right\rangle_n \left\langle \dot{\boldsymbol{x}}_{m_{n,l}}^* \otimes \bar{\boldsymbol{h}}^* \right\rangle_n \right\} \\ &+ Re\left\{ \left\langle \frac{\partial \dot{\boldsymbol{x}}_{m_{n,l}}}{\partial \phi_0} \otimes \bar{\boldsymbol{h}} \right\rangle_n \left\langle \frac{\partial \dot{\boldsymbol{x}}_{m_{n,l}}^*}{\partial \phi_0} \otimes \bar{\boldsymbol{h}}^* \right\rangle_n \right\} \end{aligned} \tag{E.17}$$

$$\begin{aligned} \frac{\partial^2 ln(L)}{\partial \eta \partial \phi_0} \quad &= -\frac{2}{\sigma^2} \sum_{m_{n,l}=m^1}^{m^{\mathcal{M}}} Re\left\{ -y_{n,l}^* \left\langle \frac{\partial^2 \dot{\boldsymbol{x}}_{m_{n,l}}}{\partial \eta \partial \phi_0} \otimes \bar{\boldsymbol{h}} \right\rangle_n \right\} \\ &+ Re\left\{ \left\langle \frac{\partial^2 \dot{\boldsymbol{x}}_{m_{n,l}}}{\partial \eta \partial \phi_0} \otimes \bar{\boldsymbol{h}} \right\rangle_n \left\langle \dot{\boldsymbol{x}}_{m_{n,l}}^* \otimes \bar{\boldsymbol{h}}^* \right\rangle_n \right\} \\ &+ Re\left\{ \left\langle \frac{\partial \dot{\boldsymbol{x}}_{m_{n,l}}}{\partial \eta} \otimes \bar{\boldsymbol{h}} \right\rangle_n \left\langle \frac{\partial \dot{\boldsymbol{x}}_{m_{n,l}}^*}{\partial \phi_0} \otimes \bar{\boldsymbol{h}}^* \right\rangle_n \right\} \end{aligned} \tag{E.18}$$

$$\frac{\partial^2 ln(L)}{\partial\epsilon\partial\eta} = -\frac{2}{\sigma^2}\sum_{m_{n,l}=m^1}^{m^{\mathcal{M}}} Im\left\{\left(\frac{2\pi}{N}\right)(m_{n,l}+1)y_{n,l}^*\left\langle\frac{\partial\dot{\boldsymbol{x}}_{m_{n,l}}}{\partial\eta}\otimes\bar{\boldsymbol{h}}\right\rangle_n\right\} \tag{E.19}$$

$$\frac{\partial^2 ln(L)}{\partial\theta_0\partial\eta} = -\frac{2}{\sigma^2}\sum_{m_{n,l}=m^1}^{m^{\mathcal{M}}} Im\left\{y_{n,l}^*\left\langle\frac{\partial\dot{\boldsymbol{x}}_{m_{n,l}}}{\partial\eta}\otimes\bar{\boldsymbol{h}}\right\rangle_n\right\} \tag{E.20}$$

$$\frac{\partial^2 ln(L)}{\partial\epsilon\partial\phi_0} = -\frac{2}{\sigma^2}\sum_{m_{n,l}=m^1}^{m^{\mathcal{M}}} Im\left\{\left(\frac{2\pi}{N}\right)(m_{n,l}+1)y_{n,l}^*\left\langle\frac{\partial\dot{\boldsymbol{x}}_{m_{n,l}}}{\partial\phi_0}\otimes\bar{\boldsymbol{h}}\right\rangle_n\right\} \tag{E.21}$$

$$\frac{\partial^2 ln(L)}{\partial\theta_0\partial\phi_0} = -\frac{2}{\sigma^2}\sum_{m_{n,l}=m^1}^{m^{\mathcal{M}}} Im\left\{y_{n,l}^*\left\langle\frac{\partial\dot{\boldsymbol{x}}_{m_{n,l}}}{\partial\phi_0}\otimes\bar{\boldsymbol{h}}\right\rangle_n\right\} \tag{E.22}$$

$$\frac{\partial^2 ln(L)}{\partial Re\{\bar{h}_q\}\partial\epsilon} = -\frac{2}{\sigma^2}\sum_{m_{n,l}=m^1}^{m^{\mathcal{M}}}\left(\frac{2\pi}{N}\right)(m_{n,l}+1)Im\left\{y_{n,l}^*\dot{x}_{m_{n,l}}^q\right\} \tag{E.23}$$

$$\frac{\partial^2 ln(L)}{\partial Re\{\bar{h}_q\}\partial\theta_0} = -\frac{2}{\sigma^2}\sum_{m_{n,l}=m^1}^{m^{\mathcal{M}}} Im\left\{y_{n,l}^*\dot{x}_{m_{n,l}}^q\right\} \tag{E.24}$$

$$\frac{\partial^2 ln(L)}{\partial Im\{\bar{h}_q\}\partial\epsilon} = -\frac{2}{\sigma^2}\sum_{m_{n,l}=m^1}^{m^{\mathcal{M}}}\left(\frac{2\pi}{N}\right)(m_{n,l}+1)Re\left\{y_{n,l}^*\dot{x}_{m_{n,l}}^q\right\} \tag{E.25}$$

$$\frac{\partial^2 ln(L)}{\partial Im\{\bar{h}_q\}\partial\theta_0} = -\frac{2}{\sigma^2}\sum_{m_{n,l}=m^1}^{m^{\mathcal{M}}} Re\left\{y_{n,l}^*\dot{x}_{m_{n,l}}^q\right\} \tag{E.26}$$

$$\begin{aligned}\frac{\partial^2 ln(L)}{\partial Re\{\bar{h}_q\}\partial\eta} &= -\frac{2}{\sigma^2}\sum_{m_{n,l}=m^1}^{m^{\mathcal{M}}} Re\left\{-y_{n,l}^*\frac{\partial\dot{x}_{m_{n,l}}^q}{\partial\eta}\right\} + 2Re\left\{\dot{x}_{m_{n,l}}^q\frac{\partial(\dot{x}_{m_{n,l}}^q)^*}{\partial\eta}Re\left\{\bar{h}_q\right\}\right\}\\ &+Re\left\{\frac{\partial\dot{x}_{m_{n,l}}^q}{\partial\eta}\sum_{i=0;i\neq q}^{v-1}(\dot{x}_{m_{n,l}}^i)^*\bar{h}_i^*\right\} + Re\left\{\dot{x}_{m_{n,l}}^q\sum_{i=0;i\neq q}^{v-1}\frac{\partial(\dot{x}_{m_{n,l}}^i)^*}{\partial\eta}\bar{h}_i^*\right\}\end{aligned} \tag{E.27}$$

$$\frac{\partial^2 ln(L)}{\partial Re\{\bar{h}_q\}\partial\phi_0} = -\frac{2}{\sigma^2}\sum_{m_{n,l}=m^1}^{m^{\mathcal{M}}} Re\left\{-y^*_{n,l}\frac{\partial \dot{x}^q_{m_{n,l}}}{\partial\phi_0}\right\} + 2Re\left\{\dot{x}^q_{m_{n,l}}\frac{\partial(\dot{x}^q_{m_{n,l}})^*}{\partial\phi_0}Re\left\{\bar{h}_q\right\}\right\}$$
$$+Re\left\{\frac{\partial \dot{x}^q_{m_{n,l}}}{\partial\phi_0}\sum_{i=0;i\neq q}^{v-1}(\dot{x}^i_{m_{n,l}})^*\bar{h}^*_i\right\} + Re\left\{\dot{x}^q_{m_{n,l}}\sum_{i=0;i\neq q}^{v-1}\frac{\partial(\dot{x}^i_{m_{n,l}})^*}{\partial\phi_0}\bar{h}^*_i\right\} \quad (E.28)$$

$$\frac{\partial^2 ln(L)}{\partial Im\{\bar{h}_q\}\partial\eta} = -\frac{2}{\sigma^2}\sum_{m_{n,l}=m^1}^{m^{\mathcal{M}}} Im\left\{y^*_{n,l}\frac{\partial \dot{x}^q_{m_{n,l}}}{\partial\eta}\right\} + 2Im\left\{\bar{h}_q\right\}Re\left\{\dot{x}^q_{m_{n,l}}\frac{\partial(\dot{x}^q_{m_{n,l}})^*}{\partial\eta}\right\}$$
$$+Im\left\{\frac{\partial(\dot{x}^q_{m_{n,l}})^*}{\partial\eta}\sum_{i=0;i\neq q}^{v-1}\dot{x}^i_{m_{n,l}}\bar{h}_i\right\} + Im\left\{(\dot{x}^q_{m_{n,l}})^*\sum_{i=0;i\neq q}^{v-1}\frac{\partial \dot{x}^i_{m_{n,l}}}{\partial\eta}\bar{h}_i\right\} \quad (E.29)$$

$$\frac{\partial^2 ln(L)}{\partial Im\{\bar{h}_q\}\partial\phi_0} = -\frac{2}{\sigma^2}\sum_{m_{n,l}=m^1}^{m^{\mathcal{M}}} Im\left\{y^*_{n,l}\frac{\partial \dot{x}^q_{m_{n,l}}}{\partial\phi_0}\right\} + 2Im\left\{\bar{h}_q\right\}Re\left\{\dot{x}^q_{m_{n,l}}\frac{\partial(\dot{x}^q_{m_{n,l}})^*}{\partial\phi_0}\right\}$$
$$+Im\left\{\frac{\partial(\dot{x}^q_{m_{n,l}})^*}{\partial\phi_0}\sum_{i=0;i\neq q}^{v-1}\dot{x}^i_{m_{n,l}}\bar{h}_i\right\} + Im\left\{(\dot{x}^q_{m_{n,l}})^*\sum_{i=0;i\neq q}^{v-1}\frac{\partial \dot{x}^i_{m_{n,l}}}{\partial\phi_0}\bar{h}_i\right\} \quad (E.30)$$

The elements of the FIM are obtained by taking expectation of the above second order partial derivatives. The entries the negatives of the expectations given below.

$$E\left\{\frac{\partial^2 ln(L)}{\partial Re\{\bar{h}_q\}^2}\right\} = -\frac{2}{\sigma^2}\sum_{m_{n,l}=m^1}^{m^{\mathcal{M}}}|\dot{x}^q_{m_{n,l}}|^2 \quad (E.31)$$

$$E\left\{\frac{\partial^2 ln(L)}{\partial Im\{\bar{h}_q\}^2}\right\} = -\frac{2}{\sigma^2}\sum_{m_{n,l}=m^1}^{m^{\mathcal{M}}}|\dot{x}^q_{m_{n,l}}|^2 \quad (E.32)$$

$$E\left\{\frac{\partial^2 ln(L)}{\partial Re\{\bar{h}_q\}Re\{\bar{h}_p\}_{q\neq p}}\right\} = -\frac{2}{\sigma^2}\sum_{m_{n,l}=m^1}^{m^{\mathcal{M}}}Re\{\dot{x}^q_{m_{n,l}}(\dot{x}^p_{m_{n,l}})^*\} \quad (E.33)$$

$$E\left\{\frac{\partial^2 ln(L)}{\partial Im\{\bar{h}_q\}Im\{\bar{h}_p\}_{q\neq p}}\right\} = -\frac{2}{\sigma^2}\sum_{m_{n,l}=m^1}^{m^{\mathcal{M}}}Re\{\dot{x}^q_{m_{n,l}}(\dot{x}^p_{m_{n,l}})^*\} \quad (E.34)$$

$$E\left\{\frac{\partial^2 ln(L)}{\partial Re\{\bar{h}_q\} Im\{\bar{h}_p\}_{q\neq p}}\right\} = -\frac{2}{\sigma^2}\sum_{m_{n,l}=m^1}^{m^{\mathcal{M}}} Im\{\dot{x}^q_{m_{n,l}}(\dot{x}^p_{m_{n,l}})^*\} \tag{E.35}$$

$$E\left\{\frac{\partial^2 ln(L)}{\partial Re\{\bar{h}_q\} Im\{\bar{h}_q\}}\right\} = 0 \tag{E.36}$$

$$E\left\{\frac{\partial^2 ln(L)}{\partial \epsilon^2}\right\} = -\frac{2}{\sigma^2}\sum_{m_{n,l}=m^1}^{m^{\mathcal{M}}} \left\{\left(\frac{2\pi}{N}\right)^2 (m_{n,l}+1)^2 \left|\left\langle \dot{\boldsymbol{x}}_{m_{n,l}} \otimes \bar{\boldsymbol{h}}\right\rangle_n\right|^2\right\} \tag{E.37}$$

$$E\left\{\frac{\partial^2 ln(L)}{\partial \theta_0^2}\right\} = -\frac{2}{\sigma^2}\sum_{m_{n,l}=m^1}^{m^{\mathcal{M}}} \left\{\left|\left\langle \dot{\boldsymbol{x}}_{m_{n,l}} \otimes \bar{\boldsymbol{h}}\right\rangle_n\right|^2\right\} \tag{E.38}$$

$$E\left\{\frac{\partial^2 ln(L)}{\partial \epsilon \partial \theta_0}\right\} = -\frac{2}{\sigma^2}\sum_{m_{n,l}=m^1}^{m^{\mathcal{M}}} \left\{\left(\frac{2\pi}{N}\right) (m_{n,l}+1) \left|\left\langle \dot{\boldsymbol{x}}_{m_{n,l}} \otimes \bar{\boldsymbol{h}}\right\rangle_n\right|^2\right\} \tag{E.39}$$

$$E\left\{\frac{\partial^2 ln(L)}{\partial \eta^2}\right\} = -\frac{2}{\sigma^2}\sum_{m_{n,l}=m^1}^{m^{\mathcal{M}}} \left\{\left|\left\langle \frac{\partial \dot{\boldsymbol{x}}_{m_{n,l}}}{\partial \eta} \otimes \bar{\boldsymbol{h}}\right\rangle_n\right|^2\right\} \tag{E.40}$$

$$E\left\{\frac{\partial^2 ln(L)}{\partial \phi_0^2}\right\} = -\frac{2}{\sigma^2}\sum_{m_{n,l}=m^1}^{m^{\mathcal{M}}} \left\{\left|\left\langle \frac{\partial \dot{\boldsymbol{x}}_{m_{n,l}}}{\partial \phi_0} \otimes \bar{\boldsymbol{h}}\right\rangle_n\right|^2\right\} \tag{E.41}$$

$$E\left\{\frac{\partial^2 ln(L)}{\partial \eta \partial \phi_0}\right\} = -\frac{2}{\sigma^2}\sum_{m_{n,l}=m^1}^{m^{\mathcal{M}}} Re\left\{\left\langle \frac{\partial \dot{\boldsymbol{x}}_{m_{n,l}}}{\partial \eta} \otimes \bar{\boldsymbol{h}}\right\rangle_n \left\langle \frac{\partial \dot{\boldsymbol{x}}^*_{m_{n,l}}}{\partial \phi_0} \otimes \bar{\boldsymbol{h}}^*\right\rangle_n\right\} \tag{E.42}$$

$$E\left\{\frac{\partial^2 ln(L)}{\partial \epsilon \partial \eta}\right\} = -\frac{2}{\sigma^2}\sum_{m_{n,l}=m^1}^{m^{\mathcal{M}}} Im\left\{\left(\frac{2\pi}{N}\right) (m_{n,l}+1) \left\langle \dot{\boldsymbol{x}}^*_{m_{n,l}} \otimes \bar{\boldsymbol{h}}^*\right\rangle_n \left\langle \frac{\partial \dot{\boldsymbol{x}}_{m_{n,l}}}{\partial \eta} \otimes \bar{\boldsymbol{h}}\right\rangle_n\right\} \tag{E.43}$$

$$E\left\{\frac{\partial^2 ln(L)}{\partial \theta_0 \partial \eta}\right\} = -\frac{2}{\sigma^2}\sum_{m_{n,l}=m^1}^{m^{\mathcal{M}}} Im\left\{\left\langle \dot{\boldsymbol{x}}^*_{m_{n,l}} \otimes \bar{\boldsymbol{h}}^*\right\rangle_n \left\langle \frac{\partial \dot{\boldsymbol{x}}_{m_{n,l}}}{\partial \eta} \otimes \bar{\boldsymbol{h}}\right\rangle_n\right\} \tag{E.44}$$

$$E\left\{\frac{\partial^2 ln(L)}{\partial\epsilon\partial\phi_0}\right\} = -\frac{2}{\sigma^2}\sum_{m_{n,l}=m^1}^{m^{\mathcal{M}}} Im\left\{\left(\frac{2\pi}{N}\right)(m_{n,l}+1)\left\langle\dot{\boldsymbol{x}}^*_{m_{n,l}}\otimes\bar{\boldsymbol{h}}^*\right\rangle_n\left\langle\frac{\partial\dot{\boldsymbol{x}}_{m_{n,l}}}{\partial\phi_0}\otimes\bar{\boldsymbol{h}}\right\rangle_n\right\} \tag{E.45}$$

$$E\left\{\frac{\partial^2 ln(L)}{\partial\theta_0\partial\phi_0}\right\} = -\frac{2}{\sigma^2}\sum_{m_{n,l}=m^1}^{m^{\mathcal{M}}} Im\left\{\left\langle\dot{\boldsymbol{x}}^*_{m_{n,l}}\otimes\bar{\boldsymbol{h}}^*\right\rangle_n\left\langle\frac{\partial\dot{\boldsymbol{x}}_{m_{n,l}}}{\partial\phi_0}\otimes\bar{\boldsymbol{h}}\right\rangle_n\right\} \tag{E.46}$$

$$E\left\{\frac{\partial^2 ln(L)}{\partial Re\{\bar{h}_q\}\partial\epsilon}\right\} = -\frac{2}{\sigma^2}\sum_{m_{n,l}=m^1}^{m^{\mathcal{M}}}\left(\frac{2\pi}{N}\right)(m_{n,l}+1)Im\left\{\left\langle\dot{\boldsymbol{x}}^*_{m_{n,l}}\otimes\bar{\boldsymbol{h}}^*\right\rangle_n\dot{x}^q_{m_{n,l}}\right\} \tag{E.47}$$

$$E\left\{\frac{\partial^2 ln(L)}{\partial Re\{\bar{h}_q\}\partial\theta_0}\right\} = -\frac{2}{\sigma^2}\sum_{m_{n,l}=m^1}^{m^{\mathcal{M}}} Im\left\{\left\langle\dot{\boldsymbol{x}}^*_{m_{n,l}}\otimes\bar{\boldsymbol{h}}^*\right\rangle_n\dot{x}^q_{m_{n,l}}\right\} \tag{E.48}$$

$$E\left\{\frac{\partial^2 ln(L)}{\partial Im\{\bar{h}_q\}\partial\epsilon}\right\} = -\frac{2}{\sigma^2}\sum_{m_{n,l}=m^1}^{m^{\mathcal{M}}}\left(\frac{2\pi}{N}\right)(m_{n,l}+1)Re\left\{\left\langle\dot{\boldsymbol{x}}^*_{m_{n,l}}\otimes\bar{\boldsymbol{h}}^*\right\rangle_n\dot{x}^q_{m_{n,l}}\right\} \tag{E.49}$$

$$E\left\{\frac{\partial^2 ln(L)}{\partial Im\{\bar{h}_q\}\partial\theta_0}\right\} = -\frac{2}{\sigma^2}\sum_{m_{n,l}=m^1}^{m^{\mathcal{M}}} Re\left\{\left\langle\dot{\boldsymbol{x}}^*_{m_{n,l}}\otimes\bar{\boldsymbol{h}}^*\right\rangle_n\dot{x}^q_{m_{n,l}}\right\} \tag{E.50}$$

$$\begin{aligned}E\left\{\frac{\partial^2 ln(L)}{\partial Re\{\bar{h}_q\}\partial\eta}\right\} &= -\frac{2}{\sigma^2}\sum_{m_{n,l}=m^1}^{m^{\mathcal{M}}} Re\left\{-\left\langle\dot{\boldsymbol{x}}^*_{m_{n,l}}\otimes\bar{\boldsymbol{h}}^*\right\rangle_n\frac{\partial\dot{x}^q_{m_{n,l}}}{\partial\eta}\right\}\\ &+2Re\left\{\dot{x}^q_{m_{n,l}}\frac{\partial(\dot{x}^q_{m_{n,l}})^*}{\partial\eta}\right\}Re\left\{\bar{h}_q\right\}+Re\left\{\frac{\partial(\dot{x}^q_{m_{n,l}})^*}{\partial\eta}\sum_{i=0;i\neq q}^{v-1}\dot{x}^i_{m_{n,l}}\bar{h}_i\right\}\\ &+Re\left\{(\dot{x}^q_{m_{n,l}})^*\sum_{i=0;i\neq q}^{v-1}\frac{\partial\dot{x}^i_{m_{n,l}}}{\partial\eta}\bar{h}_i\right\}\end{aligned} \tag{E.51}$$

$$E\left\{\frac{\partial^2 ln(L)}{\partial Re\{\bar{h}_q\}\partial\phi_0}\right\} = -\frac{2}{\sigma^2}\sum_{m_{n,l}=m^1}^{m^{\mathcal{M}}} Re\left\{-\left\langle \dot{\boldsymbol{x}}^*_{m_{n,l}} \otimes \bar{\boldsymbol{h}}^*\right\rangle_n \frac{\partial \dot{x}^q_{m_{n,l}}}{\partial\phi_0}\right\}$$
$$+2Re\left\{\dot{x}^q_{m_{n,l}}\frac{\partial(\dot{x}^q_{m_{n,l}})^*}{\partial\phi_0}\right\} Re\left\{\bar{h}_q\right\} + Re\left\{\frac{\partial(\dot{x}^q_{m_{n,l}})^*}{\partial\phi_0}\sum_{i=0;i\neq q}^{v-1}\dot{x}^i_{m_{n,l}}\bar{h}_i\right\}$$
$$+Re\left\{(\dot{x}^q_{m_{n,l}})^*\sum_{i=0;i\neq q}^{v-1}\frac{\partial\dot{x}^i_{m_{n,l}}}{\partial\phi_0}\bar{h}_i\right\} \tag{E.52}$$

$$E\left\{\frac{\partial^2 ln(L)}{\partial Im\{\bar{h}_q\}\partial\eta}\right\} = -\frac{2}{\sigma^2}\sum_{m_{n,l}=m^1}^{m^{\mathcal{M}}} Im\left\{\left\langle \dot{\boldsymbol{x}}^*_{m_{n,l}} \otimes \bar{\boldsymbol{h}}^*\right\rangle_n \frac{\partial \dot{x}^q_{m_{n,l}}}{\partial\eta}\right\}$$
$$+2Im\left\{\bar{h}_q\right\} Re\left\{\dot{x}^q_{m_{n,l}}\frac{\partial(\dot{x}^q_{m_{n,l}})^*}{\partial\eta}\right\} + Im\left\{\frac{\partial(\dot{x}^q_{m_{n,l}})^*}{\partial\eta}\sum_{i=0;i\neq q}^{v-1}\dot{x}^i_{m_{n,l}}\bar{h}_i\right\}$$
$$+Im\left\{(\dot{x}^q_{m_{n,l}})^*\sum_{i=0;i\neq q}^{v-1}\frac{\partial\dot{x}^i_{m_{n,l}}}{\partial\eta}\bar{h}_i\right\} \tag{E.53}$$

$$E\left\{\frac{\partial^2 ln(L)}{\partial Im\{\bar{h}_q\}\partial\phi_0}\right\} = -\frac{2}{\sigma^2}\sum_{m_{n,l}=m^1}^{m^{\mathcal{M}}} Im\left\{\left\langle \dot{\boldsymbol{x}}^*_{m_{n,l}} \otimes \bar{\boldsymbol{h}}^*\right\rangle_n \frac{\partial \dot{x}^q_{m_{n,l}}}{\partial\phi_0}\right\}$$
$$+2Im\left\{\bar{h}_q\right\} Re\left\{\dot{x}^q_{m_{n,l}}\frac{\partial(\dot{x}^q_{m_{n,l}})^*}{\partial\phi_0}\right\} + Im\left\{\frac{\partial(\dot{x}^q_{m_{n,l}})^*}{\partial\phi_0}\sum_{i=0;i\neq q}^{v-1}\dot{x}^i_{m_{n,l}}\bar{h}_i\right\}$$
$$+Im\left\{(\dot{x}^q_{m_{n,l}})^*\sum_{i=0;i\neq q}^{v-1}\frac{\partial\dot{x}^i_{m_{n,l}}}{\partial\phi_0}\bar{h}_i\right\} \tag{E.54}$$

References

[1] P. H. Moose, "A technique for orthogonal frequency division multiplexing frequency offset correction," *IEEE Transactions on Communications*, vol. 42, pp. 2908–2914, October 1994.

[2] T. M. Schmidl and D. C. Cox, "Robust frequency and timing synchronization for ofdm," *IEEE Transactions on Communications*, vol. 45, pp. 1613–1621, December 1997.

[3] K. Y. Kim, J. Y. Lee, H. J. Choi, and H. Kim, "Symbol frame synchronization technique for OFDM burst mode transmission," *ITC-CSCC*, pp. 1697–1700, July 2002.

[4] V. Abhayawardhana and I. Wassell, "Residual frequency offset correction for coherently modulated OFDM systems," *55th IEEE Vehicular Technology Conference*, vol. 2, pp. 777–781, May 2002.

[5] M. Sliskovic, "Carrier and sampling frequency offset estimation and correction in multicarrier systems," *GLOBECOM '01*, pp. 285–289, 2001.

[6] V. Abhayawardhana and I. Wassell, "Iterative symbol offset correction algorithm for coherently modulated OFDM systems in wireless communication," *The 13th IEEE International Symposium on Personal Indoor and Mobile Radio Communications*, vol. 2, pp. 545–549, September 2002.

[7] S.-Y. Liu and J.-W. Chong, "A study of tracking algorithms of carrier frequency offset and sampling clock offset for OFDM-based WLANs," *International Conference on Communications, Circuits and Systems*, vol. 1, pp. 109–113, 2002.

[8] E. G. Larsson, G. Liu, J. Li, and G. B. Giannakis, "Joint symbol timing and channel estimation for OFDM based WLAN's," *IEEE Communications Letters*, vol. 5, August 2001.

[9] K. Nikitopoulos and A. Polydoros, "Joint channel equalization and residual frequency offset and phase noise compensation in OFDM systems," tech. rep., National and Capodistrian University of Athens, 2003.

[10] G. Golub and C. V. Loan, *Matrix Computions*. London: The John Hopings Press, 1997.

[11] European Telecommunications Standards Institute (ETSI), *Radio Broadcasting Systems: Digital Audio Broadcasting (DAB) to Mobile Portable and Fixed Receivers*, v1.3.3 ed., 2001.

[12] American National Standard for Telecommunications, *Very high bit rate Digital Subscriber Line (VDSL) Metallic Interface*, February 2003.

[13] European Telecommunications Standards Institute (ETSI), *Broadband Radio Access Networks; HIPERLAN Type 2; Physical Layer*, 1.1.1 ed., April 2000.

[14] Institute of Electrical and Electronics Engineers(IEEE), *Supplement to IEEE Standard for Information Technology - Part 11: Wireless LAN Medium Access Control(MAC) and Physical Layer (PHY) specifications High-speed Physical Layer in the 5 GHZ Band*, 1999.

[15] T. Rappaport, *Wireless Communications.* IEEE Press, 1996.

[16] E. Biglieri, J. Proakis, and S. Shamai, "Fading channels: Information theoretic and communications aspects," *IEEE Transactions on Information Theory*, vol. 44, pp. 2619–2692, October 1998.

[17] J. Proakis, *Digital Communications.* New York: McGraw-Hill, 3 ed., 1995.

[18] S. Coleri, M. Ergen, A. Puri, and A. Bahai, "Channel estimation techniques based on pilot arrangement in OFDM systems," *IEEE Transactions on Broadcasting*, vol. 48, pp. 223–229, September 2002.

[19] F. Tufvesson and T. Masseng, "Pilot assisted channel estimation for OFDM in mobile cellular systems," *47th IEEE Vehicular Technology Conference*, vol. 3, pp. 1639–1643, May 1997.

[20] O. Simeone, Y. Bar-Ness, and U. Spagnolini, "Pilot-based channel estimation for OFDM systems by tracking the delay- subspace," *IEEE Transactions on Wireless Communications*, vol. 3, pp. 315–325, January 2004.

[21] H. Minn and V. Bhargava, "An investigation into time-domain approach for OFDM channel estimation," *IEEE Transactions on Broadcasting*, vol. 46, pp. 240–248, December 2000.

[22] T. Roman, M. Enescu, and V. Koivunen, "Time-domain method for tracking dispersive channels in OFDM systems," *57th IEEE Vehicular Technology Conference*, vol. 2, pp. 1318–1321, 2003.

[23] M. Speth, S. Fechtel, G. Fock, and H. Meyr, "Optimum receiver design for OFDM-based broadband transmission - part II: A case study," *IEEE Transactions on Communications*, vol. 49, pp. 571–578, April 2001.

[24] M. Olsson, "Implementation of an IEEE802.11a synchronizer," tech. rep., Department of Electrical Engineering: Linkoping University, 2002.

[25] B. Yang, K. B. Letaief, R. S. Cheng, and Z. Cao, "Timing recovery for OFDM transmission," *IEEE Journal on Selected Areas in Communications*, vol. 18, pp. 2278–2291, November 2000.

[26] T. Keller, L. Piazzo, P. Mandarini, and L. Hanzo, "Orthogonal frequency division multiplex synchronization techniques for frequency-selective fading channels," *IEEE Journal on Selected Areas in Communications*, vol. 19, pp. 999–1008, June 2001.

[27] M. Pollet and M. Moeneclacy, "BER sensitivity of OFDM systems to carrier frequency offset and wiener phase noise," *IEEE Transactions on Communications*, vol. 43, February 1995.

[28] J. F.-G. Garcia, O. Edfors, and J. M. Paez-Borrallo, "Frequency offset correction for coherent OFDM in wireless systems," *IEEE Transactions on Consumer Electronics*, vol. 47, pp. 187–193, February 2001.

[29] K. Nikitopoulos and A. Polydoros, "Compensation schemes for phase noise and residual frequency offset in OFDM systems," *GLOBECOM '01*, vol. 1, pp. 330–333, November 2001.

[30] S. A. Fechtel, "OFDM carrier and sampling frequency synchronization and its performance on stationary and mobile channels," *IEEE Transactions on Consumer Electronics*, vol. 46, pp. 438–441, August 2000.

[31] J. Weng, S. Leung, and W. Lau, "Joint amplitude and delay estimation for CDMA systems in impulsive channels," *IEEE International Symposium on Circuits and Systems*, vol. 4, pp. 2513–2516, June 1997.

[32] B. Thapa, B. Jones, and Q. Zhu, "Non-linear control with neural networks," *Fourth International Conference on Knowledge-Based Intelligent Engineering Systems and Allied Technologies*, vol. 2, pp. 868–873, 2000.

[33] K. Pope and P. Rayner, "Non-linear system identification using Bayesian inference," *International Conference on Acoustics, Speech, and Signal Processing*, vol. 4, pp. 457–460, 1994.

[34] S. McLaughlin, "Adaptive equalisation via Kalman filtering techniques," *IEE Proceedings: Radar and Signal Processing*, vol. 138, pp. 388–396, August 1991.

[35] D. G. Manolakis, V. K. Ingle, and S. M. Kogon, *Statistical and Adaptive Signal Processing.* Boston: McGraw-Hill, 2002.

[36] S. Haykin, *Adaptive Filter Theory.* Englewood Cliffs, NJ: Prentice Hall, 3 ed., 1996. pp 573-580.

[37] K. Baum, "A synchronized coherent OFDM air interface concept for high data rate cellular systems," *48th IEEE Vehicular Technology Conference*, vol. 3, pp. 2222–2226, 1998.

[38] H. Chen and G. J. Pottie, "A comparison of frequency offset tracking algorithms for OFDM," *GLOBECOM '03*, vol. 2, pp. 1069–1073, 2003.

[39] J. Li, G. Liu, and G. B. Giannakis, "Carrier frequency offset estimation for OFDM-Based WLANs," *IEEE Signal Processing Letters*, vol. 8, pp. 80–82, March 2001.

[40] Institute of Electrical and Electronics Engineers(IEEE), *Suggested Requirements for a Consumer PAN High Rate Video/MM Link*, March 2000.

[41] H. L. V. Trees, *Detection Estimation and Modulation Theory: Part I.* New York: John Wiley & Sons Inc, 2001.

[42] S. Ljung and L. Ljung, "Error propagation properties of recursive least-squares adaptation algorithms," *Automatica*, vol. 21, no. 2, pp. 157–167, 1985.

[43] S. Haykin, *Adaptive Filter Theory.* Englewood Cliffs, NJ: Prentice Hall, 3 ed., 1996. pp 711-717.

[44] S. Haykin, A. Sayed, J. Zeidler, P. Yee, and P. Wei, "Adaptive tracking of linear time-varying systems by extended RLS algorithm," *IEEE Transactions on Signal Processing*, vol. 45, pp. 1118–1128, May 1997.

[45] Institute of Electrical and Electronics Engineers(IEEE), *Part 16: Air Interface for Fixed Broadband Wireless Access Systems - Amendment 2: Medium Access Control Modifications and Additional Physical Layer Specifications for 2-11 GHz*, 2003.